New Methods for QRS Detection and Classification in ECG Signals

A Thesis
Submitted in partial fulfillment of the requirements
for the degree of

Doctor of Philosophy

by

Tanushree Sharma
(2013REC9570)

Under the supervision of
Prof. Kamalesh Kumar Sharma

DEPARTMENT OF ELECTRONICS AND
COMMUNICATION ENGINEERING
Malaviya National Institute of Technology, Jaipur.

January, 2018

Department of Electronics and Communication Engineering

MALAVIYA NATIONAL INSTITUTE OF TECHNOLOGY

CERTIFICATE

This is to certify that the thesis entitled, **"New Methods of QRS Detection and Classification in ECG Signals"** submitted by **Ms. Tanushree Sharma** (Registration No. 2013REC9570) to the Department of Electronics and Communication Engineering, Malaviya National Institute of Technology, Jaipur, for the award of the degree of Doctor of Philosophy is a bonafide research work carried by her under my supervision and guidance. The results obtained in this thesis have not been submitted to any other university or institute for the award of any other degree.

Prof. Kamalesh Kumar Sharma
Department of Electronics and Communication Engineering,
Malaviya National Institute of Technology, Jaipur.

Declaration of Authorship

I, Tanushree Sharma, declare that this thesis titled, 'NEW METHODS OF QRS DETECTION AND CLASSIFICATION IN ECG SIGNALS' and the work presented in it are my own. The work has been carried out under the supervision of Prof. Kamalesh Kumar Sharma.

I confirm that:

- This work was done wholly or mainly while in candidature for a research degree at MNIT, Jaipur.
- Where any part of this thesis has previously been submitted for a degree or any other qualification at MNIT, Jaipur or any other institution, this has been clearly stated.
- Where I have consulted the published work of others, this is always clearly attributed.
- Where I have quoted from the work of others, the source is always given. With the exception of such quotations, this thesis is entirely my own work.
- I have acknowledged all main sources of help.
- Where the thesis is based on work done by myself jointly with others, I have made clear exactly what was done by others and what I have contributed myself.

Signed: _____

Date: _____

"God always helps those who help themselves..."

Abstract

The electrocardiogram (ECG) is a commonly used low cost, noninvasive tool used for diagnosis of various cardiovascular diseases. For example, the different types of *arrhythmias* can be detected by their signature ECG patterns. Manual identification of arrhythmias in long-term ECG recordings obtained over a period of several hours or days is a tedious task and also prone to human errors. Therefore, there is a strong motivation for automatic ECG classification. Automatic ECG classification comprises two main stages: *heartbeat segmentation* and *beat classification*. Since the QRS complex is the most distinctive feature in an ECG, it is almost invariably chosen as the fiducial point for heartbeat segmentation. Usually, fixed size beats are extracted by selecting certain fixed durations of signal on both sides of the R-peak. In the next stage, these beats are classified to identify their category. Therefore, in order to improve the performance of an automatic ECG classification system, work needs to be done on developing improved techniques for QRS detection and classification. In this thesis, we have focused on these two objectives. The standard MIT-BIH database has been used in evaluation of the proposed methods. The main challenge in QRS detection is the noise spectrally overlapping with the dominant QRS energy range. Techniques like wavelet transform, which have frequently been used in the literature for QRS detection come up short for removal of this noise, because it is difficult to select an appropriate mother wavelet, given the diverse ECG morphologies. As a solution, we propose a new method for QRS detection using the synchrosqueezed wavelet transform (SSWT), which gives a time frequency representation of a signal which is largely invariant to the choice of the mother wavelet. The proposed method gives a very low detection error rate (DER) of 0.15% and outperforms existing QRS detection techniques. In cases where the noise spectrally overlaps with the desired signal, optimization techniques can also be used to suppresss the in-band noise. Therefore, we propose another QRS detection method based on weighted least squares (WLS) optimization. This method has low computational load, and is suitable for implementation in wearable devices. It was implemented in NXP LPC1768 microcontroller, based on ARM Cortex M3 core and was found to be real-time implementable on it, in block-by-block processing mode. The algorithm gives 0.22 % DER in the offline implementation and 0.67 % in the real-time implementation. In the direction of developing real-time implementable algorithms, another algorithm based on weighted total variation (WTV) denoising is proposed. While the previous algorithm is based on ℓ_2 norm minimization, this algorithm uses ℓ_1 norm minimization. This technique uses Teager-Kaiser energy to compute weights in WTV denoising. Using a recently available WTV solver, the method performed much faster than the WLS-based technique and also, the real time implementation of the WTV method gave much lower DER than WLS-based method (0.29% versus 0.67%). Next, a novel ECG classification technique using a graph based classifier is proposed. With simpler features, the proposed classification algorithm gives accuracy nearly equal to those of techniques that use more sophisticated features. Finally, as additional work, a technique for power line interference removal from ECG signals based on wavelet transform based component-retrieval is proposed, which gives significantly better results than fixed and adaptive notch filters used for this purpose.

Acknowledgements

I would like to first thank the Almighty for giving me the strength to do this Ph.D. work. Without His blessings, it wouldn't have been possible.

Next, I would like to thank my supervisor, Prof. K. K. Sharma, for his patient guidance and for giving me the freedom to do the research work I wanted to do, and grow in the process.

I would also like to thank the Departmental Research Evaluation Committee members, Dr. M. Salim, Dr. S. J. Nanda and Dr. Ghanshyam Singh, for their valuable comments and suggestions which helped in improving this research work.

I would also like to thank Mr. Bharat Kashyap, Technical Assistant, Embedded Systems Lab for his valuable assistance in coding the microcontroller used in a QRS detection algorithm.

I'm thankful to my family for their patience and support throughout. I'm very grateful to my husband, Dr. Rishi Sharma, for his valuable suggestions that helped me a lot in my research work.

Last, but not the least, I gratefully acknowledge the help extended to me by my colleagues in various forms, throughout the Ph.D..

Contents

List of Figures

List of Tables

List of Important Abbreviations

CVD	Cardiovascular disease
CWT	Continuous wavelet transform
DSP	Digital signal processing
ECG	Electrocardiogram
PLI	Power line interference
PCA	Principal components analysis
PVC	Premature ventricular contraction
RCM	Retrieval of components and modes
SNR	Signal-to-noise ratio
SSWT	Synchrosqueezed wavelet transform
TFR	Time frequency representation
TV	Total variation
WT	Wavelet transform
WLS	Weighted least squares
WTV	Weighted total variation

List of Important Symbols

a	scale parameter
A	Weighted adjacency matrix
b	translation or shift parameter
ψ	mother wavelet
DER	detection error rate
f	frequency
G	Graph
ℓ_1	L1 norm
ℓ_2	L2 norm
n	sample number
ν	set of vertices
P^+	positive predictivity
Se	sensitivity
f	frequency
t	time
TP	true positives
FP	false positives
FN	false negatives
TN	true negatives
W	Wavelet transform

Dedicated to the Almighty...

Chapter 1

Introduction

1.1 Motivation

Cardiovascular diseases (CVDs) are the foremost cause of death globally. According to a World Health Organization report [13], an estimated 17.7 million people lost their lives to CVDs in the year 2015, which accounts for 31% of global deaths. Hence, it is important to enable early detection and management for people with high cardiovascular risk (because of diabetes, hypertension etc.), in order to mitigate mortality risks due to CVDs.

The electrocardiogram (ECG) is a very commonly used, noninvasive and low cost tool used for diagnosis of CVDs. The ECG signal, which is an electrical manifestation of heart muscle contractions, is recorded from the body surface of the subject using electrodes. Many cardiac problems manifest as characteristic ECG patterns and therefore, can be detected by analyzing the ECG. The recorded ECG may be analyzed manually by a cardiologist or automatically, by means of computer software. There are several advantages of automation of ECG analysis. For example, a 24 hour ECG recording obtained from a Holter monitor may contain close to hundred thousand beats, in which the pathological beats may occur randomly. Manual analysis of these long records is very difficult, because a human observer is prone to fatigue, boredom and distraction. Also, it has been found in studies that there is marked intra- and inter- observer variability in ECG interpretation among cardiologists, which can be reduced significantly when they are provided with computer ECG interpretation [14, 15].

The ECG signal is comprised of successive heartbeats or cycles, with each beat consisting of a P-wave, the Q, R and S-waves, which are collectively known as the QRS complex and the T-wave, as shown in the diagram in Fig. 1.1. In some cases, an additional

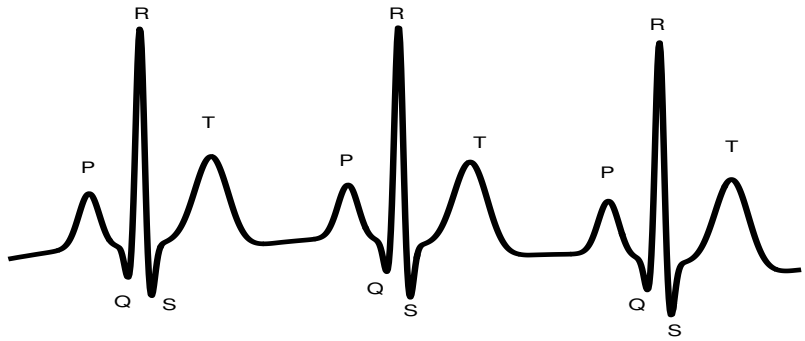

FIGURE 1.1: Three successive ECG beats

U-wave may also be present. Automatic ECG classification involves two major steps: (1) segmentation of the ECG into beats (2) classification of the beats. For extraction of a beat from the continuous ECG recording, first a fiducial point needs to be decided, with respect to which, the beat onset and offset can be determined. The QRS complex is the most distinctive feature in the ECG; therefore, it is almost invariably used as the reference for ECG segmentation. Hence, accurate detection of QRS complexes is essential for extraction of the beats. In some applications, such as ambulatory monitoring using a Holter monitor, it is also required that the detection algorithm have low computational cost and be real-time implementable. Thus, it is desirable to develop QRS detection algorithms that have high accuracy and low computational cost.

The next step in automatic ECG classification is to classify the beats. An important application is to detect the presence of *arrhythmias* in the subject. Arrhythmia refers to any abnormal rhythmic activity of the heart. Some arrhythmias are harmless, whereas some may be life threatening. For example, occurrence of three or more premature ventricular contraction (PVC) beats in succession, along with an elevated heart rate, is a condition referred to as ventricular tachycardia (VT), which may lead to ventricular fibrillation (VF). This is a state of disorganized contractions of the heart, resulting in ineffective pumping of blood and hence, is fatal. Therefore, an automatic ECG classification program needs to timely and accurately detect these arrhythmias.

In order to improve the performance of automatic ECG classification, efforts need to be made in the following directions:

- Developing improved techniques for QRS detection
- Developing improved beat classification techniques

The research work presented in this thesis describes the development of the proposed methods, aimed at achieving these two objectives.

1.2 Background

Accurate detection of QRS complexes serves as the basis for not just ECG classification, but also other tasks that depend on reliable QRS detection, such as derivation of the heart rate and hence the respiratory signal, ECG compression, delineation, biometrics, etc. However, the problem of QRS detection in ECG signals is complicated by factors such as presence of noise and artefacts (particularly those that spectrally overlap with QRS frequencies), interference from tall and pointed P- and T-waves in the ECG that resemble the QRS waves and varying QRS morphologies and signal-to-noise ratios (SNRs).

QRS detection in ECG signals is a longstanding problem and numerous techniques have been proposed in the literature for the same. QRS detection algorithms proposed over the years reflect advances in signal processing, as well as increased processing power and memory. A review of QRS detection techniques proposed prior to 2002 is given in [16]. The underlying structure common to most QRS detection algorithms consists of two stages. The first is a preprocessing stage that comprises linear and/or nonlinear filtering that aims at accentuating the QRS complexes and suppressing noise in the ECG signal. This is followed by a decision stage that usually uses heuristic rules to decide the final R-peak locations. Since QRS complexes are characterized by a steep slope, derivative-based algorithms have frequently been used in the literature [17–19]. A number of algorithms based on digital filters [18, 20–22] have also been proposed in the literature. Wavelet transforms [23–27] have frequently been used for QRS detection. Other approaches proposed in the literature include neural networks [28, 29], linear prediction [30], mathematical morphology [31], hidden Markov models [32] and Hilbert transform [33]. More recently, S-transform and Shannon energy [34], sparse derivatives [35], envelopment filter [36], quadratic filter [37], nonlinear MaMeMi filter [38] and singular value decomposition (SVD) filter [39] based techniques have been proposed. However, it is still a challenge to simultaneously reduce the number of false detections and missed detections to low values. Also, most real-time QRS detection algorithms have relatively high detection error rates.

Most of the QRS energy lies in the frequency range [5 22] Hz [27]. Bandpass filtering to select this frequency range helps in QRS detection by reducing the interference from P- and T-waves, eliminating the out-of-band noise such as baseline wander and power line interference and diminishing muscular noise, whose frequency range overlaps that of QRS complexes, but extends to higher frequencies. However, this bandpass filtering attenuates the wider QRS complexes. Also, the noise that spectrally overlaps with the QRS range still remains in the filtered signal. This complicates the QRS detection problem, as the detection of the wider and other lower amplitude QRS complexes requires the need of a

low threshold, which can lead to a greater number of false detections due to noise peaks. Thus, threshold selection becomes an issue.

In such cases, where the signal and noise overlap in frequency, wavelet denoising is a useful technique. The idea behind wavelet denoising is that the signal can be represented by a few large magnitude coefficients in the wavelet domain, whereas the noise is represented by a larger number of smaller magnitude coefficients. Thus, by thresholding in the wavelet domain, the noise can be removed. However, the wavelet representation strongly depends on the choice of the mother wavelet [40]. Therefore, in case of ECG signals, which have varying morphologies, the choice of an appropriate mother wavelet becomes difficult. Thus, a time-frequency transform that is invariant to the choice of the moter wavelet/basis needs to be sought. In this work, we have focused on seeking such techniques.

Apart from linear techniques such as the wavelet transform based filtering, nonlinear filtering based on optimization has recently been shown to be very useful in enhancement of the signal-to-noise ratio (SNR) of the ECG signal [35], which in turn leads to improved QRS detection accuracy. The technique is based on convex ℓ_1 optimization and can suppress noise spectrally overlapping with the ECG. Motivated by this, we attempt to develop an optimization based filtering technique in this work, which can improve the signal-to-noise ratio of the ECG signal, so that higher detection accuracies can be achieved.

Several methods for arrhythmia classification have also been reported in the literature. The classification schemes typically consist of a feature extraction stage, followed by a classifier. Various features have been used in the previous works, such as morphological features [41–44], hermite coefficients [45, 46], higher order statistics [44, 47], wavelet coefficients [48], etc. The classifiers most frequently used in the literature are neural networks (NNs) [49–56] and support vector machines (SVMs) [47, 57–64]. It was observed that in the literature, the focus has been on deriving effective features for classification, which is a relatively difficult task. Very little attention has been paid on exploring new methods for classification, however. Therefore, in this work, we explore the possibility of using an efficient classifier with just the raw beats or possibly beats with reduced dimensions (obtained using a suitable dimensionality reduction technique) as input and obtaining comparable values of classification accuracy.

Problem statement

Having identified the need for fast and accurate techniques for QRS detection and ECG classification through a critical analysis of the existing techniques in the literature, we

attempted to develop improved methods for the same. To this end, we formulated the following research objectives:

1. To develop a new method of QRS detection that would give higher accuracy than the existing techniques, but may not necessarily be real-time implementable.
2. To develop a new method for QRS detection that has a low computational load, and therefore, is implementable for real-time operation in wearable ECG monitoring devices. The method should also possess improved accuracy over existing such techniques.
3. To develop an improved technique for ECG classification.

The first objective of the research work presented in the thesis is to develop a new method for QRS detection that gives improved detection accuracy over existing techniques. The technique may not necessarily be real-time, as it is intended to be used for short duration signals. Potential applications of such a technique could be in clinical decision support systems, to assist cardiologists. Since, the ECG signals are nonstationary in nature, therefore, time-frequency transforms, such as the wavelet transform seem to be a suitable choice for the preprocessing stage of such a method. However, as observed earlier, wavelet transforms strongly depend on the choice of the mother wavelet. Therefore, the representation is “coloured" by the basis used [65]. This is disadvantageous from the point of view of QRS detection, because of varying QRS morphologies. The selected wavelet may not correlate well with certain morphologies, so the corresponding wavelet coefficients obtained may be low in magnitude. Therefore, we intend to seek a time-frequency transform invariant to the choice of the basis.

The second objective is to develop a QRS detection technique with low computational load, for use in wearable devices. The reduced computational load, however, should not come at the cost of low accuracy. Time-frequency transforms have higher computational and memory requirements; therefore we seek alternative methods based on optimization, to suppress the noise spectrally overlapping with QRS complexes.

The final objective is to develop improved methods for ECG classification. As observed earlier, many new feature extraction techniques have been proposed in the literature; however, not much attention has been paid on the classifier stage. In this work, we seek new classifiers that are capable of achieving high classification accuracies, without the use of sophisticated features.

1.3 Organization of the thesis

The remainder of this thesis is organized as follows.

Chapter-2 begins with a physiological overview of ECG generation, following which, a brief description of various types of arrhythmias is given. Also, a more detailed review of the earlier efforts in the areas of QRS detection and ECG arrhythmia classification is given.

In Chapter-3, a QRS complex detection algorithm using the synchrosqueezed wavelet transform (SSWT) is presented. In this method, we first obtain the SSWT of the ECG signal and select the frequency range in which the QRS energy is maximum. On the signal filtered using the SSWT, we apply a nonlinear transformation which is novel in the context of QRS detection. This nonlinear transformation aims at equalizing the QRS amplitudes before peak detection. Finally, a smooth envelope is obtained using low pass filtering, in which peaks are detected and used as guides to latch on to the actual R-peaks. The algorithm is evaluated on the MIT-BIH arrhythmia database and its performance is compared to that of existing techniques.

In Chapter-4, we develop a technique for QRS detection which has low computational load and therefore, is implementable in wearable devices. The technique is based on weighted least squares (WLS) optimization, which was originally introduced in the context of edge-preserving image denoising [66]. In the method proposed in this chapter, we use WLS-based smoothing in combination with Savitzky-Golay filtering, which is another least-squares polynomial-fitting-based smoothing technique, to smooth the ECG signal, while preserving the QRS complexes. Following this preprocessing stage, we again use the nonlinear transformation technique described in the previous chapter with some modifications, to equalize the QRS amplitudes. Finally a smooth envelope is obtained, which is used to determine the actual R-peak positions. We describe two different implementations of the proposed method: one suitable for fast offline QRS detection and other suitable for real-time implementation on block-by-block processing mode. The technique was also implemented in hardware on LPC1768 microcontroller, based on ARM Cortex M3 and was found to be implementable in real-time on this microcontroller. The method is evaluated on the standard MIT-BIH arrhythmia database and its performance is compared to that of established and sate-of-the-art techniques.

In Chapter-5, we develop another technique for QRS detection with low computational load. The technique is based on weighted total variation (WTV) minimization. A local estimate of noise in the signal block under consideration is used to determine the regularization parameter in WTV minimization, which determines the amount of

smoothing applied. This makes the denoising locally adaptive. The weights are chosen so as to give preference to preservation of QRS complexes over P- and T-waves while smoothing. Thus, the technique can simultaneously reduce the higher frequency noise as well as the lower frequency interference from P- and T-waves, in spite of the fact that they have overlapping spectra with the QRS complexes. The proposed method is evaluated on the MIT-BIH arrhythmia database and gives improved detection accuracy over established and state-of-the-art techniques. The technique has low computational load, therefore, it can be used for fast offline QRS detection in long duration ECG records, as well as real-time QRS detection in block-by-block processing mode.

In Chapter-6, we describe a new method for ECG arrhythmia classification using a graph-based classifier. In the proposed method, we first apply principal components analysis (PCA) on raw ECG beats, to reduce their dimensionality. The resulting lower dimensional transformed vectors are combined with RR interval information to form the input vectors. Using these input vectors, a K-nearest neighbour graph is built using the city-block distance as the similarity measure. The unknown labels are determined by finding a smooth graph signal with mimimum total variation. The proposed method is evaluated on the MIT-BIH arrhythmia database. The performance of the graph-based classifier is compared to support vector machines with the same inputs. Also, the overall classification performance is compared to that of other methods proposed in the literature.

In Chapter-7, as additional work, we use the wavelet transform for power line interference removal from ECG signals. The techniques for PLI removal proposed in the literature are mostly based on fixed notch and adaptive filters. The fixed notch filters perform poorly in case of PLI frequency variations, whereas adaptive filters suffer from issues such as slow convergence and requirement of an external reference signal. In this chapter, we propose an alternative approach for PLI removal from the ECG signal, which overcomes the limitations of both fixed and adaptive filters. We model the PLI as an AM-FM component and use a wavelet transform (WT) based component retrieval technique that is inspired by the synchrosqueezing framework [67] to retrieve the PLI component, which is subtracted from the contaminated signal to remove the interference. The proposed method is evaluated in two worst-case scenarios of PLI frequency and amplitude variation, for healthy and pathological cases and the results are compared to those of other techniques.

Finally, in Chapter-8, we present the conclusions of the research work presented in the thesis.

Chapter 2

Physiological Background of ECG and Literature Review

2.1 Overview

In this chapter, we first give a brief overview of the physiological processes that underlie the ECG, focusing mainly on the processes that are relevant to the topics considered in the thesis. After describing the ECG generation mechanism, we briefly describe various ways of measuring the ECG. Since we have focused on arrhythmia classification in this thesis, we next discuss the different kinds of arrhythmia and how they are generated. Finally, we give a literature review covering the earlier efforts made by researchers in the areas of QRS detection and ECG classification.

2.2 Physiological basis of the ECG

2.2.1 The anatomy of the heart

The heart is made up of muscle known as the *myocardium*, which rhythmically contracts to pump blood throughout the body. It consists of four chambers. The upper chambers or *atria* are responsible for the collection of blood, whereas the lower chambers or *ventricles* pump the blood throughout the body. The relaxation of a chambers is referred to as *diastole*, whereas its contraction is known as *systole*. The four chambers of the heart and the major connecting vessels are depicted in the diagram in Fig. 2.1.

The impure blood fills the right atrium (RA) via the superior and inferior vena cavae. When the atria contract, this impure blood is pumped from the RA to the right ventricle

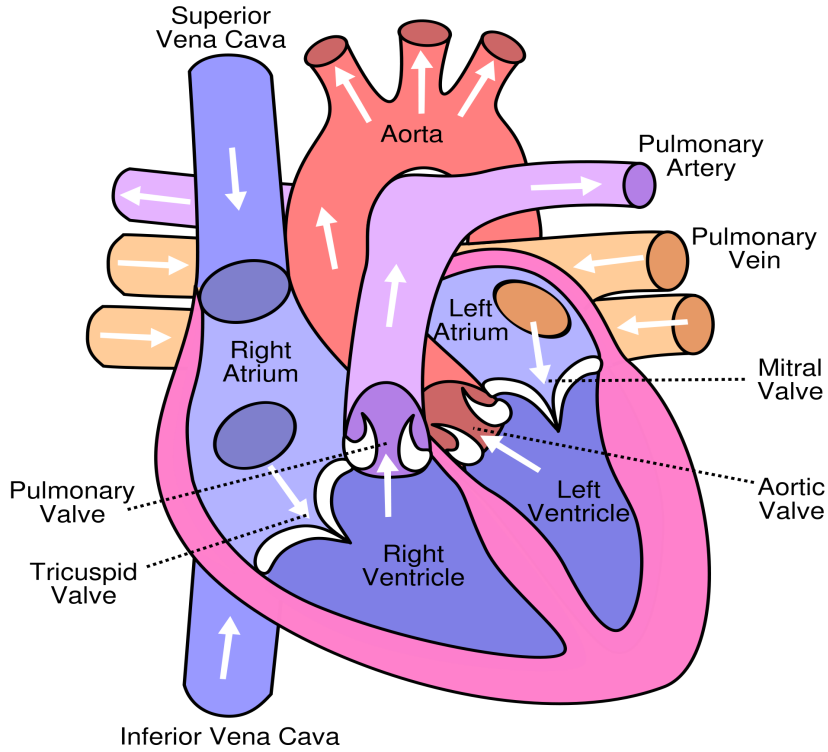

FIGURE 2.1: Anatomy of the heart. [1]

(RV) through the tricuspid valve. When the ventricles contract, this impure blood in the right ventricle is pumped to the lungs for oxygenation, through the pulmonary valve [68]. After purification by the lungs, this blood is received in the left atrium (LA), and is pumped into the left ventricle (LV) through the mitral valve on contraction.

2.2.2 The action potential

Each myocardial cell or cardiac *myocyte* has a trans-membrane *resting potential* of around -80 to -90 mV with respect to the external surrounding fluid [69]. The membrane has several voltage-gated channels that open or close in response to changes in voltage. These channels allow the flow of different ions, including sodium (Na^+), potassium (K^+), calcium (Ca^+) and chloride (Cl^-) through the membrane. Because of the inflow and outflow of the ions through the gate over time, there are changes in the trans-membrane potential over time, which constitute action potential [69]. A typical action potential waveform for a ventricular cell is depicted in Fig. 2.2, in which four different phases (0-3) are shown. Also shown below are the corresponding waves produced on the ECG. When myocytes are depolarized to a *threshold* voltage of about -70 mV, which can happen as a result of conduction of another action potential from a neighboring cell, a rapid depolarization phase (phase 0) occurs, which is caused by an increase in Na^+ channel conductance and hence, greater Na^+ influx. This is followed by an initial

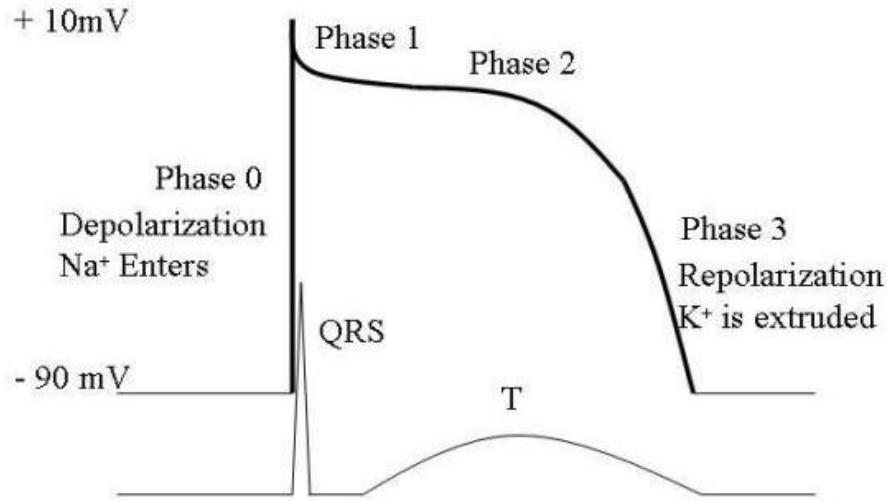

FIGURE 2.2: A typical ventricular action potential waveform. [2]

repolarization phase (phase 1), which is caused by efflux of K^+ ions due to opening of K^+ channels. During phase 2, there is a plateau in action potential due to approximate balance between influx of Ca^+ ions and efflux of K^+ ions [69]. In phase 3, the cell again repolarizes due to increased K^+ conductivity and decrease in Ca^+ conductivity. Finally, the cell comes back into the resting state, which is characterized by open K^+ channels [69].

2.2.3 Pacemaker cells

Under normal functioning, the cardiac rhythm is controlled by the sinoatrial (SA) node, which is located at the junction of the superior vena cava and the right atrium [68]. It consists of special pacemaker cells, which possess the property of *automaticity*, i.e., they can spontaneously depolarize, and act as pacemaker cells for the rest of the heart [69]. However, pacemaker cells are not found only in the SA node, but also in the atrio-ventricular (AV) node and some specialized conduction systems within the atria and the ventricles [69]. In these cells, the resting phase is not stable, but exhibits spontaneous depolarization and when the cell potential reaches a threshold, an action potential is generated, after which, the cell returns back to the resting phase and the cycle repeats [69].

Myocardial cells are tightly coupled to transmit the action potentials from one cell to another, by means of low-resistance gap junctions. These gap junctions allow the flow of ionic currents from cell to cell, and the heart electrically behaves as a syncytium. Thus, an action potential originating at any myocyte will propagate throughout the heart, causing a coordinated mechanical contraction [69]. The autonomous and central

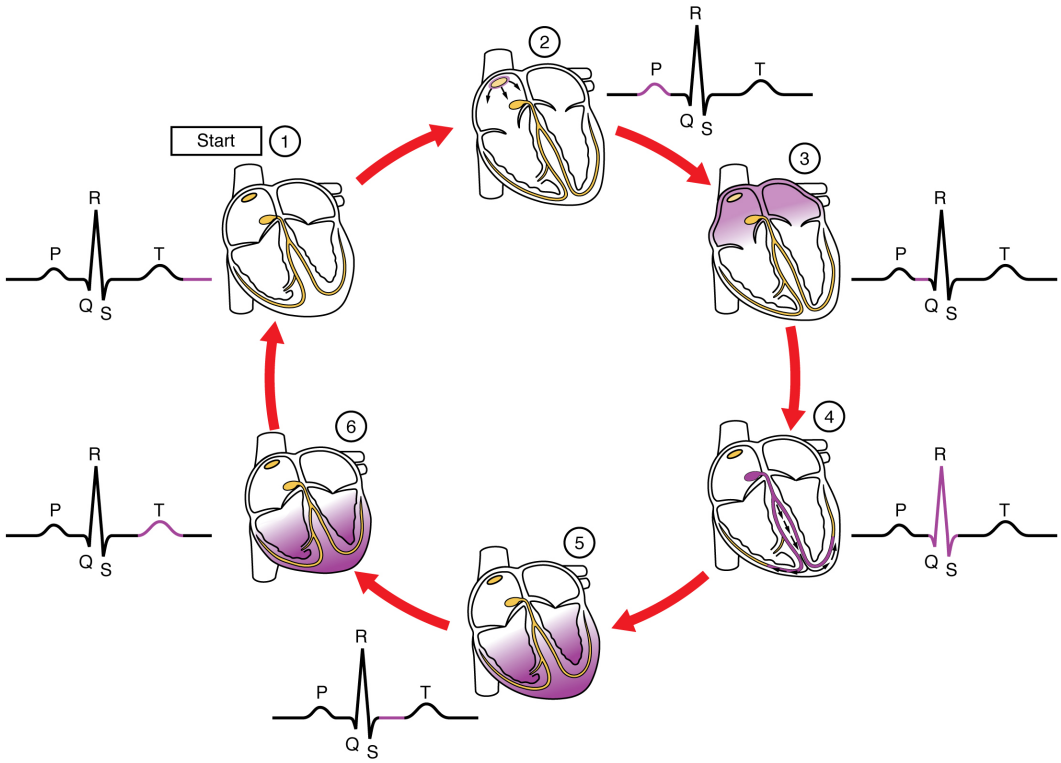

FIGURE 2.3: Stages in the cardiac cycle correlated with the ECG tracing. [3]

nervous systems control the firing rate of the SA node through neurotransmitters [68]. The intrinsic firing rate of the SA node is the highest under normal functioning; therefore it determines the heart rate under normal functioning, the lower pacemakers being reset in each cardiac cycle. However, in some pathological conditions, the firing rate of lower pacemakers can be faster than that of the SA node, and can determine the overall heart rate [69].

2.2.4 Generation of the ECG signal

The series of events in a single cardiac cycle, and their correlation with different waves and segments in the ECG training is depicted in Fig. 2.3. Each stage is described as follows: [68]:

1. Under normal functioning, the cardiac cycle begins with generation of action potential by the SA node. The impulse propagates through the atria at a relatively low speed, causing them to contract. This results in the generation of a slowly varying, low-amplitude P-wave because of the slow contraction of the atria and their relatively small size. The amplitude of P-waves is typically in the range of 0.1 - 0.2 mV and their duration is about 60 - 80 ms [68].

2. When the excitation wave arrives at the AV node, it faces a propagation delay. This delay causes the iso-electric PQ segment of duration 60-80 ms in the ECG tracing. This delay helps the atria to pump all the blood into the ventricles [68].

3. After the propagation delay, the excitation waves arrives at the bundle of His, which branches into the left and right bundle branches, that lead to the network of purkinje fibres. The wave travels through this conduction system and causes the ventricles to contract rapidly. This produces a sharp QRS wave in the ECG, which is the most distinctive wave in the ECG of amplitude about 1 mV and 80 ms duration [68].

4. The action potential duration in the ventricles is relatively longer, at about 300 - 350 ms. The plateau portion of the action potential results in a normally iso-electric ST segment in the ECG of about 100 - 120 ms duration, following the QRS complex (please see Fig. 2.2) [68].

5. Diastole of the ventricles causes a slow T-wave in the ECG, with a nominal amplitude of 0.1 - 0.3 mV and duration between 120 - 160 ms [68].

2.2.5 ECG measurement

Because of the electrical activity of the cells, current flows within the body and potential differences are established on the skin. These potential differences can be measured using surface electrodes. The recording of these body surface potentials as a function of time is known as the ECG [69].

The standard 12-channel ECG is obtained using four limb leads and six chest leads, with the reference electrode placed on the right leg [68]. It comprises three sets of leads: *limb leads*, *augmented leads* and *precordial* or chest leads. The limb leads I, II, and III are obtained using the left arm, right arm, and the left leg. By averaging the left arm, right arm, and left leg leads, the Wilson's central terminal is obtained, which is used as the reference for chest leads. The augmented limb leads, which are known as aVR, aVL, and aVF (aV denotes the augmented lead, R denotes the right arm, L denotes the left arm, and F denotes the left foot) are obtained by using the exploring electrode on the limb indicated by the lead name and using the Goldberger's central terminal as the negative input. The Goldberger's central terminal is an average of inputs from two limb electrodes, other than the exploring electrode.

Fig. 2.4 shows a hypothetical equilateral triangle formed by leads I, II, and III, which is known as the Einthoven 's triangle. Also indicated in the figure are the directions of the axes the six limb leads form. The center of the triangle, which corresponds to the

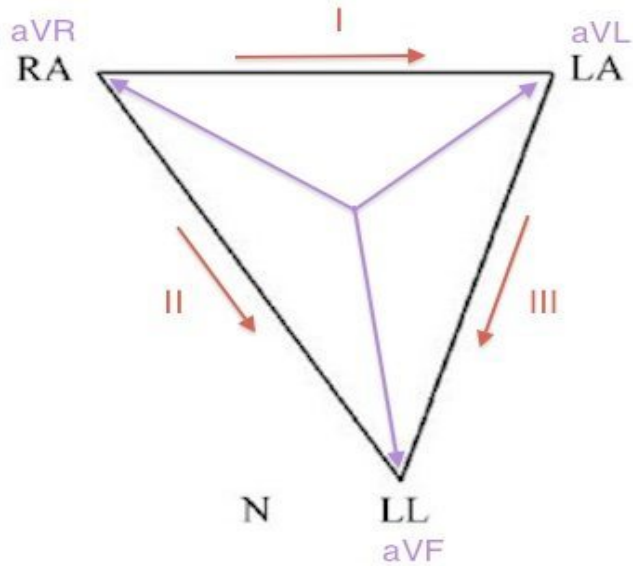

FIGURE 2.4: The Einthoven's triangle and the six limb leads [4]

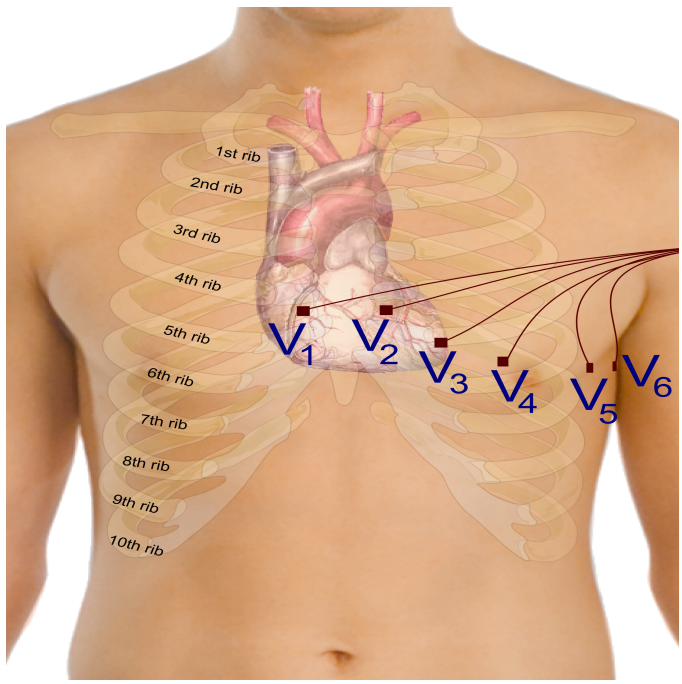

FIGURE 2.5: Placement of the six precordial leads [5]

Wilson's central terminal, where the heart is assumed to be placed [68]. The six leads are actually projections of the three-dimensional (3D) cardiac electrical vector onto the axes illustrated in Fig. 2.4, where each axis samples the $0° - 180°$ range in steps of approximately 30° [68]. The projections facilitate observation of electrical activity of the heart from different perspectives, in the frontal plane [68].

The six precordial leads (written as V1 - V6) are obtained from six standardized chest positions, with Wilson's central terminal as the reference [68]. The positions for placement

FIGURE 2.6: Atrial premature contractions in ECG. [6].

of the precordial leads are shown in Figure 2.5.

The six chest leads provide different perspectives of the cardiac electrical vector in a cross-sectional plane. Of all chest leads, V5 and V6 provide the most information about left ventricular activity, V3 and V4 are most sensitive to septa1 activity, whereas V1 and V2 are most sensitive to activity in the right-half of the heart [68].

2.2.6 Arrhythmias

Any abnormality in the heart rhythm is referred to as arrhythmia. One way to categorize arrhythmias is on the basis of the heart rate. Accordingly, arrhythmias can be classified as follows [69].

2.2.6.1 Ectopy, tachycardia and fibrillation

One category of arrhythmias is associated with elevated heart rates. When the trigger to depolarize originates at a location other than the SA node, i.e. in some other part, it is called *ectopic* depolarization and the resulting beats are known as ectopic beats [69]. They may be caused as a result of certain drugs, infection of the myocardium or inflammation or damage of part of the heart [69].

The ectopic beats can further be classified on the basis of origin of the beat. Ectopic beats originating in the atria are referred to as *premature atrial beats*, or *atrial premature contractions* (APCs), an example of which is shown in Fig. 2.6. In this case, an abnormal P wave of non-sinus origin is followed by a QRS complex.

When ectopic beats originate in the ventricles, they are known as *premature ventricular beats* or *premature ventricular contractions* (PVCs), as shown in Fig. 2.7. It may be noted that the morphology of a PVC beat is very different from that of a sinus beat. Also, it is typically wider, because its excitation wave propagates slowly through the myocardium rather than through the high-speed Purkinje fibers [69]. Sometimes there

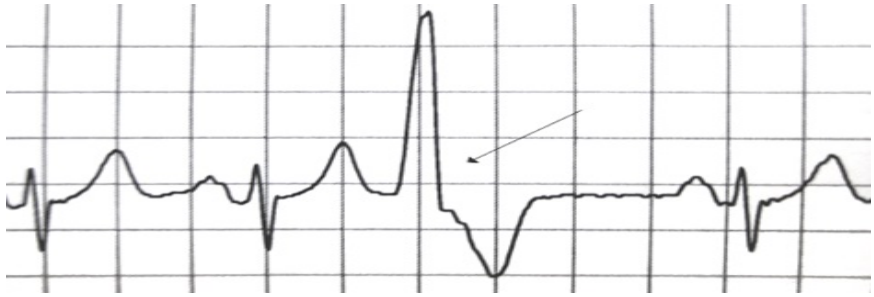

FIGURE 2.7: Premature ventricular contraction marked with an arrow [7].

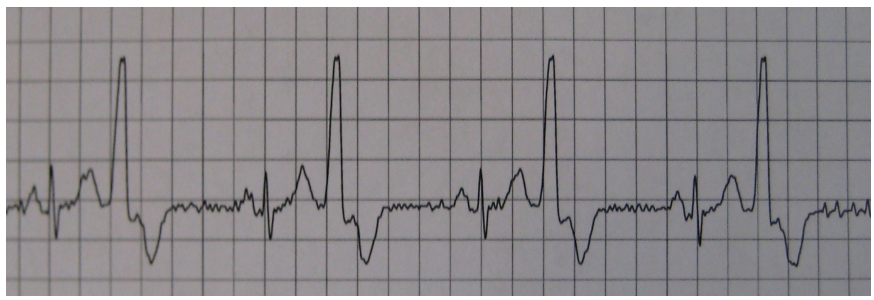

FIGURE 2.8: Ventricular bigeminy in ECG. [8].

occurs a repeating pattern of "sinus beat - PVC - sinus beat - PVC -" and so on, which is termed as *ventricular bigeminy*, as shown in Fig. 2.8. Also, sometimes, there can be occurrence of many ectopic beats, because of which, the overall heart rate may be higher than normal [69].

In some cases, the wavefront of excitation circulates repeatedly through the heart, leading to repeated waves of tissue depolarization at an abnormally high rate, in a phenomenon known as *reentrant arrhythmia* [69]. An example of this reentrant pattern is *ventricular tachycardia* (VT), as shown in Fig.-2.9.

These states can be rapidly fatal, because the pumping of the blood is not effective. If a run of three or more successive PVC beats occurs, and the heart rate is over 100 beats per minute, then the condition corresponds to VT. If the VT lasts up to 15 seconds (or 30 seconds, according to some conventions), then it is called nonsustained VT; otherwise it is known as sustained VT [69].

In some cases, the wavefront of excitation breaks down into numerous smaller wavefronts that circulate over the myocardium, leading to totally uncoordinated contraction and the myocardium quivers. This condition is known as *fibrillation*. In *atrial fibrillation* (AF), the AV node act as a gatekeeper for these disorganized atrial wavefronts,and therefore, the ventricular depolarization is organized and the QRS complexes are normal [69]. However, the ventricular rhythm is usually quite irregular and the heart rate is higher. In case the ventricular rate becomes excessively high, the cardiac output can be reduced as the

FIGURE 2.9: Ventricular tachycardia observed in ECG. [9].

FIGURE 2.10: Ventricular fibrillation observed in ECG. [10].

ventricles do not fill up sufficiently. Also, in the long run, untreated AF can lead to formation of clots that can reenter the circulation and cause arterial blockages [69].

As opposed to atrial fibrillation, untreated *ventricular fibrillation* (VF), as shown in Fig. 2.10 an lead to death in seconds to minutes, as it causes the termination of blood flow through the cardiovascular circuit [69].

2.2.6.2 Conduction blocks, bradycardia, and escape rhythms

In the other category of arrhythmias, the heart rhythms are excessively slow and there are abnormal blockages in propagation of the excitation wave [69].

Pathological conditions that are responsible for these excessively slow rhythms and blockages include conduction abnormalities in the AV node. In first-degree AV block (shown in Fig. 2.11), the excitation impulses coming from the atria are delayed at the AV node, resulting in lengthening of the PR interval. In second degree AV block, the AV node may fail to conduct some of the atrial excitation wavefronts [69]. In the case of third degree AV block, the AV node fails to conduct all impulses coming from the atria.

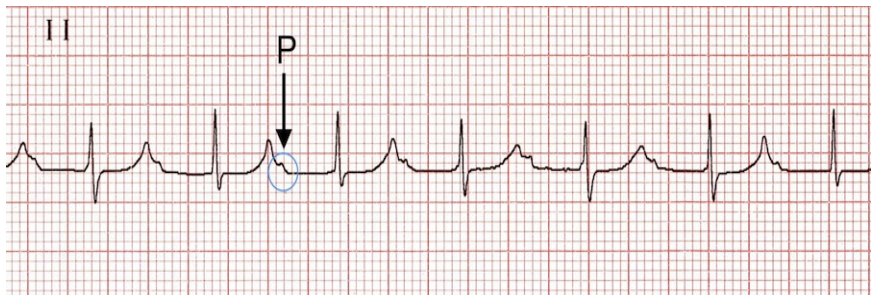

FIGURE 2.11: First degree AV block observed in ECG. [11].

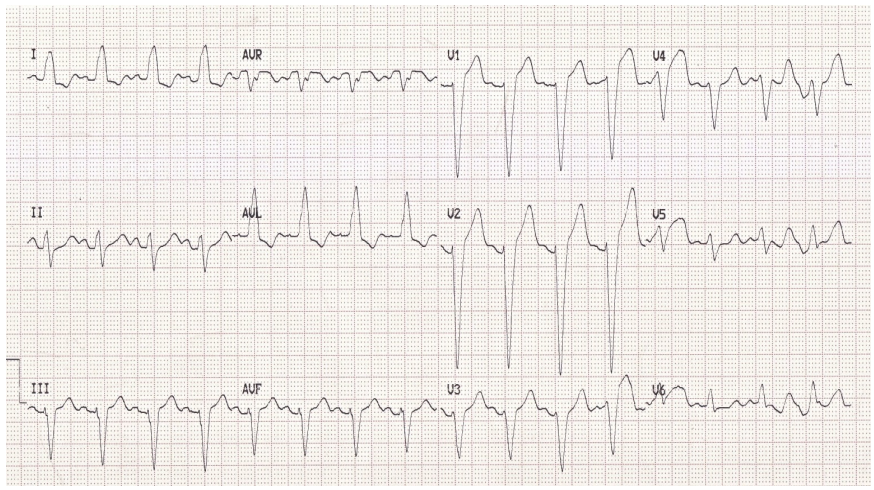

FIGURE 2.12: Left bundle branch block observed in ECG. [12].

On the other hand, blockages in the right and left conduction bundles, termed as right bundle branch block (RBBB) and left bundle branch block (LBBB) (shown in Fig. 2.12), respectively, do not affect the pumping efficacy significantly, but can cause dramatic changes in the ECG morphology. They can mask ECG changes crucial to diagnosis of other diseases such as myocardial ischemia. Also in some cases, these conduction abnormalities are indicative of some other pathological condition.

When there is an excessively long pause in initiation of heart beat by the SA node, the heartbeat may be initiated by other cardiac cells, as a normal, compensatory response. Such beats are known as *escape beats* [69]. Though these beats are of non-sinus origin, just like the ectopic beats, however an important difference is that in case of escape beats, the pathology is aberrant automaticity, whereas in case of escape beats, the pathology is abnormal conduction; therefore there treatments are quite different [69]. While ectopic beats are generally premature, the escape beats appear at the end of a prolonged RR interval. An example of an escape beat is a *ventricular escape beat*, which is a ventricular beat that occurs in the condition of third-degree heart block [69]

2.3 QRS detection techniques

As discussed earlier, the QRS complex represents ventricular depolarization. It is the most noticeable feature in the ECG, characterized by a steep slope. Therefore, it is used as the reference for delineation of other waves and segments in the ECG [70]. Also, QRS detection is used to obtain additional clinically useful information from the ECG, such as the heart rate and the respiratory signal [71], for extraction of beat segments for classification [72], ECG compression [73], biometrics [74], etc. Detection of QRS complexes in the ECG signal is complicated by factors such as presence of noise, pointed P- and T-waves resembling QRS complexes, QRS-like artefacts and varied QRS morphologies.

As mentioned earlier, the underlying structure common to most QRS detection algorithms consists of two stages, as shown in Fig. 2.13. The first is a preprocessing stage that comprises linear and/or nonlinear filtering that aims at accentuating the QRS complexes and suppressing noise in the ECG signal. This is followed by a peak detection stage that usually uses heuristic rules to decide the final R-peak locations. Numerous QRS detection techniques have been proposed in the literature, that use different ways of preprocessing the ECG. A review of the techniques proposed prior to 2002 is given in [16].

Among the earlier techniques, the real-time, derivative-based algorithm proposed by Pan and Tompkins [21] is a classic and popular real-time QRS detection algorithm. It detects QRS complexes based upon analysis of slope, amplitude, and width. The ECG signal is first passed through a digital bandpass filter to attenuate the noise, which comprises cascaded highpass and lowpass filters. This is followed by a derivative stage that gives information about the slope of the QRS complexes. Then, a squaring operation is used to intensify the slope of the frequency response curve of the derivative, which aids in reduction of false positives caused by tall and pointed T-waves. This is follwed by moving window integration that produces information about both the slope and the width of the QRS complexes. The algorithm uses automatic adaptation of thresholds to adapt to changing ECG morphology and heart rate. Though the algorithm has a low computational load, its accuracy, however, is low for noisy records. Improvements of this algorithm [75], as well as many other algorithms that use derivative [17–19] and digital filters [18, 20, 22] have been proposed in the literature.

As mentioned earlier in Chapter-1, most of the QRS energy lies in the frequency range [5 22] Hz [27]. Bandpass filtering to select this frequency range helps in QRS detection by reducing the interference from P- and T-waves, eliminating the out-of-band noise such as baseline wander and power line interference and diminishing muscular noise, whose frequency range overlaps that of QRS complexes, but extends to higher frequencies.

However, this bandpass filtering attenuates the wider QRS complexes, for example, the PVC beats. Also, the noise that spectrally overlaps with the QRS range still remains in the filtered signal. This complicates the QRS detection problem, as the detection of the wider and other lower amplitude QRS complexes requires the need of a low threshold, which can lead to a greater number of false detections due to noise peaks. Thus, threshold selection becomes difficult.

Because of the nonstationary nature of ECG signals, time-frequency analysis using wavelet transform is more suitable for QRS detection, as compared to pure frequency analysis using Fourier transform. Also, as mentioned earlier in Chapter-1, in such cases, where the signal and noise overlap in frequency, wavelet denoising is a useful technique. The idea behind wavelet denoising is that the signal can be represented by a few large magnitude coefficients in the wavelet domain, whereas the noise is represented by a larger number of smaller magnitude coefficients. Thus, by thresholding in the wavelet domain, the noise can be removed. Therefore, approaches based on wavelet transforms [23–27, 76] have frequently been used in the literature. A noteworthy algorithm is that proposed in [76]. This algorithm uses a quadratic spline wavelet. In the wavelet transform obtained using this wavelet, every uniphase wave is represented by a positive-maximum-negative minimum pair of coefficients at different scales. The moduli of these maxima or minima corresponding to the same edge are referred to as the modulus maximum line. For R-peak detection, characteristic scales, where R-peak energy is maximum are selected and then the modulus maximum lines are determined. From these, the modulus maxima lines less than a threshold are discarded, and the from the remaining ones, the isolated modulus maxima lines are further eliminated, as they correspond to motion artifact and muscle noise. The final set of modulus maxima lines is then used to detect the R-peaks. The method gives a high accuracy of 99.8 % , but the size of the data used for evaluation was much smaller [35].

Recently, empirical mode decomposition (EMD) and its variants that overcome its mode-mixing problem have emerged as powerful time-frequency decomposition tools because of the use of adaptive basis, in contrast to the fixed basis wavelet methods. In [77], an EMD-based method for QRS detection has been proposed. However, the difficulty with EMD is that there is still no established technique for its online implementation.In [34], another time-frequency technique, S-transform has been used for QRS detection. The S-transform can be seen as phase-corrected wavelet transform. In this approach, first the time-frequency representation of the ECG signal is obtained using the S-transform. Following this, the normalized Shannon energy (NSE) of the signal is computed over the frequency range in which the QRS energy is maximum. The advantage of using Shannon energy is that is emphasizes the low and medium amplitude QRS complexes better than the classical squared energy. After obtaining the NSE, a threshold is used to determine

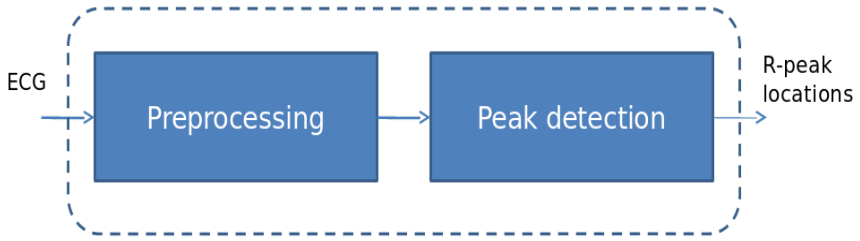

FIGURE 2.13: Typical QRS detection stages.

the R-peak locations. The method was shown to give improved results over wavelet transform based approach in [27].

Apart from linear techniques such as the Fourier and wavelet transform based filtering, which have limitations as discussed earlier, nonlinear filtering based on optimization has recently been shown to be very useful in enhancement of the signal-to-noise ratio (SNR) of the ECG signal [35]. In [35], Ning and Selesnick have proposed a novel ECG enhancement method based on sparse derivatives. In this method, the clean ECG signal is modeled as a sum of two signals whose second and third-order derivatives (differences) are sparse respectively. The denoised signal is obtained as the solution to a convex ℓ_1 optimization problem, in which a signal which has sparse second and third order derivatives is sought. Enhancement of the ECG signal using this technique was shown to improve QRS detection accuracy.

Another recently proposed method worth mentioning is the matched filtering and Hilbert transform based technique [140] proposed by Chanwimalueang *et al.* which achieves distinctly higher positive predictivity in low SNR ECG obtained from wearable devices, as compared to the Pan-Tompkins algorithm.

Some of the other approaches proposed in the literature include neural networks [28, 29], linear prediction [30], mathematical morphology [31], hidden Markov models [32] and Hilbert transform [33]. More recently, envelopment filter [36], quadratic filter [37], nonlinear MaMeMi filter [38] and singular value decomposition (SVD) filter [39] based techniques have been proposed.

As highlighted earlier, the main challenge in QRS detection is posed by the noise which lies in the same spectrum as the dominant QRS energy. Time-frequency transforms such as the wavelet transform can help in removing this noise to some extent, however, given the diverse QRS morphologies, the choice of a suitable wavelet basis is very difficult. Thus, a

time-frequency representation that is invariant to the choice of the basis needs to be sought nonlinear optimization based techniques seem very promising in removing this in-band noise. Therefore, an ECG enhancement technique based on optimization can be used to reduce this noise and improve QRS detection accuracy. We have attempted to explore such techniques in this thesis.

2.4 ECG Classification techniques

In an automatic ECG classification system, the first stage involves detection of QRS locations, which are used as fiducial marks for heartbeat segmentation. The next step is to classify these heartbeats into the correct class. Arrhythmia detection is an important application of ECG classification. Each class of arrhythmia is associated with its signature ECG pattern, which can be used to detect it. The various types of arrhythmia were discussed in detail in Section 2.2.6. In this section, we give a review of some of the techniques for arrhythmia classification proposed in the literature.

Arrhythmia classification involves two main stages: Feature extraction or feature selection, and classification. There is a difference between feature extraction and feature selection. While feature extraction refers to extraction of information from an input to discriminate its type, feature selection refers to choosing a subset of most representative features [78].

The most commonly used feature in the literature for heartbeat classification is the cardiac rhythm, or simply, the RR interval [78]. The RR interval can be used as a feature for arrhythmia classification, because the variations in RR interval are correlated with variations in morphology, frequently caused by arrhythmia [78]. Therefore, in some works, these have been used as the sole features for arrhythmia classification [79, 80].

Some methods have used time domain features directly [41, 42, 81]. The difficulty with time domain features, such as onset and offset, height and width of component waves is that they are susceptible to noise and uncertainty in detection of boundaries.

As in QRS detection, wavelet transforms have frequently been used for arrhythmia classification also [82–85]. However, as highlighted earlier, the main difficulty with wavelet transformation is the choice of appropriate mother wavelet, given the diverse ECG morphologies.

Several other types of features have also been used in the literature, such as Hermite coefficients [45, 46], higher order statistics [44, 47], linear predictive coding [86], local fractal dimension [87], etc.

The classifiers most frequently used in the literature are neural networks (NNs) [49–56] and support vector machines (SVMs) [47, 57–64]. In the recent works, SVMs have more commonly been used. Some of the other less frequently used classifiers include linear discriminants [41, 43] , decision trees [88], optimum-path forest [89], conditional random fields [44], etc.

As mentioned earlier, it has been observed that in the literature, the focus has mainly been on deriving effective features for classification. The classifier stage has received much less attention, however. Therefore, in this work, we explore the possibility of using an efficient classifier that can obtain comparable values of classification accuracy with the use of just the raw beats, or possibly beats with reduced dimensions (obtained using a suitable dimensionality reduction technique).

Chapter 3

QRS Complex Detection in ECG signals using the Synchrosqueezed Wavelet Transform

3.1 Overview

In this chapter, a QRS detection technique based on the synchrosqueezed wavelet transform (SSWT) is proposed. The SSWT is obtained from the continuous wavelet transform (CWT) by application of a frequency-reassignment technique known as *synchrosqueezing*, resulting in higher resolution. While the CWT gives a time-scale representation of a signal, the SSWT gives its time-frequency representation (TFR). The SSWT has been shown to be largely invariant to the choice of the mother wavelet [90], unlike the CWT. Also, thresholding of the wavelet coefficients is part of the SSWT implementation process, which aids in removal of additive Gaussian noise. The SSWT has recently been used for various applications such as the analysis of seismic signals [91, 92], paleoclimate records and incoming solar radiation (insolation) [90] and damping identification in a vibration system [93]. In the context of ECG signals, it has been used for obtaining breathing dynamics from ECG signals [94] and for diagnosis of paroxysmal atrioventricular block using the ECG [95]. Its application to QRS detection in ECG signals, however, has not yet been explored.

The remainder of this chapter is organized as follows. An overview of the SSWT is provided in Section 3.2. Section 3.3 describes the methodology and in Section 3.4 the experimental results are presented. Finally, Section 3.5 concludes the chapter.

3.2 Review of the synchrosqueezed wavelet transform

Synchrosqueezing was originally introduced in the context of analysing auditory signals [96]. It is a special case of reallocation methods [97–99] which aim to "sharpen" a TFR, i.e., enhance its resolution. Synchrosqueezing was recently further studied in [100] and shown to capture the flavour and philosophy of the empirical mode decomposition (EMD) [101], albeit using a different approach, and a firm theoretical foundation, which is not available for EMD. Also, it allows exact reconstruction of constituent components, like EMD and unlike classical TFR techniques [90]. It is worth mentioning, though that recently, the Multivariate EMD algorithm [137] and its extensions, noise-assisted EMD [138] and EMD via MEMD [139] have been proposed, which are strong competition for the SST and sometimes even outperform it.

A brief overview of wavelet based synchrosqueezing, originally described in [100], is given below. A more detailed description can be found in [100].
To obtain the SSWT, one starts with the CWT of a signal $s(t)$, given by:

$$W\left(a,b\right)=\int a^{-1/2}\psi^{*}\left(\frac{t-b}{a}\right)s\left(t\right)dt, \tag{3.1}$$

where, $W(a,b)$ are wavelet coefficients, a is the scale parameter, b is the translation parameter and $\psi^{*}(t)$ denotes the complex conjugate of the mother wavelet $\psi(t)$.
The wavelet ψ is chosen such that it is concentrated on the positive frequency axis, i.e.

$$\hat{\psi}(\xi)=0 \text{ for } \xi<0.$$

By using Plancheral's theorem, (3.1) can be written as

$$W(a,\ b)=\int\hat{s}(\xi)\hat{\psi}^{*}(a\xi)e^{i2\pi b\xi}d\xi\ . \tag{3.2}$$

In synchrosqueezing, for every (a,b) under consideration, for which $W(a,b)>\gamma$, instantaneous frequency,

$$\omega_{s}\left(a,b\right)=-i(W\left(a,b\right))\quad\frac{\partial}{\partial b}W\left(a,b\right) \tag{3.3}$$

is computed, where γ is a threshold chosen as described in the next section.

$\omega_s(a,b)$ in (3.3) can be considered to be an FM demodulated estimate that cancels out the effect of the mother wavelet on the wavelet coefficients [90].

the information from the time-scale plane is mapped to the time-frequency plane according to the map $(b,a) \rightarrow (b, s(a,b))$ in an operation termed synchrosqueezing. The synchrosqueezed wavelet transform $T_s(\omega, b)$, is given by:

$$T_s(\omega, b) = \int_{A(b)} W(a,b) a^{-3/2} \delta(\omega_s(a,b) - \omega) da, \tag{3.5}$$

where, $A(b) = \{a;\ W(a,b) \neq 0\}$ and $\delta(\cdot)$ is the Dirac delta function. The signal $s(t)$ can be recovered from its SSWT using the reconstruction formula:

$$s(t) = \Re e \left[C'_{\Psi} \int_0^{\infty} T_s(\omega, t)\ \mathrm{d}\omega \right], \tag{3.6}$$

where, C'_{Ψ} is a constant that depends only on Ψ[100].

To understand the effect of synchrosqueezing, consider a purely harmonic signal given by:

$$x(t) = Acos(2\pi ct),$$

Its wavelet transform is given by:

$$W_x(a,\ b) = \frac{A}{2} \int [\delta(\xi - c) + \delta(\xi + c)]\ \hat{\psi}^*(a\xi) e^{i2\pi b\xi} d\xi = \frac{A}{2} \hat{\psi}^*(a\ c) e^{i2\pi b\ c} \tag{3.7}$$

the information from the time-scale plane is mapped to the time-frequency plane according to the map $(b,a) \rightarrow (b, s(a,b))$, in an operation termed synchrosqueezing.

From (3.7), we see that if $\psi(\xi)$ is concentrated around $\xi = 1$, then $W(a,b)$ will be concentrated around the horizontal line $ac = 1$. This will cause the problem that we can't separate the IFs from their CWTs if they are close.

However, using (3.3) and (3.7), it can be seen that though the wavelet transform is spread out in a, its oscillatory behavior in b points to the original frequency c, regardless of a .

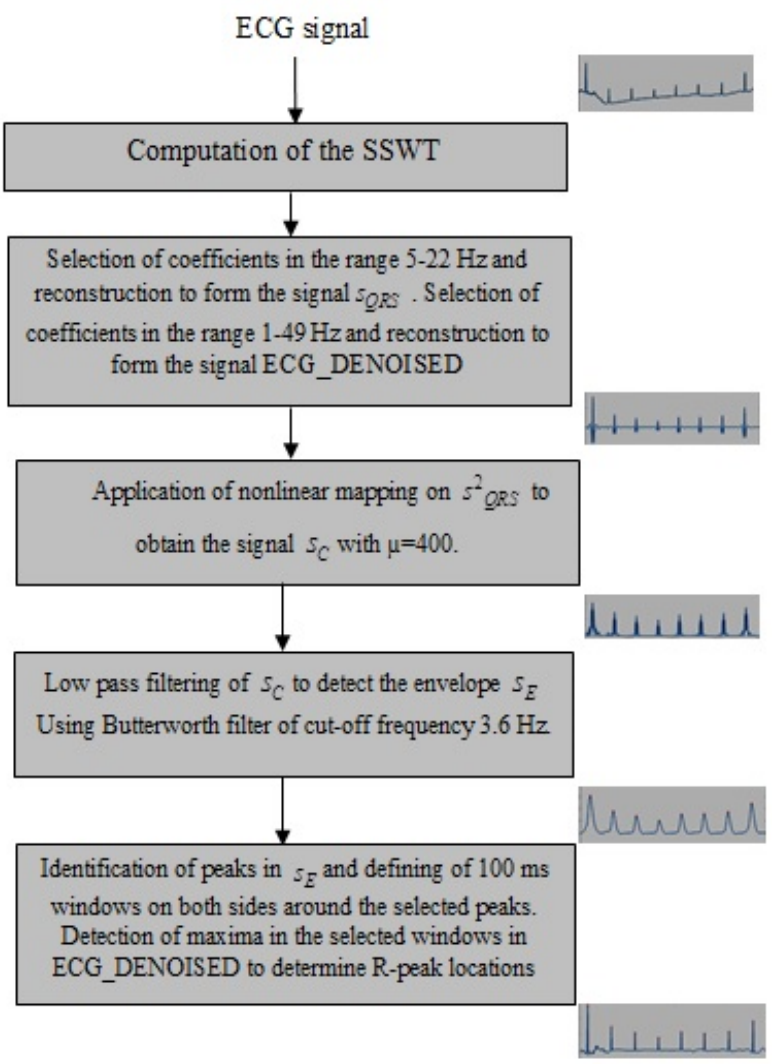

FIGURE 3.1: Schematic representation of the overall technique

3.3 Methods

A schematic representation of the proposed method is shown in Figure 3.1. The various processing steps used are described below.

Step-1: In the first step, the SSWT of the signal is obtained. The digitized ECG signal $\tilde{s}(m),\ m = 0, ..., M-1$, is a uniform discretization of the continuous time ECG signal $s(t)$ sampled at the time instants $t_m = t_0 + m\Delta t$. To prevent boundary effects, $\tilde{s}(m)$ is symmetrically padded on both sides, by using reflecting boundary conditions and converted in the form of a vector $\tilde{s}_p \in \mathbb{R}^n,\ \ n = 2^{L+1}$, where L is a nonnegative integer [90]. The maximum measurable frequency (Nyquist frequency) of the signal $\tilde{s}_n$ is given by $f_M = 1/2\Delta t$, where, Δt is the sampling interval and the minimum measurable frequency (fundamental frequency) is given by $f_m = 1/T$, where, $T = (M-1)\Delta t$ is the signal

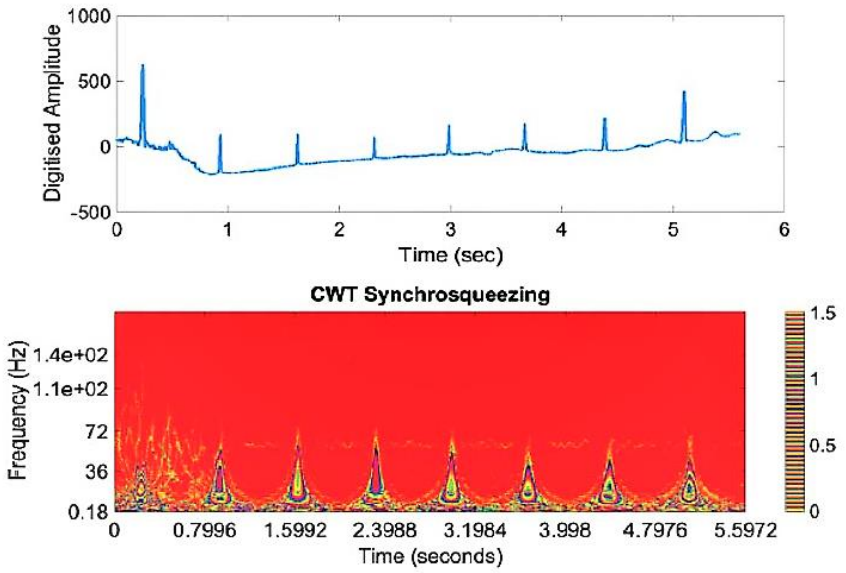

FIGURE 3.2: ECG signal and the corresponding SSWT (top) ECG signal (bottom) corresponding SSWT

duration. The SSWT of the signal $\tilde{s}_p$ is obtained over linearly spaced frequencies ranging from f_m to f_M. The total number of frequencies considered is $n_f = Ln_v$, where, n_v is a user defined parameter, known as the voice number [90].

A hard-threshold parameter $\gamma > 0$ is chosen which effectively decides the lowest CWT magnitude at which the instantaneous frequency can be reliably computed. Any points where $|W(a,b)| \leq \gamma$ are disregarded in SSWT computation [90]. Thus, γ can be seen as a hard threshold on the wavelet representation, whose value determines the level of filtering. In [90], Thakur et al have suggested the use of the threshold

$$\gamma = 1.4826\sqrt{2\log n} \cdot \text{MAD}\ (|\tilde{W}_{\tilde{f}}|_{1\,:\,n_v}), \tag{3.8}$$

where MAD denotes median absolute deviation of $|\tilde{W}_{\tilde{f}}|_{1\,:\,n_v}$ which are the wavelet coefficients at the n_v finest scales and 1.4826 is a multiplicative constant that relates the Gaussian distribution to its standard deviation.

In this work, we have used only the aforementioned thresholding operation in SSWT computation, which aids in filtering Gaussian noise. However, it is worth mentioning that some techniques have been proposed in the literature that can be used to obtain a better TFR with a sharp localization of components and reduced noise fluctuations. For example, in [102], multitapering is applied to reassigned spectrograms, which leads to coherent averaging of the chirp components and incoherent averaging in the noise regions, thereby leading to smoothing of the noise fluctuations. In [103], synchrosqueezing a highly redundant time-frequency transform with over-complete samples in a and different mother wave packets have been suggested. This generates many estimates from

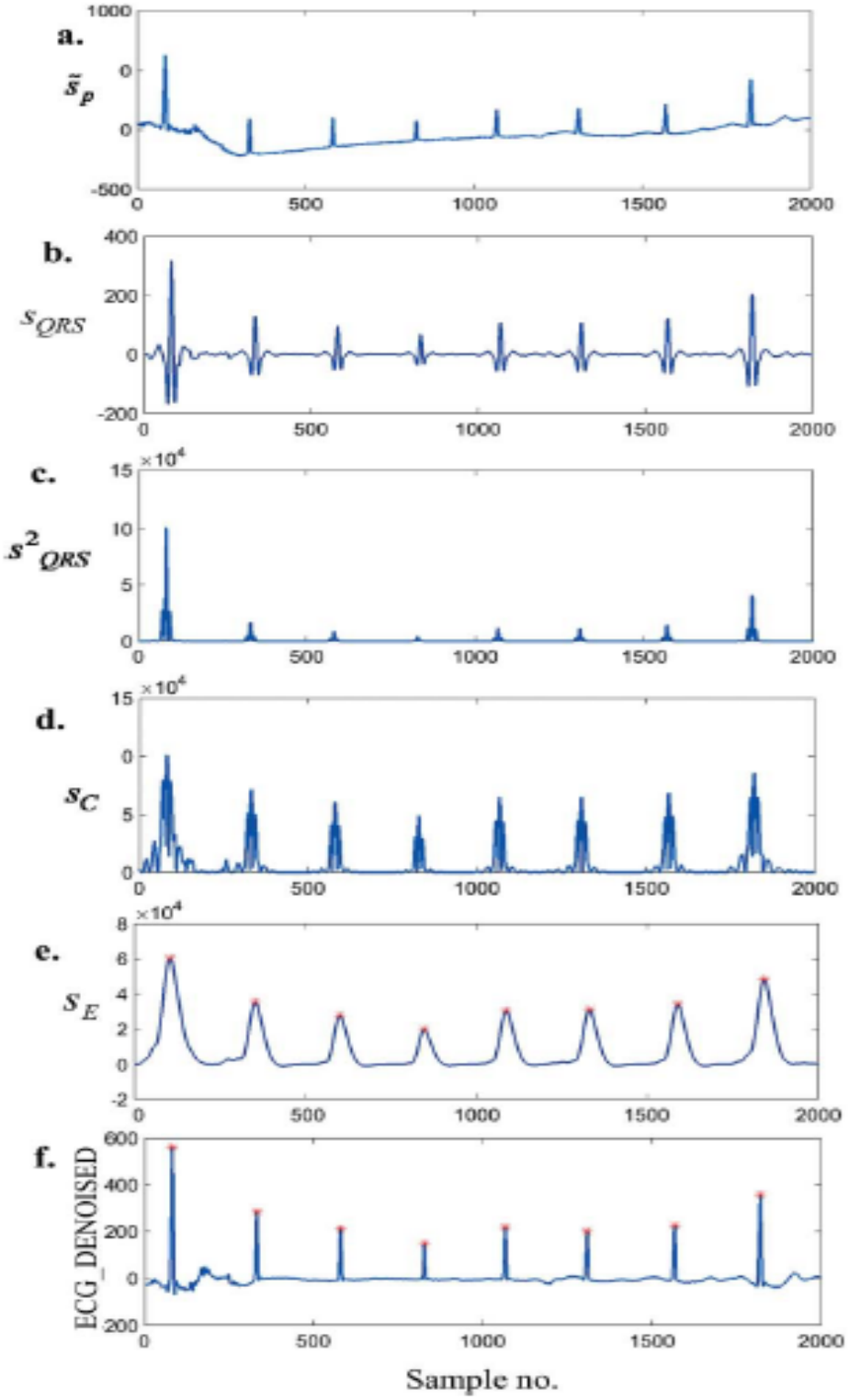

FIGURE 3.3: Signals obtained at various stages of processing for R-peak detection.

a single realization of noisy signal. Since the estimation of the instantaneous frequency is independent of a and the mother wavelet/wave packet, therefore, these estimates can be averaged to give a better result because of coherent averaging for signal components and incoherent averaging for noise. The use of different mother wave packets is essentially the

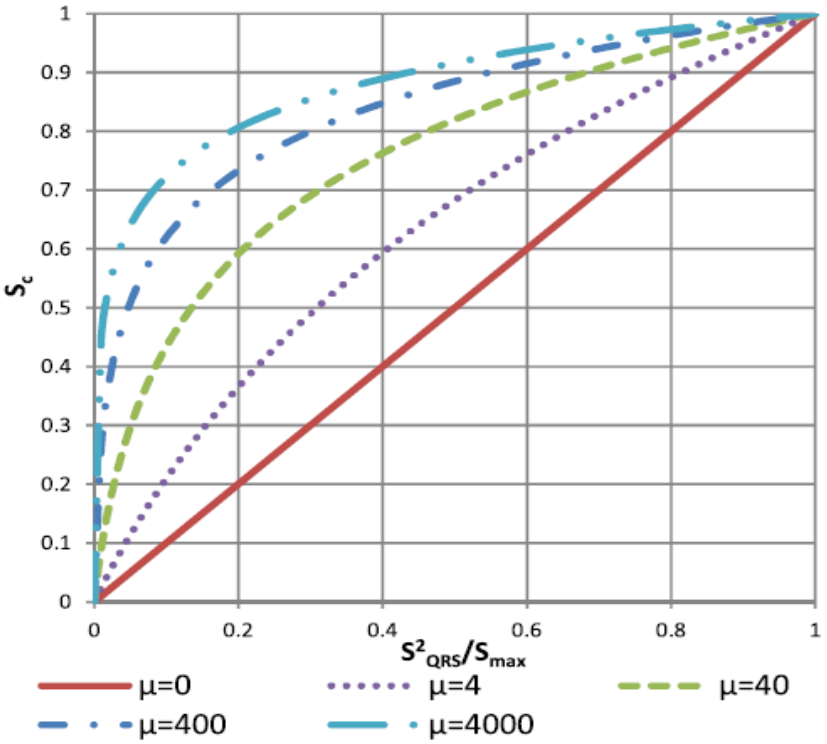

FIGURE 3.4: Logarithmic compression curves for different values of μ.

same as multitapering [103]. An ECG signal and its TFR obtained using the SSWT are shown in Figure 3.2, for illustration. It can be seen that the individual QRS complexes are well localized in time in the SSWT.

Step-2: The energy of the QRS complex is found to be concentrated in the frequency range 5-22 Hz [27]. Hence, SSWT coefficients corresponding to this frequency range are reconstructed by taking inverse SSWT, to obtain the signal s_{QRS}. It is worth mentioning that recently, some reconstruction issues with SSWT have been highlighted [104] , when component retrieval from ridge in the TFR is required. In fact, the recently proposed synchrosqueezed wave packet transform (SSWPT) [105] has been shown to have a higher resolution and much superior component identification ability as compared to the SSWT. However, in the present case, the specific frequency range is directly reconstructed, as the individual QRS complexes are well localized in time in this range, i.e. no ridge retrieval is used. Hence, no reconstruction issue arises in the present case. It may be noted that the selection of this frequency band automatically excludes baseline wander, which lies at frequencies below 1 Hz and the high frequency noise. Also, low frequency P- and T-waves, which could have amplitudes larger than the QRS complex are suppressed. Another signal, $ECG\_DENOISED$ is also obtained, by reconstruction using coefficients in the frequency range 1-49 Hz. Figure 3.3 shows an ECG signal and the signal s_{QRS} obtained from it. The signal $ECG\_DENOISED$ is also shown in the bottom.

Step-3: As a result of the filtering operation in the previous step using the SSWT, the P- and T-waves and the noise peaks are greatly suppressed. However, there are still very low amplitude contributions from these peaks which need to be further suppressed in order to avoid false detections. For this purpose, the signal s_{QRS} is further processed in a series of steps. First, the signal s_{QRS} is squared and then a nonlinear mapping is applied to ${s^2}_{QRS}$, as follows:

$$s_C = s_{\max} \frac{\ln[1 + \mu({s^2}_{QRS}/s_{\max})]}{\ln(1+\mu)}, \tag{3.9}$$

where, $s_{\max}$ is the maximum value of ${s^2}_{QRS}$ and μ is a positive constant. It may be noted that (3.9) may be seen as the well-known μ-law logarithmic compression used in pulse code modulation (PCM) systems, applied to the square of the signal s_{QRS}. To the best of our knowledge, it has not been used in the context of QRS detection earlier. The squaring operation makes all data points positive, further suppresses the undesired low amplitude peaks and further boosts the higher amplitude QRS complex peaks, as is evident from Fig. 3.3(c). However, as an undesirable effect, this also further attenuates the low amplitude QRS complexes. Therefore, to compensate for squaring operation, logarithmic compression is applied, which basically boosts the low and medium intensity QRS complexes, to bring their amplitudes closer to the highest amplitude complexes. Thus, the range of variations of the input is compressed. This is illustrated in Figure 3.3(d), where it can be seen that the QRS amplitudes have been equalized. How logarithmic compression achieves this equalization can be understood with the help of the curves in Figure 3.4, in which the logarithmically compressed output s_C is plotted against the normalized input ${s^2}_{QRS}/s_{\max}$ for various values of compression factor μ. For reference, the case of no compression ($\mu = 0$) is also shown. It is seen that as μ is increased, the low and mid-range intensities are boosted more and more. In the present work, $\mu = 400$ is empirically found to be an appropriate value. The reason why this equalization is required is as follows. The threshold used in this work for QRS detection is fixed and dependent on the maximum (peak) value of the signal under consideration. As such, if a very large amplitude QRS complex occurs along with a very small QRS complex in the signal duration under consideration, false negatives may occur as a result of failed detection of the small QRS complexes. Logarithmic compression boosts the low and mid-range amplitude QRS complexes, thereby reducing the false negatives.

Step-4: After application of nonlinear mapping, the envelope s_E of the signal s_C is extracted using a low pass filter, as shown in Figure 3.3. In this work, a second order Butterworth filter with cut-off frequency 3.6 Hz has been used.

Step-5: In the final step, the peaks are detected in the envelope signal. For the purpose of peak detection, three detection parameters: threshold, minimum peak separation and

minimum peak prominence are used. The threshold is empirically determined and set to 27% of the maximum value of the envelope signal. The minimum peak separation is set as 200ms. This is chosen because of the physiologically determined refractory period of 200ms between two consecutive QRS complexes [21]. Another parameter, peak prominence is also used that measures how much the peak stands out due to its intrinsic height and its location relative to other peaks. The minimum peak prominence is set to 33% of the peak value of the envelope signal. The use of this parameter is found to significantly reduce the number of false positives. It has been explained in more detail in Section 4.2.5 of the next chapter. Finally, in each beat, windows of 100 ms are defined around the detected peaks on both sides. The maxima occurring in these windows in the signal $ECG\_DENOISED$ are determined as R-peaks, as shown in Figure 3.3. It may be noted that the peaks are detected in the signal $ECG\_DENOISED$ instead of the initial ECG signal, because the initial ECG can contain baseline wander and power line interference, which could lead to erroneous detection of peaks if the spurious peaks crated by these lie in the 100 ms windows defined around the R-peak locations in envelope. The example ECG used in Figure 3.3 does not have high baseline wander, muscular noise or other artefacts. The performance of the proposed method when these interferences are present is shown in the next section.

3.4 Results and discussion

The proposed technique is evaluated on the MIT-BIH arrhythmia database [106]. In this database, 48 annotated recordings of 30 minutes duration from two channels are available for every record. The recordings are digitized at 360 samples per second. The first channel corresponding to the modified limb lead II is used in this work. For SSWT computation, the MATLAB Synchrosqueezing Toolbox [107] by Thakur *et al* [90] has been used. The SSWT has been computed using the bump wavelet over dyadic frequencies, with 64 log-spaced bins per octave, i.e. $n_v = 64$.The algorithm is applied on the ECG signal taking 3-second segment at a time, so that an outlier high amplitude peak in any segment does not affect threshold value for the entire signal. In this sense, the threshold can be considered to be locally adaptive. To evaluate the efficacy of the proposed technique, three parameters: sensitivity (Se), positive predictivity (P^+) and error rate (DER) are used, which are defined as follows:

$$Se = \frac{TP}{TP + FN} \times 100\% \tag{3.10}$$

$$P^+ = \frac{TP}{TP + FP} \times 100\% \tag{3.11}$$

$$DER = \frac{FP + FN}{TB} \times 100\%, \tag{3.12}$$

where, TP denotes the number of true positives, i.e., correctly detected R-peaks, FN denotes the number of false negatives, i.e., failure to detect an R-peak, FP denotes the number of false positives, i.e. a falsely detected R-peak and TB denotes the actual total number of beats. The experimental results are shown in Table-3.1. Overall sensitivity, specificity and error rate values of 99.92%, 99.93% and 0.15%, respectively, are obtained. To demonstrate the QRS detection ability of the proposed algorithm on ECG signals containing different wave morphologies and different kinds of noise, its performance on some selected ECG segments from different records is illustrated. Fig. 3.5 shows the performance of the algorithm on a segment from record 104 containing muscular noise. The detected peaks are marked with asterisk. As can be seen, all peaks are successfully detected with no false positives due to noise peaks. Fig. 3.6 shows another ECG segment containing large baseline wander. Again, the R-peaks are successfully detected. The frequency content of QRS complexes can vary because of different morphologies. Fig. 3.7 shows the performance of the algorithm on ECG signals with different wave morphologies taken from records 208, 222 and 109 of the MIT BIH database, respectively. Record 208 contains premature ventricular contraction (PVC) beats which have wider than normal QRS complexes with abnormal morphology. Record 222 consists of unusual wave morphologies and record 109 corresponds to left bundle branch block. The proposed algorithm detects R-peaks in all these beat types successfully.

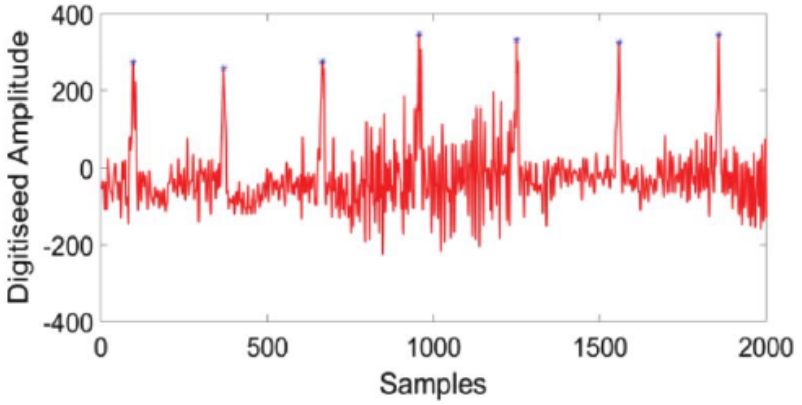

FIGURE 3.5: R-peak detection in a segment from record 104 containing muscular noise.

The performance of the proposed method is also compared with some established and state-of-the-art QRS detection algorithms proposed in the literature in Table-3.2. It can be seen that the proposed method significantly outperforms the referenced methods. It can be seen that the proposed method gives better results than the discrete wavelet transform (DWT), CWT and S-transform based methods. However, the improved performance of the proposed method cannot be attributed to the use of the SSWT alone.

TABLE 3.1: Experimental results of QRS detection on MIT-BIH database

Record	**Total Beats**	**TP**	**FP**	**FN**	**Se**(%)	**P**+ (%)	**Er** (%)
100	2273	2273	0	0	100	100	0.00
101	1865	1863	3	2	99.89	99.84	0.27
102	2187	2187	0	0	100	100	0.00
103	2084	2084	0	0	100	100	0.00
104	2229	2228	5	1	99.96	99.78	0.27
105	2572	2567	5	10	99.61	99.81	0.58
106	2027	2026	2	1	99.95	99.9	0.15
107	2137	2137	0	0	100	100	0.00
108	1763	1742	13	21	98.81	99.26	1.93
109	2532	2532	0	0	100	100	0.00
111	2124	2124	0	0	100	100	0.00
112	2539	2539	0	0	100	100	0.00
113	1795	1795	0	0	100	100	0.00
114	1879	1878	1	1	99.95	99.95	0.11
115	1953	1953	1	1	99.95	99.95	0.10
116	2412	2401	7	13	99.46	99.71	0.83
117	1535	1535	0	0	100	100	0.00
118	2278	2278	0	0	100	100	0.00
119	1987	1987	0	0	100	100	0.00
121	1863	1862	0	1	99.95	100	0.05
122	2476	2476	0	0	100	100	0.00
123	1518	1518	0	0	100	100	0.00
124	1619	1619	0	0	100	100	0.00
200	2601	2601	3	0	100	99.88	0.12
201	1963	1962	0	1	99.95	100	0.05
202	2136	2135	0	3	99.86	100	0.14
203	2980	2973	12	7	99.77	99.6	0.64
205	2656	2656	0	0	100	100	0.00
207	1860	1860	0	0	100	100	0.00
208	2955	2948	3	7	99.76	99.9	0.34
209	3005	3005	0	0	100	100	0.00
210	2650	2649	2	1	99.96	99.92	0.11
212	2748	2748	3	4	99.85	99.89	0.25
213	3251	3251	0	0	100	100	0.00
214	2262	2262	0	0	100	100	0.00
215	3363	3362	0	1	99.97	100	0.03
217	2208	2207	1	1	99.95	99.95	0.09
219	2154	2154	1	1	99.95	99.95	0.09
220	2048	2048	0	0	100	100	0.00
221	2427	2427	0	0	100	100	0.00
222	2483	2483	0	0	100	100	0.00
223	2605	2605	1	0	100	99.96	0.04
228	2053	2051	4	5	99.76	99.81	0.44
230	2256	2256	0	0	100	100	0.00
231	1571	1571	0	0	100	100	0.00
232	1780	1780	10	0	100	99.44	0.56
233	3079	3077	0	2	99.94	100	0.06
234	2753	2753	0	0	100	100	0.00
Ov-erall	109494	109428	77	84	99.92	99.93	0.15

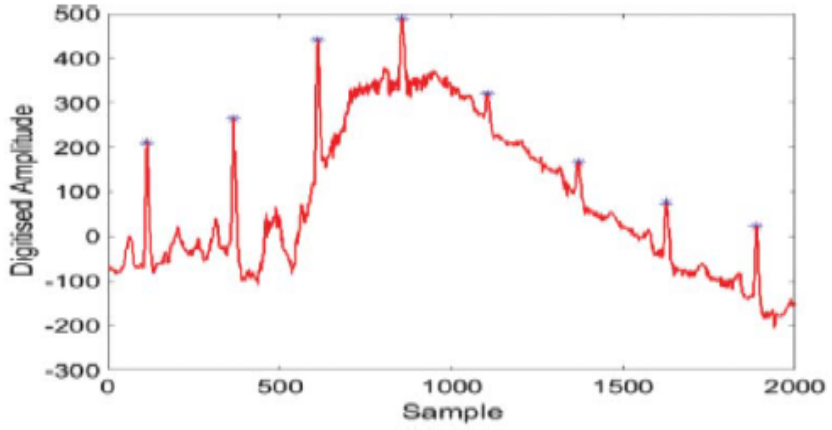

FIGURE 3.6: R-peak detection in a segment from record 121 containing large baseline wander.

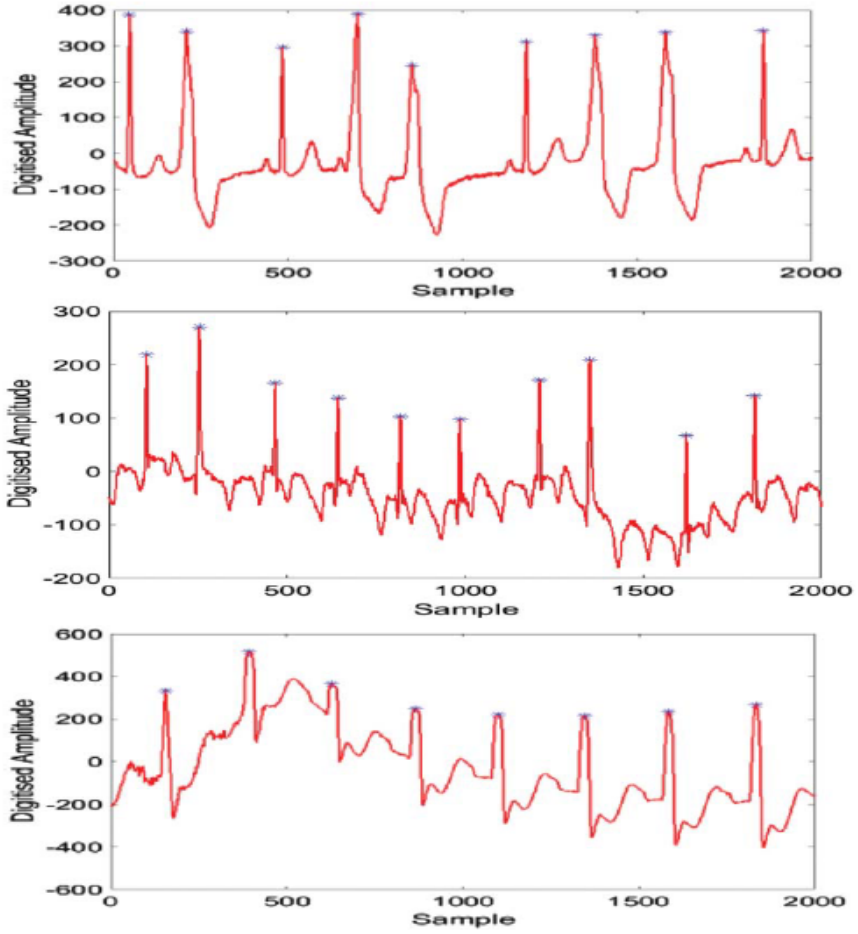

FIGURE 3.7: R-peak detection in ECG signals with different wave morphologies from records 208 (top) 222 (middle) and 109 (bottom).

The nonlinear transformation stage and the improved decision logic that uses three criteria, viz. threshold, minimum peak separation and minimum peak prominence also play

TABLE 3.2: Comparison of performance of the proposed method with other methods on the MIT-BIH arrhythmia database

Reference	**Method**	**FN**	**FP**	**Se** (%)	**P+** (%)	**DER** (%)
Pan and Tompkins (1985) [10]	First derivative followed by squaring	277	507	99.54	99.75	0.712
Zidelmal et al (2014) [19]	S- transform and Shannon energy	171	97	99.84	99.91	0.25
Martinez et al (2004) [15]	Discrete Wavelet transform	220	153	99.8	99.86	0.34
Bouaziz et al (2014) [17]	Discrete Wavelet transform	140	232	99.87	99.79	0.34
Yochum et al (2016) [34]	Continuous Wavelet transform	160	574	99.85	99.48	0.67
Phukpattaranont (2015) [18]	Quadratic filtering	202	210	99.82	99.81	0.38
Proposed method	SSWT and nonlinear transformation	84	77	99.92	99.93	0.15

a very important role.

3.5 Conclusion

In this chapter, a novel technique for QRS detection in ECG signals is proposed. The detection algorithm uses the recently proposed SSWT to obtain a TFR of the ECG signal. The coefficients in the frequency range corresponding to the QRS complex are selected and reconstructed to form a signal on which further processing including a nonlinear mapping is applied to reduce false positives and negatives. The peaks are detected in the envelope of the signal thus obtained and mapped to corresponding peaks in the denoised signal. The algorithm is shown to successfully detect QRS complexes in various noise conditions and in cases of varying QRS morphologies. The algorithm is evaluated on the MIT-BIH arrhythmia database and overall sensitivity, positive predictivity and percentage error values of 99.92%, 99.93% and 0.15%, respectively, are obtained.

Chapter 4

A New Method for QRS Detection in ECG Signals using QRS-Preserving Filtering Techniques

4.1 Overview

As mentioned earlier, most of the QRS energy lies in the frequency range [5 22] Hz, for both normal and abnormal signals [27]. Though the selection of this frequency range by means of a bandpass filter eliminates the out-of-band noise, the noise still remaining in the selected frequency band can cause false positive detections. Muscular noise is a major contributing factor to this noise. Because of spectral overlap with the QRS complexes, it is very challenging to eliminate this noise without affecting the R-peaks. Similar problem is faced in image enhancement, where edge-preserving filtering techniques are required for smoothing out the noise without blurring the edges in the image. In [66], Farbman et al proposed an edge-preserving smoothing approach based on the weighted least squares (WLS) optimisation framework. This approach aims at smoothing the image everywhere, except where significant gradients (edges) are present. The QRS complexes in an ECG signal are also characterized by a high slope. Therefore, by applying WLS-based smoothing on the ECG signal, it can be smoothed without loss of QRS complexes. In the method proposed in this chapter, we use WLS-based smoothing in combination with Savitzky-Golay filtering, which is another least-squares polynomial-fitting based smoothing technique that can preserve the high frequency content of the signal. These two techniques can be used to obtain a much cleaner ECG signal in which

noise peaks are reduced to very low amplitudes. To the signal thus obtained, a novel nonlinear transformation technique is applied that equalizes the QRS amplitudes without boosting the low amplitude noise peaks. This helps in obtaining a smooth envelope after low pass filtering, in which the R-peaks can be detected with a constant fixed threshold and prominence value, independent of any signal attributes. The proposed algorithm has low computational load and can be applied for fast offline QRS detection in a long duration Holter recording, for example, or in a real- time scenario.

The remainder of this chapter is organized as follows. The step-by-step procedure and design considerations are discussed in section 4.2. In section 4.3, we give the implementation details and the results obtained using the proposed method and also illustrate its performance on some of the most critical cases in the database. Also, the performance of the proposed method is compared with existing methods. Finally, the chapter is concluded in section 4.4.

4.2 The proposed method

The proposed R-peak detection method is depicted in the block diagram in Fig. 4.1. The first stage is preprocessing that aims at suppressing noise and accentuating the QRS complexes. It consists of the operations of bandpass filtering, Savitzky-Golay filtering, first-order backward differencing, weighted least squares optimization based filtering, amplitude normalization and logarithmic compression, followed by two stages of moving average filters. The aim of the preprocessing stage is to suppress noise and equalize the QRS amplitudes to obtain a smooth envelope, from which the R-peaks can be detected. Before the filtering operations, symmetric reflective padding is done on both ends of the signal to exclude the edge effects. The padding is discarded after filtering. The second stage is peak detection. In this stage, peaks are detected in the envelope obtained from the previous stage, which are used as guides to latch on to the actual R-peak locations in the original ECG signal in the final step. Each operation in both stages is discussed in more detail in the following subsections.

4.2.1 Bandpass filtering

The ECG signal $x(n)$ is first bandpass filtered to select most of the QRS energy, eliminate out-of-band noise such as baseline wander and power line interference and to suppress muscular noise and the interference from P- and T-waves to some extent. For this purpose, we design an FIR bandpass filter of passband [6 22] Hz and a linear phase response, in order to avoid phase distortion to the filtered signal. As for the filter design

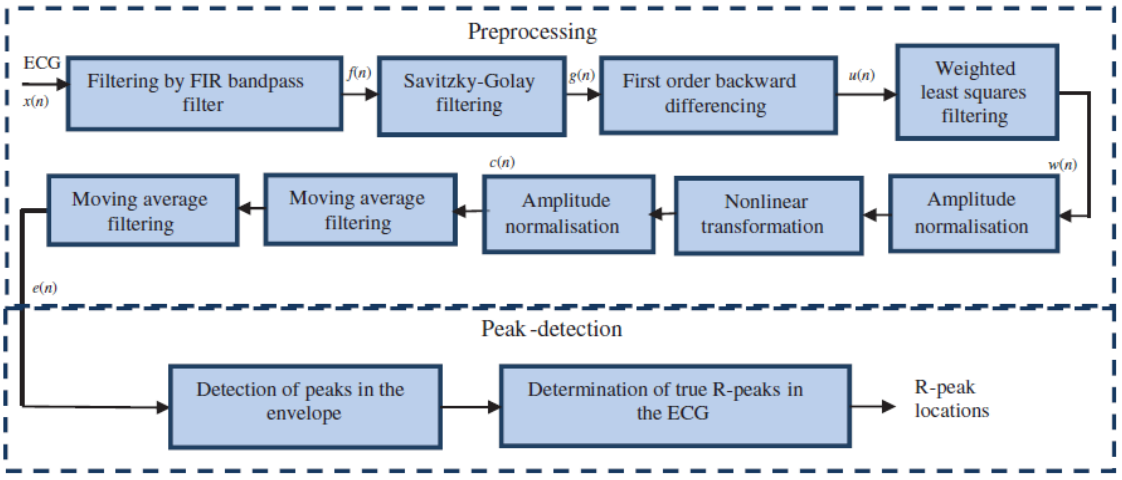

FIGURE 4.1: Block Diagram of the proposed method

method, window design is a simple technique for FIR filters, but it is not optimal and designs a filter with higher order as compared to equiripple and least squares designs. We choose least squares design here, because it gives greater overall stop-band attenuation.

4.2.2 Savitzky-Golay filtering and first order backward differencing

There is still significant noise in the bandpass filtered ECG signal $f(n)$ that spectrally overlaps with the QRS complexes and therefore is difficult to separate. In order to suppress this noise without smoothing out the R-peaks, the signal $f(n)$ is filtered using a Savitzky-Golay FIR smoothing filter [108]. This filter is particularly aimed at suppressing the muscular noise, which can cause a large number of false positive detections. Savitzky-Golay filters, which are also known as polynomial smoothing filters, are generalizations of the FIR moving average filter that preserve the high frequency content of the signal better than the latter, at the cost of not removing as much noise [109]. In this filtering technique, for each data point f_i, a polynomial of order m is least-square fitted to the neighbouring L points lying in a window. The data point f_i is replaced by the value of the polynomial at that point. Savitzky and Golay showed [108] that a set of pre-derived integers can be used as weighting coefficients for filtering, as it is equivalent to fitting a polynomial. This makes the filtering very simple and computationally efficient. As a rough guideline, for best results, the width L of the window must be between 1 to 2 times the FWHM of the desired feature in the signal [109]. In this case, the desired feature is the QRS complex, which has an average duration of 77 ms [110], though its duration can vary among different subjects and pathological conditions. For our sampling rate of 360 samples/s, $L = 23$ (64 ms) and $m = 3$ were found to be appropriate values.

Next, the derivative of the resultant filtered signal $g(n)$ is computed by first order backward differencing as

$$u(n) = g(n) - g(n-1). \tag{4.1}$$

This operation further suppresses the lower frequency P- and T-waves and accentuates the QRS complexes because of their higher slope.

4.2.3 Weighted Least Squares Smoothing

Even after the preceding filtering stages, there is still significant noise remaining in the signal which needs to be removed in order to obtain a smooth envelope containing only the R-peaks. The target is to obtain a signal that is as close as possible to the original signal and smooth everywhere except at QRS complex locations, which are characterised by a high slope. Weighted least squares smoothing [66] is a technique that helps in achieving these possibly contradictory goals. For a one-dimensional signal, the problem can be formulated as seeking the signal $w(t)$ which is as close as possible to the input signal $u(t)$ and as smooth as possible everywhere except for places where the gradient in $u(t)$ is significant. Mathematically, this can be expressed as seeking

$$\arg\min_{w} J(w) = (w(t) - u(t))^2 dt + \lambda \int a_t(u) w'(t)^2 dt, \tag{4.2}$$

where $\lambda > 0$ is a trade-off parameter between the first term which is the data fidelity term and the second term which is the weighted regularization term; greater value of λ leads to greater smoothness. $w'(t)$ denotes the derivative of $w(t)$ and $a_t(u)$ denotes the smoothness weight that depends on $u(t)$ given by [66]

$$a_t(u) = \left(\left| \frac{du(t)}{dt} \right|^{\alpha} + \varepsilon \right)^{-1}, \tag{4.3}$$

where α determines the sensitivity to the gradients of $u(t)$ and ε is a small constant (taken as 0.0001 here). In discrete form, (4.3) can be expressed in vector-matrix notation as

$$\arg\min_{\mathbf{w}} J(\mathbf{w}) = \|\mathbf{w} - \mathbf{u}\|^2 + \lambda \left\| \mathbf{A}^{\frac{1}{2}} \mathbf{D} \mathbf{w} \right\|^2, \tag{4.4}$$

where $\mathbf{w}$ and $\mathbf{u}$ are both M-dimensional vectors, if M is the length of the signal. $\mathbf{A}$ is an $(M-1) \times (M-1)$ weight matrix and $\mathbf{D}$ is an $(M-1) \times M$ dimensional matrix. In discrete form, (4.3) can be expressed in vector-matrix notation as

$$\arg\min_{\mathbf{w}} J(\mathbf{w}) = (\mathbf{w} - \mathbf{u})^T (\mathbf{w} - \mathbf{u}) + \lambda (\mathbf{w}^T \mathbf{D}^T \mathbf{A} \mathbf{D} \mathbf{w}), \tag{4.5}$$

where **u** and **w** are vectors representing discrete signals, **A** is a diagonal matrix containing the smoothness weights, **D** is the difference operator of the form

$$\mathbf{D} = \begin{bmatrix} -1 & 1 & 0 & \cdots & 0 \\ 0 & -1 & 1 & \cdots & 0 \\ \vdots & \ddots & \ddots & \ddots & \vdots \\ 0 & 0 & \cdots & -1 & 1 \end{bmatrix}. \tag{4.6}$$

The vector **w** that minimizes 4.4 is given by the solution of the linear system

$$(\mathbf{I} + \lambda\mathbf{L})\mathbf{w} = \mathbf{u}, \tag{4.7}$$

where $\mathbf{L} = \mathbf{D^T A D}$. It may be noted that $(\mathbf{I} + \lambda\mathbf{L})$ is a very sparse, tridiagonal matrix and therefore, fast solution to (4.7) is obtained using a tridiagonal solver. Thus, using this weighted least-squares optimization based smoothing technique a smooth signal **w** can be obtained from the input signal **u** obtained in the previous step, while preserving the QRS complexes, which have significant gradient.

4.2.4 Amplitude normalization, nonlinear transformation and envelope extraction

After WLS smoothing, the signal **w** is amplitude normalized as

$$w(n) \ := \frac{w(n)}{\max\limits_{n}\left(|w(n)|\right)}. \tag{4.8}$$

Following normalization, a nonlinear transformation is applied to the square of the signal $w(n)$ as

$$c(n) = \ln\left(1 + \frac{Kw^2(n)}{m_{w^2}}\right), \ n{=}1 \ ... \ N, \tag{4.9}$$

where K is a constant and N denotes the length of the signal **w**.

$$m_{w^2} = \tfrac{1}{N}\sum_{n=1}^{N} w^2(n) \tag{4.10}$$

denotes the mean value of the squared signal. The nonlinear transformation in (4.9) involves squaring and logarithmic transformations. The squaring operation further reduces the amplitude of the noise peaks that have been reduced to low values by the preceding filtering operations. On the other hand, the QRS complexes which are larger as compared to noise peaks become even larger, i.e. the difference in the amplitudes of noise peaks

and QRS complexes is accentuated. In (4.9), there is also a logarithmic transformation, whose purpose is to basically compresses the range of input amplitudes by boosting the mid-range intensities, making them comparable to the higher intensities, as illustrated in Fig. 4.2. It may be noted that the lowest amplitudes peaks are mostly due to noise, therefore, the compression scheme should not boost these amplitudes. The compression curves obtained for different values of K in (4.9) are illustrated in Fig. 4.2. It can be seen that too high a value of K can boost the low amplitude noise peaks excessively, whereas too low a value of K gives inadequate enhancement to the mid range. We have found $K = 5$ to be an appropriate value. This value of K boosts the mid-range intensities, which are due to QRS complexes, without enhancing the low amplitude noise. Another advantage of the logarithmic transformation is that by equalizing the QRS amplitudes, it enables use of a single fixed threshold for all ECG signals, independent of any signal attributes. The mean value m_{w^2} has been used for norrmalization in (4.9) instead of the maximum value, because there are often outlying, very high amplitude peaks in the ECG, caused by electrode artefacts and some QRS complexes.

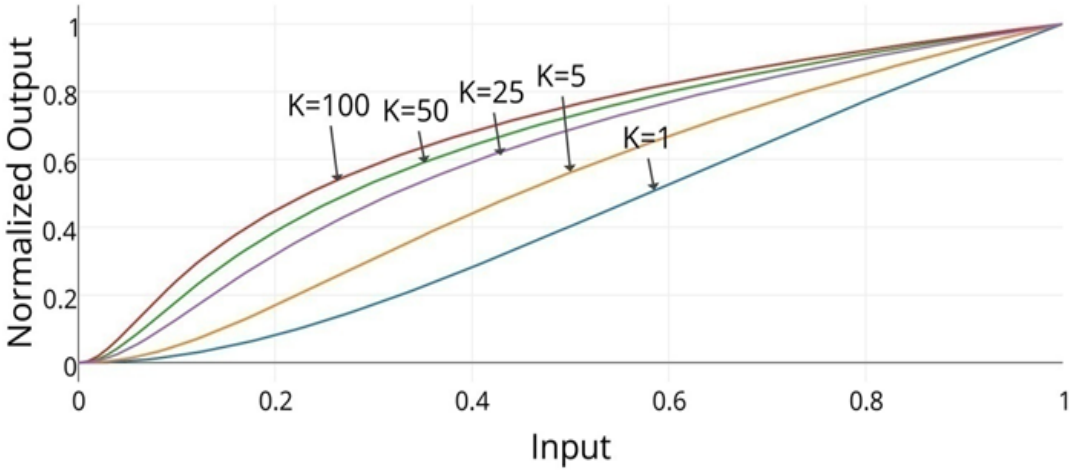

FIGURE 4.2: Nonlinear transformation curves for different values of K

After the nonlinear transformation, the amplitude is again normalized by division with the peak value, as in (8) and then a smooth signal envelope **e** is extracted by low pass filtering **c** using two-cascade moving average filters. For our sampling rate of 360 samples/s the window size for MA filters is chosen as $M = 75$, which is nearly equal to the physiological refractory period of 200 ms between two consecutive QRS complexes.

4.2.5 Peak-finding and decision logic

Finally, peaks that exceed a certain threshold Th and prominence value MPP are detected in the envelope. A peak is said to occur at $e(n)$ if $e(n) > e(n-1)$ and $e(n) > e(n+1)$.

The peak prominence is measured as follows. For a given peak, the range from the peak to the end point or the point at which a higher peak is encountered, whichever is closer to the peak, is considered on both sides. The minimum of the signal in each of the two intervals is found. The higher of the two minima is used as the reference level. The peak prominence is defined as the height of the peak above this level. Thus, peak prominence measures the height of the peak relative to neighbouring peaks. This is illustrated in Fig. 4.3. Fig. 4.3(a) shows an ECG signal and Fig. 4.3(b) shows the corresponding envelope signal**e**, in which the peak prominence values are given by the length of the vertical lines. It can be seen that the reference for peak prominence measurement is different for every peak, depending upon the neighbouring peaks. Thus, by using a certain minimum peak prominence criterion, the false peaks due to noise can be rejected. The peak prominence criterion, as described, has been implemented in the peak detection utility in MATLABR2014b software. The detected peak positions in the envelope signal **e** are used as guides to latch on to the true R-peaks in the ECG signal within ±15 samples (42 ms). For illustration, the outputs of the different stages in the proposed method are shown in Fig. 4.4 for a noisy ECG signal from record 104 of the MIT-BIH arrhythmia database [106].

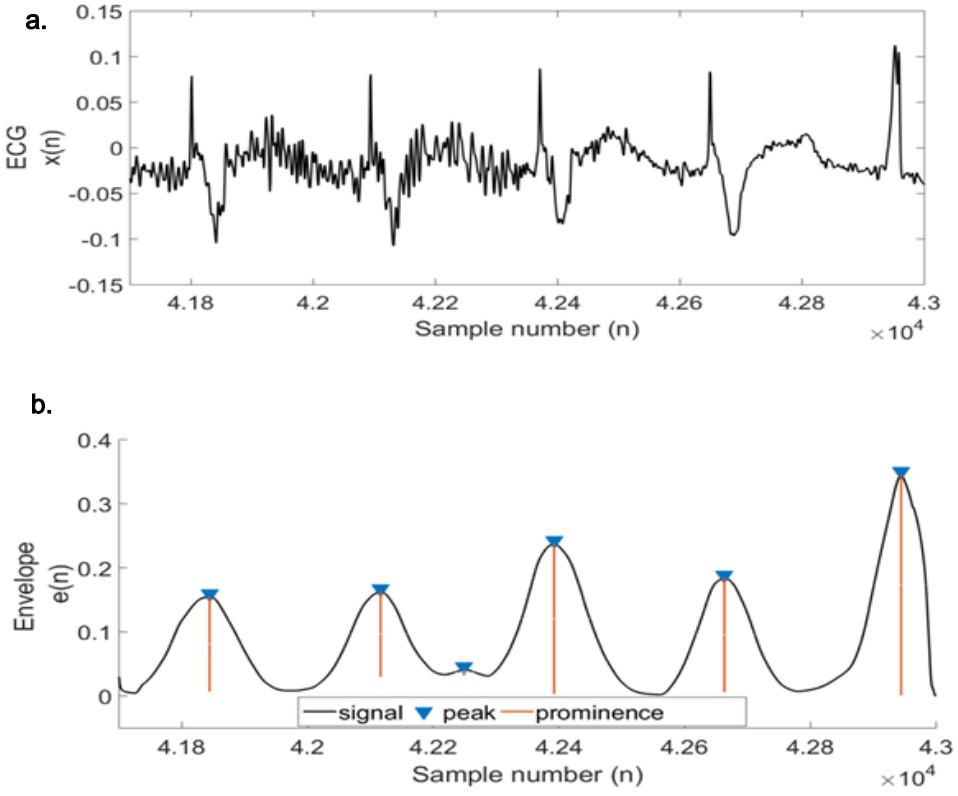

FIGURE 4.3: (a) ECG signal from record 104 of the MIT-BIH database (115.8-119.4 s) (b) Corresponding envelope signal with peak prominence values indicated by vertical lines.

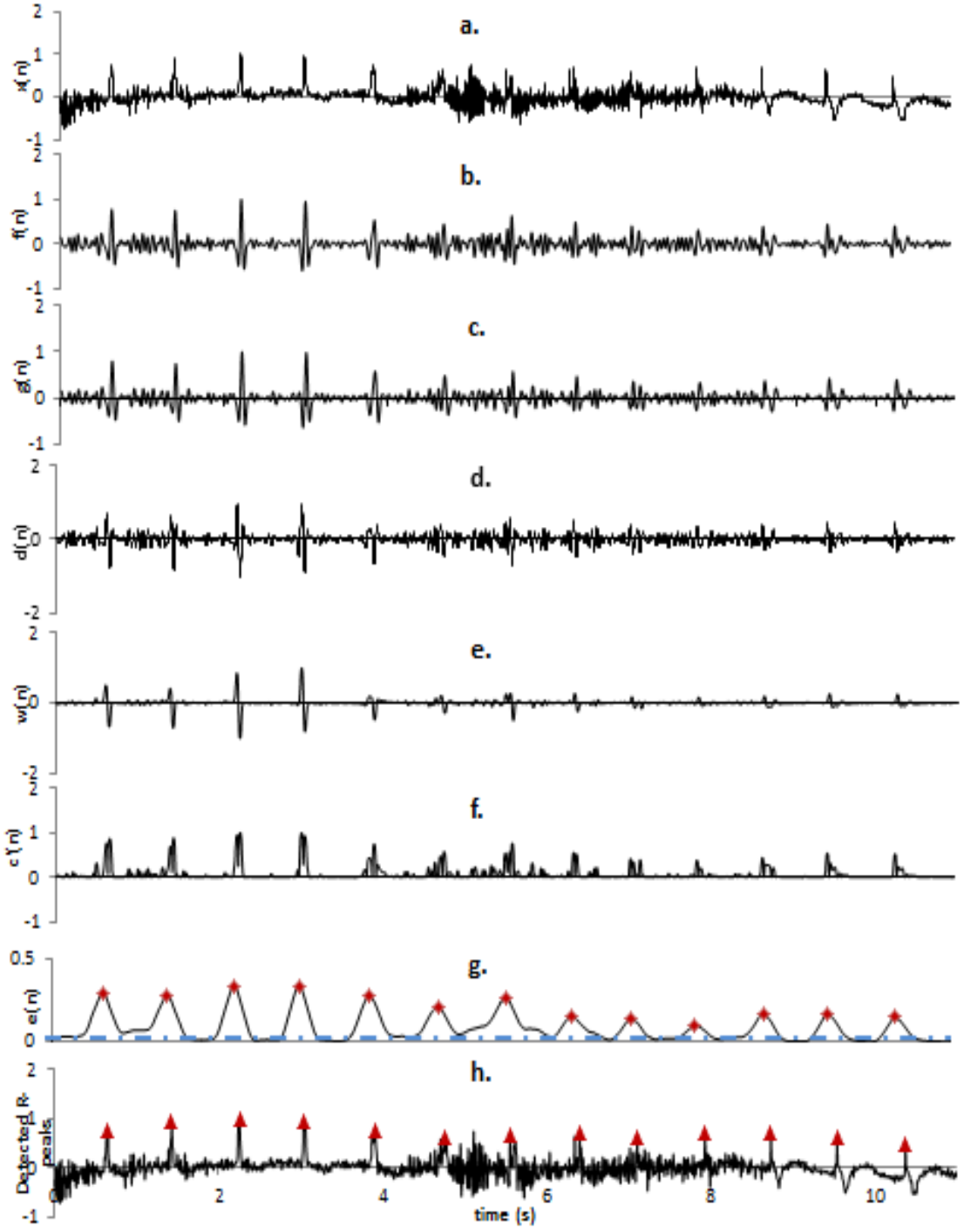

FIGURE 4.4: Signals obtained at various stages in the proposed method: (a) Original ECG signal taken from record 104 (b) the signal obtained by bandpass filtering (c) the signal obtained after SG filtering (d) the signal after first order backward differencing (e) the signal obtained by weighted least-squares filtering (f) the signal obtained after logarithmic transformation (g) the smooth envelope (threshold indicated by dashed line) and (h) the detected R-peaks.

4.3 Implementation, results and discussion

4.3.1 Data

For evaluation of the proposed method, we use the MIT-BIH arrhythmia database [106], which was also used in the previous chapter. This database contains varied QRS, P- and T-wave morphologies belonging to both healthy and arrhythmia categories. The signals in this database contain various kinds of noise that occur in a clinical setting, such as baseline wander, electrode artefacts, power line interference, muscular noise, etc. We choose the MLII recording for evaluation of the proposed method. As mentioned in the previous chapter, the recordings are digitized at 360 samples per second per channel.

4.3.2 Performance evaluation criteria

To evaluate the performance of the proposed technique, three parameters: sensitivity (Se), positive predictivity ($P+$) and detection error rate (DER) are used, which were defined in the previous chapter. The method is evaluated using the WFDB tools available on `www.physionet.org`. The data and the tools used for evaluation conform to the relevant ANSI guidelines [111] given by AAMI [112], as discussed in [69].

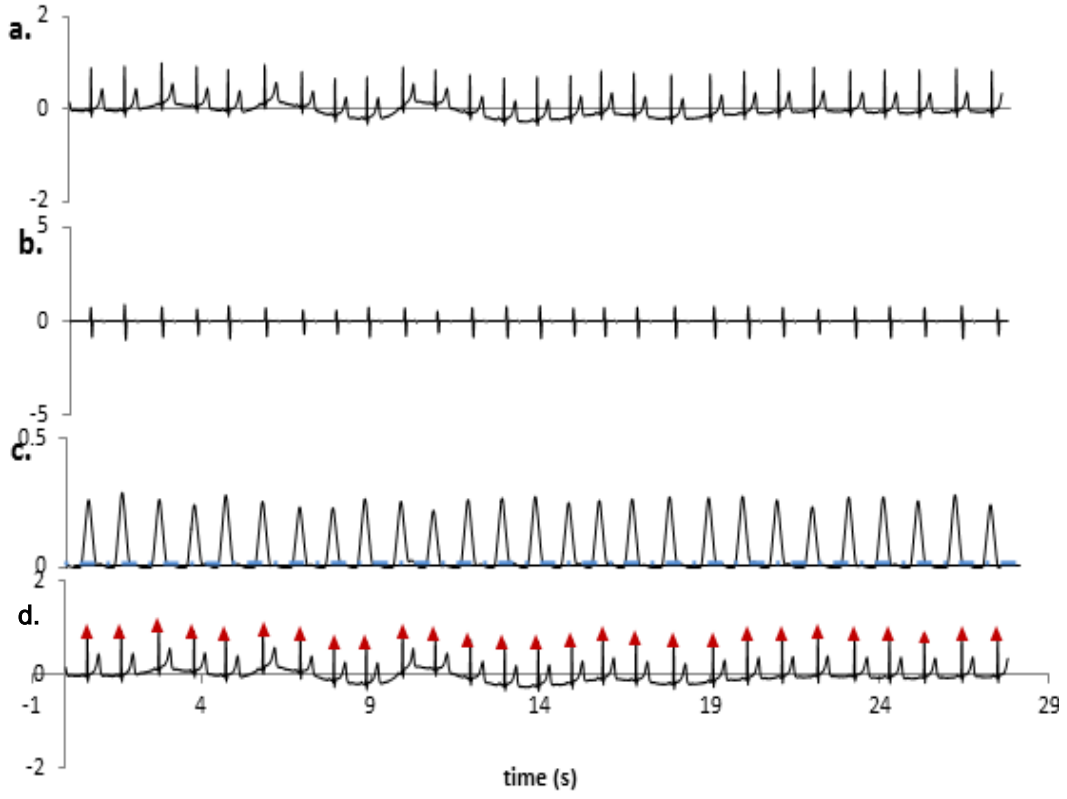

FIGURE 4.5: (a) ECG signal from record 113 (b) Output obtained after weighted least-squares filtering (c) smooth envelope obtained after logarithmic compression and low pass filtering (threshold indicated by dashed line) (d) Detected R-peaks.

TABLE 4.1: Results for R-peak detection using the proposed method evaluated on the MIT-BIH arrhythmia database (Offline implementation).

Record	**Total Beats**	**TP**	**FN**	**FP**	**Se** (%)	**P**$^{+}$ (%)	**DER**(%)
100	2273	2273	0	0	100	100	0.00
101	1865	1864	1	3	99.95	99.84	0.21
102	2187	2187	0	0	100	100	0.00
103	2084	2084	0	0	100	100	0.00
104	2229	2226	3	4	99.87	99.82	0.31
105	2572	2561	11	33	99.57	98.73	1.72
106	2027	2025	2	0	99.9	100	0.10
107	2137	2136	1	1	99.95	99.95	0.09
108	1763	1755	8	8	99.55	99.55	0.91
109	2532	2532	0	0	100	100	0.00
111	2124	2123	1	1	99.95	99.95	0.09
112	2539	2539	0	0	100	100	0.00
113	1795	1795	0	7	100	99.61	0.39
114	1879	1875	4	2	99.79	99.89	0.32
115	1953	1953	0	0	100	100	0.00
116	2412	2392	10	2	99.58	99.92	0.50
117	1535	1535	0	0	100	100	0.00
118	2278	2278	0	1	100	99.96	0.04
119	1987	1987	0	0	100	100	0.00
121	1863	1862	1	1	99.95	99.95	0.11
122	2476	2476	0	0	100	100	0.00
123	1518	1518	0	0	100	100	0.00
124	1619	1619	0	1	100	99.94	0.06
200	2601	2599	2	2	99.92	99.92	0.15
201	1963	1957	6	0	99.69	100	0.31
202	2136	2133	3	0	99.86	100	0.14
203	2980	2945	35	14	98.83	99.53	1.66
205	2656	2651	5	0	99.81	100	0.19
207	1860	1858	2	5	99.89	99.73	0.38
208	2955	2940	15	3	99.49	99.9	0.61
209	3005	3005	0	0	100	100	0.00
210	2650	2646	4	3	99.85	99.89	0.26
212	2748	2748	0	0	100	100	0.00
213	3251	3250	1	0	99.97	100	0.03
214	2262	2258	4	1	99.82	99.96	0.22
215	3363	3362	1	0	99.97	100	0.03
217	2208	2205	3	1	99.86	99.95	0.18
219	2154	2154	0	0	100	100	0.00
220	2048	2048	0	0	100	100	0.00
221	2427	2427	0	0	100	100	0.00
222	2483	2479	4	1	99.84	99.96	0.20
223	2605	2605	0	0	100	100	0.00
228	2053	2052	1	14	99.95	99.32	0.73
230	2256	2256	0	0	100	100	0.00
231	1571	1571	0	0	100	100	0.00
232	1780	1780	0	2	100	99.89	0.11
233	3079	3076	3	1	99.9	99.97	0.13
234	2753	2753	0	0	100	100	0.00
Overall	**109494**	**109353**	**131**	**111**	**99.88**	**99.9**	**0.22**

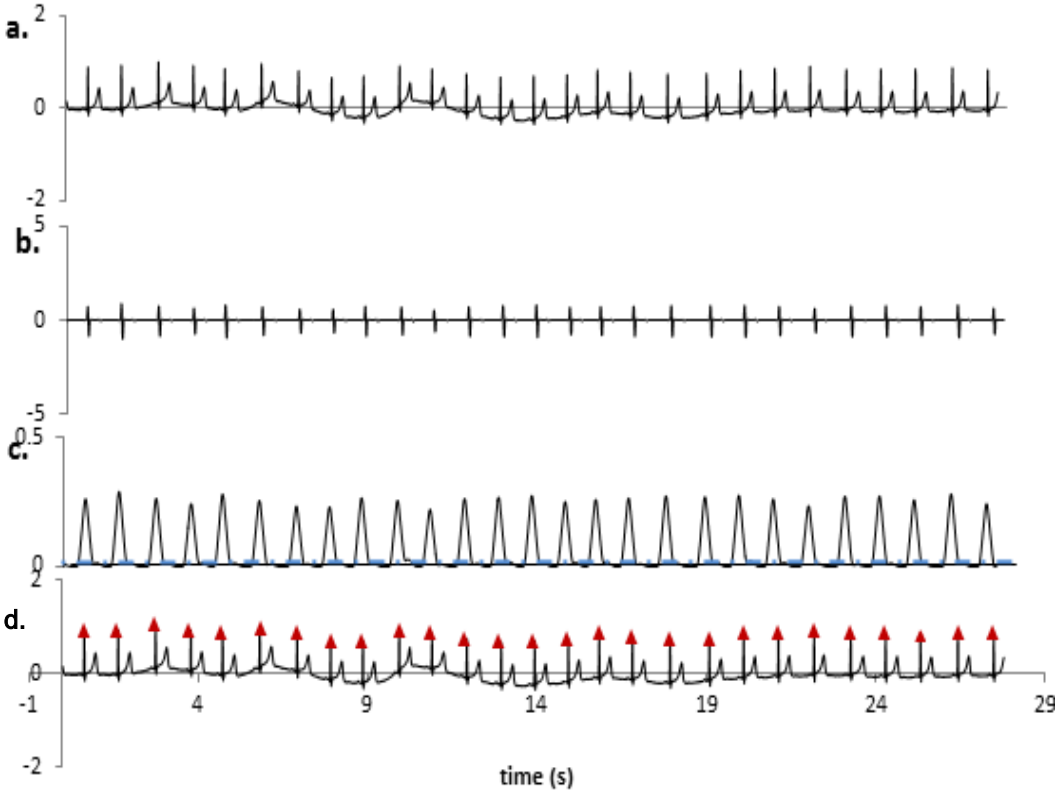

FIGURE 4.6: (a) ECG signal from record 119 (b) Output obtained after weighted least-squares filtering (c) smooth envelope obtained after logarithmic compression and low pass filtering (threshold indicated by dashed line) (d) Detected R-peaks.

4.3.3 Results for R-peak detection using offline implementation of the proposed method

In offline implementation, the proposed method as described in Section 4.2 is directly applied to each record of 30 minutes duration, using the entire record as input. The bandpass filter is designed with order 100. For WLS filtering, the parameters are selected as $\lambda = 0.6$ and $\alpha = 1$. The threshold and peak prominence values are chosen as $Th = 0.01$ and $MPP = .006$, respectively. The remaining parameters are selected as described in Section 4.2. The offline implementation was carried out using MATLAB R2014b software. The record-wise results for R-peak detection in ECG signals from the MIT-BIH arrhythmia database using the offline implementation of the proposed method are summarized in Table-4.1. Like many other methods, the most FPs occur for record 105 which contains high-grade noise and QRS-like artefacts and the most FNs occur for record 203, which contains a high number of multiform PVCs. However, it can be seen that the proposed method achieves high overall positive predictivity and sensitivity values and low detection error rates. The performance of the proposed method on some of the challenging scenarios is illustrated in Fig. 4.5- 4.7. Fig. 4.5(a) shows an ECG signal from record 113 with pointed T-waves resembling QRS complexes. It can be seen

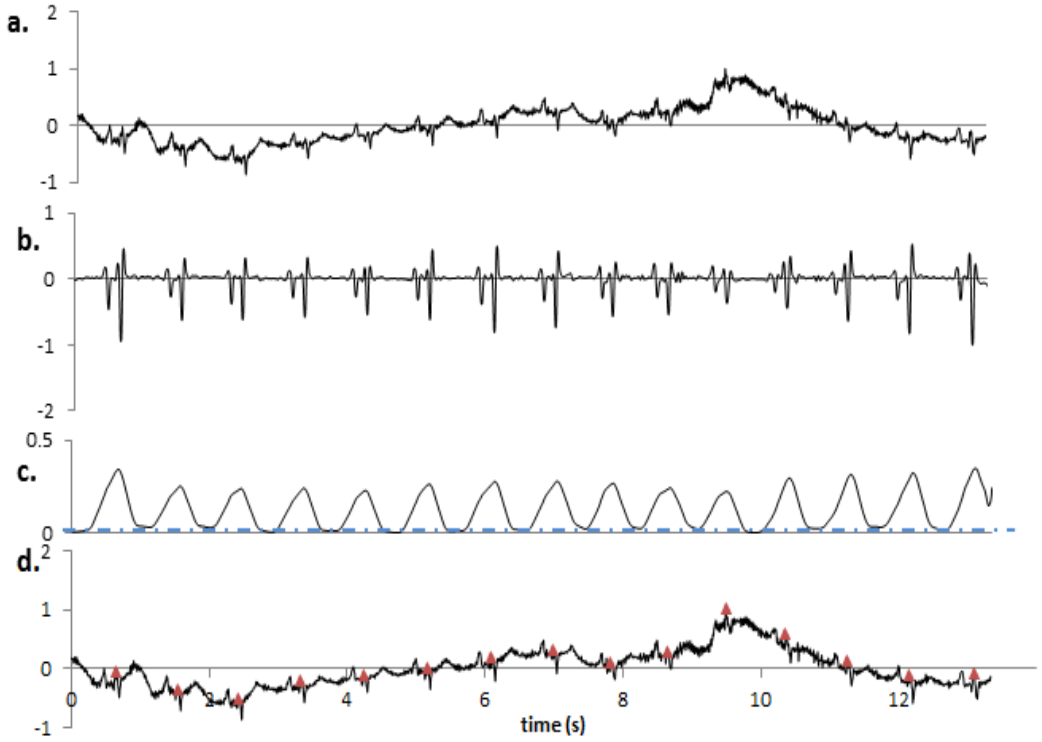

FIGURE 4.7: (a) ECG signal from record 108 (b) Output obtained after weighted least-squares filtering (c) smooth envelope obtained after logarithmic compression and low pass filtering (threshold indicated by dashed line) (d) Detected R-peaks.

that the T-waves are effectively suppressed and the smooth envelope contains only very small peaks due to the T-waves, which are rejected because of the threshold and peak prominence criteria. Fig. 4.6(a) shows an ECG segment taken from the record 119. The signal consists of several wide PVC beats. It can be seen in Fig. 4.6(b)-(c) that the PVC beats are preserved after filtering and correctly detected. Fig. 4.7(a) shows another challenging ECG signal from record 108 which contains muscular noise, baseline wander as well as pointed P-waves, which can be mistaken as R-waves. However, the proposed method is able to detect all the R-peaks correctly. In the offline implementation, the time required by the proposed method for QRS detection in a signal of duration 30 minutes and sampling rate 360 Hz is 0.88 seconds, therefore, the per sample execution time of the proposed method is only 1.35 μs on an Intel Core i3 2.50 GHz processor with 2 GB RAM. Hence, the proposed method is very useful for fast QRS detection in pre-recorded ECG signals, particularly long records such as those obtained from Holter monitoring. The offline implementation of the proposed method is compared with several established and state-of-the-art methods in Table-4.2. It can be seen that the proposed method shows improved performance over existing methods.

TABLE 4.2: Comparison of performance of the offline implementation of the proposed method with other R-peak detection methods on the MIT-BIH database.

Reference	**Method**	**FN**	**FP**	**Se** (%)	**P+** (%)	**DER** (%)
Pan and Tompkins (1985) [21]	First derivative followed by squaring	277	507	99.54	99.75	0.712
Zidelmal et al (2014) [34]	S- transform and Shannon energy	171	97	99.84	99.91	0.25
Martinez et al (2004) [25]	Discrete Wavelet transform	220	153	99.8	99.86	0.34
Dohare et al (2014) [122]	Median filtering and sixth power of the signal	870	728	99.21	99.34	1.46
Bouaziz et al (2014) [123]	Discrete Wavelet transform	140	232	99.87	99.79	0.34
Yochum et al (2016) [124]	Continuous Wavelet transform	160	574	99.85	99.48	0.67
Castellas-Rufas and Carrabina (2015) [38]	Non-linear MaMeMi filter	614	353	99.43	99.67	0.88
Chen et al (2006) [26]	Wavelet denoising and moving averaging	459	529	99.55	99.49	0.96
Phukpattaranont (2015) [37]	Quadratic filtering	202	210	99.82	99.81	0.38
Jung and Lee (2012) [39]	Singular value decomposition filter	581	579	99.47	99.47	1.05
Proposed method	R-peak preserving filtering and logarithmic compression	131	111	99.88	99.9	0.22

4.3.4 Real-time implementation

For real-time implementation, the block-by-block processing approach can be used. The incoming data is stored in a memory buffer of size M and it is processed when the buffer is full. In order to satisfy real-time requirements, the block processing must be completed before the next block of M samples arrives. Thus the total duration of I/O overheads and processing time must be less than the time it takes for a block of samples to be generated [113]. The proposed method described in section 4.2 can be implemented in this mode with a small change. If a peak is detected in the last 100 ms of a block, a blanking period of 100 ms is used in the beginning of the next block, i.e., no peak is detected in the first 100 ms of the subsequent block. This total duration of 200 ms corresponds to the refractory period following a QRS complex, during which another QRS cannot

TABLE 4.3: Comparison of performance of the real-time implementation of the proposed method with other real-time R-peak detection methods on the MIT-BIH database.

Reference	**Method**	**FN**	**FP**	**Se** (%)	**P+** (%)	**DER** (%)
Pan and Tompkins (1985) [23]	First derivative followed by squaring	277	507	99.54	99.75	0.712
Castellas-Rufas and Carrabina (2015) [7]	Non-linear MaMeMi filter	614	353	99.43	99.67	0.88
Chen S.-W. et al (2006)[8]	Wavelet denoising and moving averaging	459	529	99.55	99.49	0.96
Proposed method	R-peak preserving filtering and logarithmic compression	180	556	99.84	99.49	0.67

occur. This blanking period is used so that there is only one peak corresponding to a QRS complex that is shared between two consecutive blocks. The values of the parameters of the various processing blocks are the same as that in the offline implementation. The real-time scenario is simulated in MATLAB R2014b software and for a block size of $M = 5000$ samples, the average values of sensitivity, positive predictivity and detection error rate obtained on the MIT-BIH database are 99.84%, 99.49% and 0.67% respectively. The proposed algorithm was also implemented on an NXP LPC1768 microcontroller with a 32-bit ARM Cortex M3 core with clock frequency 96 MHz, 512KB flash and 64KB on-chip RAM. A data block of size M samples from the MIT-BIH database was read from a buffer by the microcontroller and after processing, the output was observed on a terminal emulator window on a computer. It was found that the time taken to process a data block of duration 5.56s (M=2000 samples at 360 samples/s) is 2.34s, which could be even faster with an optimized code. Hence, the algorithm can be used for real-time QRS detection in a wearable device, for the purpose of Holter monitoring. It can be observed that there is a drop in the values as compared to the offline implementation. Particularly, the false positives have increased. The increased detection errors mainly occur at the edges of the blocks when a beat falls in two consecutive blocks and two QRS complexes are attributed to the same beat. This is more frequent in case of signals with pointed P- and T- waves. In the offline implementation, this problem does not occur because the moving average filtering merges the entire beat into a single smooth pulse-like waveform with its peak at the location of the R-peak. However, in spite of the drop in accuracy as compared to offline implementation, the proposed method still performs better than existing real time methods in terms of the overall detection error rate, as shown in Table-4.3. In the future, some more measures may be devised to address this

issue of false positive detection at the block edges.

4.4 Conclusions

In this chapter, offline and real-time implementations of a novel method for QRS detection are presented. The ECG signal is first bandpass filtered to suppress the out-of-band noise and select the QRS frequency range. This is followed by Savitzky-Golay filtering which suppresses the noise peaks, without smoothing out the R-peaks. This is further followed by first-order backward differencing, which accentuates the QRS complexes because of their higher slope. Next, weighted least squares smoothing is applied, which is an edge-preserving smoothing technique used for image enhancement. This technique greatly suppresses the noise peaks, without loss of QRS complexes. As a result of the preceding operations, noise is reduced to very low amplitudes and the QRS complexes correspond to medium and high signal intensities. Next, a novel nonlinear transformation technique is applied, which boosts the mid-range R-peaks to equalise their amplitude with the high amplitude R-peaks, without boosting the noise level. This achieves the twofold purpose of obtaining a smooth signal envelope in which the QRS peaks are dominant and allowing use of a single fixed threshold and peak prominence value for all signals, independent of any signal parameters. Finally, in the last step, the peaks are detected in the smooth envelope, which act as guides to latch on to the true R-peak positions in the ECG signal. The proposed method exhibits improved performance over existing methods, with overall sensitivity, positive predictivity and detection error rate values of 99.88%, 99.90% and 0.22%, respectively for the offline implementation and 99.84%, 99.49% and 0.67%, respectively for the real-time implementation.

Chapter 5

QRS Complex Detection in ECG signals Using Locally Adaptive Weighted Total Variation Denoising

5.1 Overview

As mentioned earlier, nonlinear filtering based on optimization has recently been shown to be very useful in enhancement of the signal-to-noise ratio (SNR) of the ECG signal [35]. This in turn, leads to improved QRS detection accuracy. The technique in [35] is based on compound total variation (TV) denoising. TV minimization is a denoising technique that was originally introduced in the context of edge-preserving image denoising by Rudin et al in [114]. In discrete form, TV of a signal is given by summation of the absolute value of its first order difference. Signals with high TV have excessive detail which is possibly contributed by noise. TV denoising is an optimization problem that seeks to find an estimate of a signal from its noisy version by minimizing the TV, such that the denoised signal is close to the original signal. In this chapter, we propose a novel preprocessing technique based on the WTV minimization framework. The use of weights allows attenuation of the in-band P- and T-waves, in addition to the noise. The ECG signal is first bandpass filtered to select most of the QRS energy. This filtering operation diminishes the amplitude of the lower frequency P- and T-waves and the higher frequency muscular noise. However, because of spectral overlap, some muscular noise as well as P- and T- waves still remain in the filtered signal. The filtered signal is differentiated to emphasize the QRS complexes that are characterized by a high slope and further reduce the amplitude of the P- and the T-waves. This is followed by WTV denoising, which denoises the signal by TV minimization. Additionally, by using weights,

the discrete derivatives can be individually penalized such that the QRS complexes are preserved preferentially over P- and T-waves. Thus, the WTV denoising framework helps in suppression of both the in-band noise and the P- and T-waves. The selection of the regularization parameter that determines the degree of smoothing is critical in WTV denoising. We use a measure of local noise to determine the regularization parameter, which is varied adaptively. The proposed technique is evaluated on a standard database and the performance of the proposed method is compared with established and state-of-the-art techniques.

The rest of the chapter is organized as follows. The proposed method is detailed in Section 5.2. In Section 5.3, we evaluate the proposed method on a standard database and illustrate its performance in some of the challenging scenarios. The results of the proposed method are analyzed in Section 5.4. Finally, the conclusions are given in Section 5.5.

5.2 Materials and methods

5.2.1 Data

The data used for evaluation of the proposed method has been taken from the MIT-BIH arrhythmia database [106], which has been described earlier. This database has a wide variety of QRS complexes and P- and T-wave morphologies and the records have noise and artefacts that occur in a clinical setting. We choose the MLII recordings from all the records in the database for evaluation of the proposed method. The episodes of ventricular flutter in record 207 of the database have been excluded in the evaluation.

To demonstrate the performance of the proposed method on signals from other databases, records from the Fantasia and the European ST-T database were also used for evaluation. The Fantasia database comprises ECG and respiration signal recordings from twenty young (21 - 34 years old) and twenty elderly (68 - 85 years old) healthy subjects of duration 120 minutes each. Some records also have non-invasive blood pressure signal. The sampling rate of the ECG, respiration, and (where available) blood pressure signals is 250 samples/s. The heartbeats were annotated using an automated arrhythmia detection algorithm, and the beat annotations were verified by visual inspection.

The European ST-T database consists of 90 annotated excerpts of ambulatory ECG recordings from 79 subjects. Each record is of two hours duration and contains two signals, each sampled at 250 samples per second with 12-bit resolution over a nominal 20 millivolt input range. We use the second channel recordings for evaluation. For

this database also, an initial set of beat labels was produced by a slope-sensitive QRS detector, and later verified by cardiologists.

5.2.2 Performance evaluation criteria

For evaluation of performance of the proposed method, we use the criteria of Se, P^+ and DER, which have also been used in the earlier chapters.

5.2.3 The proposed method

Similar to most other QRS detection techniques, the proposed method consists of two stages: a preprocessing stage and a peak detection stage, as shown in the block diagram in Fig. 5.1. The preprocessing is carried out block-by-block, the size of each block being N, to have a local estimate of noise in the denoising operation. The preprocessing is carried out in a series of steps that aim at suppressing the noise peaks and the P- and T-waves, and accentuating the QRS complexes. Since the preprocessing is done block-by-block, edge effects can occur after filtering, because of abrupt truncation, and hence, false peaks can be detected at the block boundaries. To avoid this issue, symmetric padding is done on the blocks on both sides before filtering, by using reflecting boundary conditions. The padding is discarded after the filtering operation. Also, before application of the proposed algorithm, the signal is clipped at ± 11 mV, to limit the amplitudes of possible artefacts. The ECG signal amplitude is much lesser.

After preprocessing, a smooth envelope is obtained, in which peaks are detected. These peaks are used as guides to determine the actual R-peak locations in the ECG signal. Each of the steps are detailed in the following subsections.

5.2.3.1 Bandpass filtering and differentiation

The ECG signal $x(n)$ is first bandpass filtered to select the frequency-range [6 22] Hz, in order to select most of the QRS energy and eliminate the out-of-band noise such as power line interference, which occurs at the power line frequency of 50/60 Hz and baseline wander, which lies at frequencies less than 1 Hz. This also diminishes the amplitude of the lower frequency P- and T- waves. The bandpass filter is designed as a constrained least squares FIR filter of order M. In designing this filter, it is not required to explicitly define the transition bands in the magnitude response [115]. This is useful in situations such as the present problem, where noise and signal overlap in spectra and therefore, a rigid transition band cannot be defined. Instead, only the cutoff frequencies and the

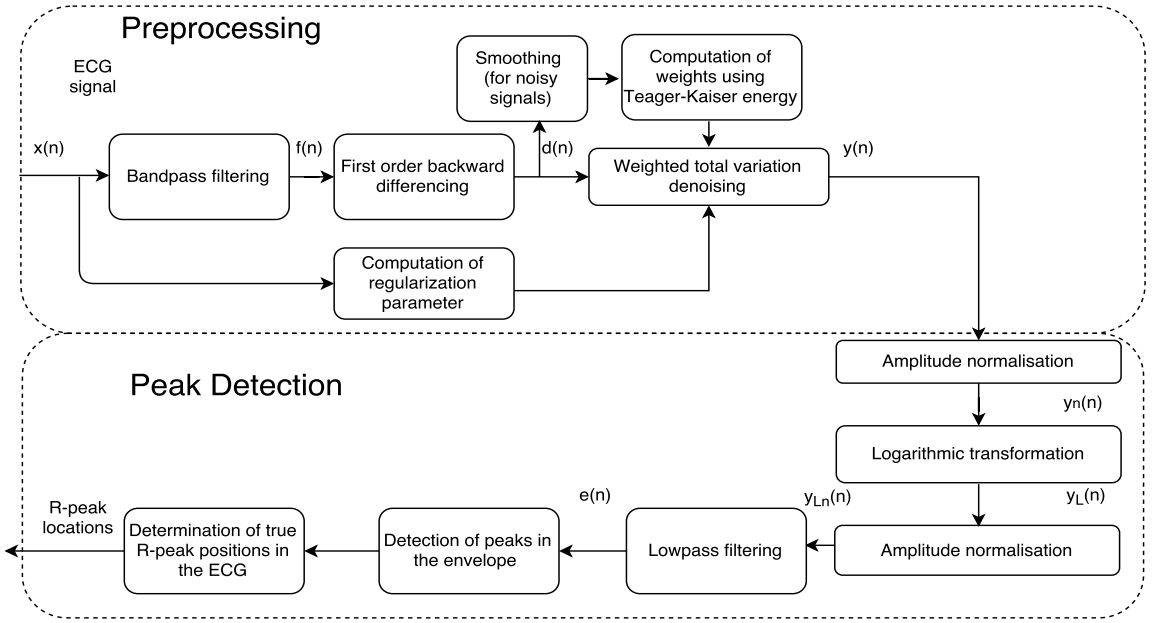

FIGURE 5.1: Block Diagram of the proposed method

lower and upper limits of the passband ripple and the stopband attenuation are to be specified.

For illustration, Fig. 5.2 (a) shows an ECG signal and the corresponding filtered signal $f(n)$ is shown in Fig. 5.2 (b). After filtering, the signal is differentiated to accentuate the QRS complexes, which are characterized by a high slope. This also further suppresses the lower frequency P- and T- waves. The differentiation operation is approximated by first order backward differencing as

$$d(n) = f(n) - f(n-1). \tag{5.1}$$

The difference signal $d(n)$ is illustrated in Fig. 5.2(c).

5.2.3.2 Weighted total variation denoising

The signal $d(n)$, which is obtained after bandpass filtering and differentiating the ECG, still contains noise, which lies in the same frequency range as the QRS complexes. Hence, this noise is difficult to remove using the linear Fourier transform based filtering techniques. Muscle noise (Electromyogram) is a major source of this noise. To suppress this noise without smoothing out the QRS complexes, optimization techniques such as TV filtering can be used. The TV of $y(n)$, $0 \leq n \leq N-1$ is given by

$$TV(\mathbf{y}) = \sum_{n=1}^{N-1} |y(n) - y(n-1)|, \tag{5.2}$$

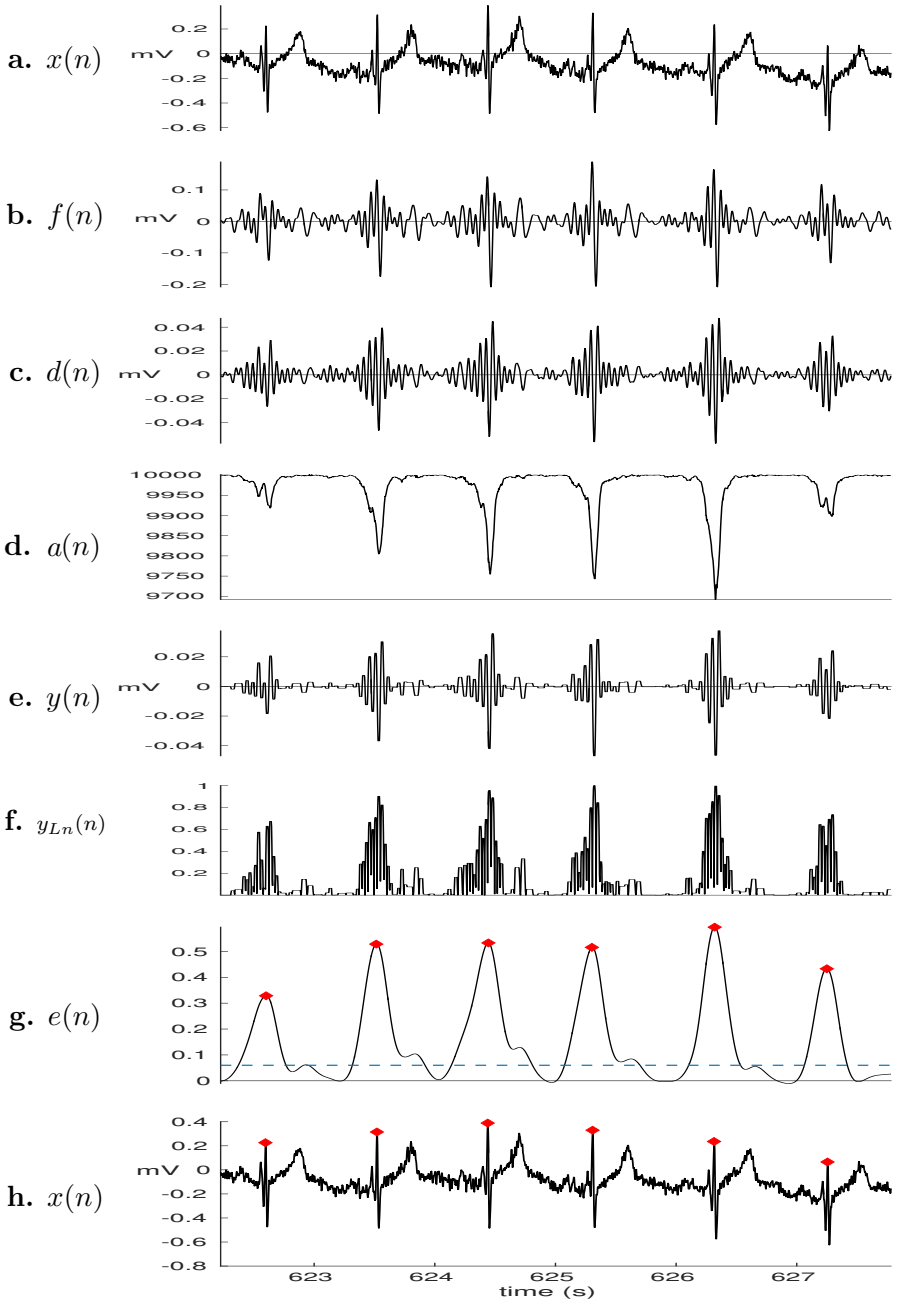

FIGURE 5.2: Outputs obtained at different stages of the algorithm (a) ECG signal from record 114 of MIT-BIH arrhythmia database (b) Signal obtained bandpass filtering (c) signal obtained by first order backward differencing of filtered signal (d) The weights obtained using Teager-Kaiser energy (e) The signal obtained after WTV minimisation (f) the signal obtained after logarithmic compression and normalisation (g) The envelope obtained using lowpass filtering and the detected peaks. Threshold indicated by dashed line (h) Peaks mapped to original ECG

i.e. summation of absolute value of the first order derivative of $\mathbf{y}$. We use upper and lower case boldface to denote vectors. Thus, the N-point signal vector $\mathbf{y}$ is given by $\mathbf{y} = [y(0), y(1), ..., y(N-1)]^T$, where $[\cdot]^T$ denotes the transpose of $[\cdot]$.

In this work, we use WTV denoising, which can be expressed as the optimization problem

$$\arg\min_{\mathbf{y}\in\mathbb{R}^{\mathbf{N}}} \Big\{ \frac{1}{2} \sum_{n=0}^{N-1} (d(n) - y(n))^2 + \lambda \sum_{n=1}^{N-1} a(n)|y(n) - y(n-1)| \Big\}, \tag{5.3}$$

which seeks a solution $\mathbf{y}$ which is as close as possible to the input $\mathbf{d}$ in the least-square sense and is smooth everywhere except at places where the weights $a(n)$ (all positive) are low. λ is the regularization parameter that determines the trade-off between the first term and the second term in (5.3). The first term, which is the *data fidelity* term, aims at approximating the input in the least squares sense, whereas the second term, which is the *regularization* term, imposes a smoothness constraint. If the value of λ is higher, greater weight is given to the smoothness constraint, at the cost of the filtered output not being as close to the input. The value of λ needs to be chosen in proportion to the amount of noise in the input signal.

In vector-matrix notation, (5.3) can be expressed as

$$\arg\min_{\mathbf{y}\in\mathbb{R}^{\mathbf{N}}} \frac{1}{2} \|(\mathbf{d} - \mathbf{y})\|^2{}_2 + \lambda \, \mathbf{A} \, \|\mathbf{D}\mathbf{y}\|_1, \tag{5.4}$$

where $\mathbf{A}$ is a diagonal matrix containing the weights $a(n)$, $\mathbf{D}$ is the $(N-1) \times N$ first order difference matrix of the form:

$$\mathbf{D} = \begin{bmatrix} -1 & 1 & & & & \\ & -1 & 1 & & & \\ & & \ddots & \ddots & & \\ & & & -1 & 1 & \\ & & & & -1 & 1 \end{bmatrix}, \tag{5.5}$$

$\|\cdot\|_1$ denotes the ℓ_1 norm and $\|\cdot\|_2$ denotes the ℓ_2 norm.

Since the objective function in (5.4) is non-differentiable, it is fairly challenging to solve. In [116], Barbero and Sra have developed a fast and low-memory algorithm using an optimized taut-string approach to solve the WTV minimization in (5.4), which is used in this work. An overview of this algorithm is given in the following subsection.

5.2.3.2.1 Overview of optimized taut-string approach based WTV solver

In [116], the WTV minimization problem in (5.3) is solved via its dual

$$\min_{\mathbf{u}\in\mathbb{R}^{\mathbf{N-1}}} \frac{1}{2}\|(\mathbf{D^T u})\|_2^2 - \mathbf{u^T D d}, \text{ subject to } |u(n)| \leq \lambda w(n),\ 0 \leq n < N-1. \tag{5.6}$$

If $\mathbf{u}^*$ is the dual solution, then using Karush-Kuhn-Tucker conditions, the primal solution

$$\mathbf{y}^* = \mathbf{d} - \mathbf{D^T u}^* \tag{5.7}$$

can be obtained. For a feasible dual variable $\mathbf{u}$, a candidate primal solution $\mathbf{y} = \mathbf{d} - \mathbf{D^T u}$ can be computed, with the corresponding duality gap given by

$$\mathbf{gap}(\mathbf{y}, \mathbf{u}) = \lambda\|\mathbf{Dy}\| - \mathbf{u^T Dy}. \tag{5.8}$$

The objective in (5.6) can be replaced by $\|\mathbf{D^T u} - \mathbf{d}\|_2^2$, which can be expressed as

$$\big(u(0) - d(0)\big)^2 + \sum_{n=1}^{N-2}(-u(n-1) + u(n) - d(n))^2 + (-u(N-2) - d(N-1))^2\big)^{\ 2}. \tag{5.9}$$

Thus, introducing the fixed extreme points $u(-1) = u(N-1) = 0$, (5.6) can be replaced by

$$\min_{\mathbf{u}} \sum_{n=0}^{N-1}(d(n) - u(n) + u(n-1))^2, \text{ subject to } |u(n)| \leq \lambda w(n),\ \ 0 \leq n < N-1. \tag{5.10}$$

Next, on performing a change of variable $\mathbf{s} = \mathbf{r} - \mathbf{u}$, where $r_n = \sum_{k=1}^{n} d_k$ is the cumulative sum of input values, (5.10) can be written as

$$\min_{\mathbf{s}} \sum_{n=0}^{N-1}(d(n) - r(n) + s(n) + r(n-1) - s(n-1))^2, \text{ subject to } |s(n) - r(n)| \leq \lambda w(n),$$
$$0 \leq n < N-1, \quad r(-1) - s(-1) = s(N-1) = r(N-1) = 0, \tag{5.11}$$

which can be simplified as

$$\min_{\mathbf{s}} \sum_{n=0}^{N-1} (s(n) - s(n-1))^2, \text{ subject to } |s(n) - r(n)| \leq \lambda w(n), \\ 0 \leq n < N-1, \quad s(-1) = 0,\ s(N-1) = r(N-1). \tag{5.12}$$

Now, the key trick here is that (5.12) can be shown to have the same minimum as

$$\min_{\mathbf{s}} \sum_{n=0}^{N-1} \sqrt{1 + (s(n) - s(n-1))^2}, \text{ subject to } |s(n) - r(n)| \leq \lambda w(n), \\ 0 \leq n < N-1, \quad s(-1) = 0,\ s(N-1) = r(N-1). \tag{5.13}$$

The objective in (5.13) can be seen as the Euclidean length of a polyline through the points $(n, s(n))$; therefore, (5.13) can be visualized as seeking the *taut string* (minimum length polyline) crossing a tube composed of segments of variable width $\lambda w(n)$, with the center being the cumulative sum $\mathbf{r}$ and fixed endpoints $(s(-1),\ s(N-1))$. Hence, the method has been named taut string optimization. For a detailed description of how the taut string is found, the interested reader is referred to the algorithm in [116].

After finding the taut string, the primal-dual relation in (5.7) is used to obtain the final solution as

$$s(n)-s(n-1) = r(n)-u(n)-(r(n-1)-u(n-1)) = d(n)-u(n)+u(n-1) = y(n). \tag{5.14}$$

A MATLAB implementation of this WTV solver in [116] has been made available by its authors at https://github.com/albarji/proxTV and has been used in this work.

5.2.3.2.2 Choice of weights

In the context of the present problem, (5.3) can be used to seek a smooth signal $\mathbf{y}$ from the difference signal $\mathbf{d}$ while preserving the QRS complexes, by using a suitable choice of weights. In this work, we choose the weights in (5.3) as the Teager-Kaiser energy (TKE) of the difference signal d. The TKE of the discrete-time signal $\mathbf{d}$ is defined as [117]

$$TK(d(n)) = d^2(n) - d(n-1)d(n+1), \tag{5.15}$$

where $TK(\cdot)$ denotes the TKE operator. From (5.15), it is evident that the TKE operator is nonlinear. Unlike the conventional energy measure in signal processing, which is only proportional to the squared signal amplitude, it can be shown that the TKE is

proportional to both the squared amplitude and squared frequency of the signal [118]. This property of TKE can be used in the present problem to accentuate the QRS complexes and suppress the P- and T- waves. The signal **d** has relatively higher amplitude of QRS complexes as compared to the P- and T-waves, because of the preceding band-pass filtering and differencing operations. Also, the P- and T-waves have relatively lower frequency compared to the QRS complexes. Thus, the TKE operator can be applied on **d** to further accentuate the QRS complexes relative to the P- and T- waves and the resultant signal can be used to determine the weights given by

$$a(n) = (0.01(TK(d(n))) + \epsilon)^{-1}, \tag{5.16}$$

where ϵ is a small positive constant. The multiplication factor of 0.01 is due to the fact that $d(n)$ is in millivolts. If $d(n)$ is in units of volts, for example, the corresponding multiplication factor would be $10e4$. In (5.16), since the weights are inversely proportional to the TKE of **d**, therefore in (5.3), low smoothing is performed at the instants where TKE is high , i.e. at QRS complex locations . This is because the QRS complexes have higher frequencies as compared to the P- and the T-waves . The resultant signal **d** is a smooth signal, in which the noise and the P- and T- waves are suppressed.

For signals in which the noise exceeds a certain threshold $\mathcal{N}_T$, a smoothing operation is performed before computation of weights using TKE, in order to avoid boosting the noise. For smoothing, we use a moving average filter with window length 36 ms. The chosen window length is less than the QRS complex duration (nominal QRS duration is 100 ms $\pm$ 20 ms [69]), so that the QRS complexes are not smoothed out. A technique for estimating the noise is described in the next subsection.

5.2.3.2.3 Choice of regularization parameter

The regularization parameter, λ determines the degree of smoothing . Its value needs to be chosen in proportion to the amount of noise in the signal. Higher amounts of noise in the signal would require higher value of λ for denoising. For denoising, first the amount of this noise needs to be estimated and then a value of λ needs to be chosen accordingly. We compute a measure of noise in the signal as

$$\mathcal{N} = \sum_n |d_2(n)|, \tag{5.17}$$

where $d_2(n)$ denotes the second order derivative of the ECG signal $x(n)$, given by

$$d_2(n) = \sum_n |d_1(n) - d_1(n-1)|, \tag{5.18}$$

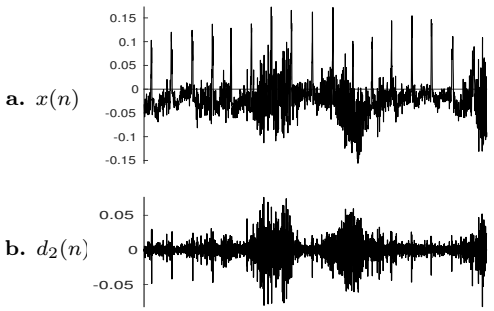

FIGURE 5.3: (a) An ECG signal with high noise and (b) the corresponding second order difference.

where $d_1(n)$ denotes the first order derivative given by

$$d_1(n) = \sum_n |x(n) - x(n-1)|. \tag{5.19}$$

The noise measure $\mathcal{N}$ in (5.17) is actually the TV of the first derivative of the ECG signal. For illustration, Fig. 5.3 shows an ECG signal with high noise and its second order derivative. It is seen that in the second order derivative, the noise is dominant. Thus, the sum of the absolute value of the second order derivative can be used as a measure of noise. We vary the regularization parameter in direct proportion to the noise as

$$\lambda = K\mathcal{N}, \tag{5.20}$$

where K is a constant. Thus, for signals with higher noise, the value of λ is higher and hence, greater smoothing is done. Using (5.17) and (5.20), (5.3) can be written as

$$\arg\min_{\mathbf{y}\in\mathbb{R}^{\mathbf{N}}} \left\{ \frac{1}{2} \sum_{n=0}^{N-1} (d(n) - y(n))^2 + K \sum_{n=2}^{N-1} |d_2(n)| \sum_{n=1}^{N-1} a(n)|y(n) - y(n-1)| \right\}, \tag{5.21}$$

Since λ also depends on K, therefore, K is a critical parameter. If the value of K is too high, then even the QRS complexes can be smoothed out. On the other hand, if the value of K is too small, then smoothing may be insufficient, leading to a large number of false positives. A range of suitable values of K has been estimated in Section 3.

5.2.3.3 Logarithmic transformation

ECG signals have different amplitude levels and because of the preceding operations like filtering and WTV denoising, some QRS complexes, particularly the PVCs have a reduced amplitude . This is because the PVC beats are wider , i.e., have lower frequency components than the normal beats. To enable use of a single fixed Th and MPP value

for all ECG records and to ensure the detection of these low amplitude QRS complexes, we equalize the QRS amplitudes, without boosting the noise peaks (which have been suppressed or reduced to low amplitudes because of the preceding operations). We follow this step by amplitude normalization. For amplitude equalization, we use a logarithmic transformation of the following form, which was used in the previous chapter also, but has been repeated here for easy reference,

$$y_L(n) = \log_e \Big(1 + \frac{C y_n^2(n)}{m_{y_n^2}(n)}\Big), \tag{5.22}$$

where C is a constant, $y_n(n)$ denotes the normalized signal given by

$$y_n(n) = \frac{y(n)}{\max_n |y(n)|} \tag{5.23}$$

and $m_{y_n^2}$ denotes the mean value of y_n^2 given by

$$m_{y_n^2} = \frac{1}{N} \sum_{n=0}^{N-1} y_n^2. \tag{5.24}$$

After logarithmic transformation, the signal is again normalized as

$$y_{Ln}(n) = \frac{y_L(n)}{\max_n |y_L(n)|}, \tag{5.25}$$

so that it lies in the range [0 1].

The constant C is the same as the constant K in the previous chapter. In (5.22), the signal y_n is first squared and then normalized with respect to the mean, before the logarithmic transformation. The squaring operation further diminishes the low amplitude noise peaks in y_n with respect to the higher amplitude QRS peaks and makes all signal values positive. The effect of logarithmic transformation can be understood with the help of Fig. 5.4, which plots the normalized output $y_{Ln}(n)$ of logarithmic compression against the normalized input $y_n(n)$, for various values of C. It is observed that as the value of C increases, the lower and the mid-range input amplitudes are boosted to a greater degree, which leads to an equalization of amplitudes. Since the lowest amplitudes are due to noise (which has been diminished because of preceding filtering operations), we do not want these to be intensified significantly. So, we choose a value of C that enhances the mid-range input intensities, without amplifying the noise significantly and choose a threshold for subsequent peak detection accordingly.

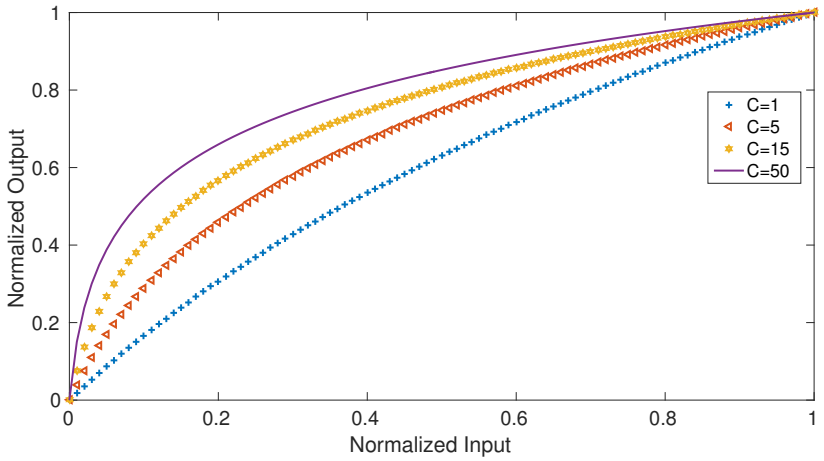

FIGURE 5.4: Logarithmic compression curves for various values of compression factor, C.

5.2.4 Lowpass filtering

The signal $y_{Ln}(n)$ is next low pass filtered to obtain a smooth envelope $e(n)$. For this purpose, we use a second order digital lowpass Butterworth filter of cut-off frequency 3 Hz and perform zero-phase filtering, in which the input data is first filtered in the forward direction, then the filtered sequence is reversed and filtered again [119]. The resulting transfer function equals squared magnitude of the original filter transfer function and the filtered sequence has the desirable characteristic of zero phase distortion.

5.2.5 Peak detection

For determination of peaks in the envelope, we use the threshold (Th), minimum peak prominence (MPP) and minimum peak separation (MPS) criteria. Peak prominence is the height of the peak relative to a reference level that is determined as follows. The range from the peak to the end point or the point at which a higher peak is encountered, whichever is closer to the peak, is considered on both sides, and the higher of the signal minima in these intervals is used as the reference. This is illustrated in Fig. 5.5 which shows an ECG signal and the corresponding envelope signal $e(n)$, in which the peak prominence values are given by the length of the vertical lines. In this example, Th is set as 0.06 and the MPP is set as zero. There are two falsely detected peaks that are encircled. However, if in addition to the threshold, we also use an equal value of $MPP = 0.06$, both false detections can be avoided, even though the actual heights of the peaks measured with respect to zero, are greater than the threshold. Thus, the MPP criterion helps in reducing the number of false positives. An optimal range of values of

Th and MPP have been estimated in Section 3. The MPS is set as 200 ms, which is the physiologically determined refractory period between two consecutive QRS complexes.

After detection of peaks in the envelope signal, R-peaks are now detected in the original signal as the peak values lying within ±15 samples (42 ms) of the detected peaks in the envelope.

It may be noted that in the preprocessing stage, it is assumed that the ECG signal $x(n)$ is in units of millivolts. If the ECG signal has a different unit of measurement, the parameters $\mathcal{N}_T$ and the TKE in (5.16) can be scaled accordingly. The selection of $\mathcal{N}_T$ is discussed in the next section.

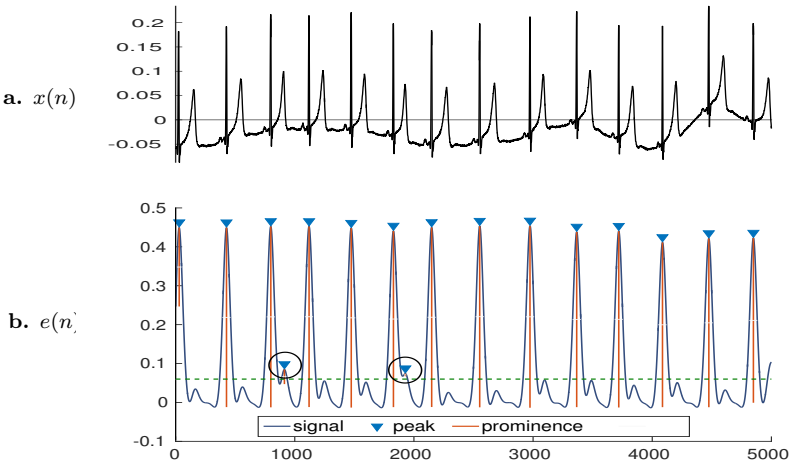

FIGURE 5.5: (a) ECG signal $x(n)$ (b) the corresponding envelope $e(n)$ with the detected peaks obtained using threshold $Th = 0.06$ and $MPP = 0$.

5.3 Results

The proposed method has been implemented in MATLAB R2015b and executed on 2.50 GHz, Intel Core i3 CPU with 4 GB RAM and 64-Bit Ubuntu 14.04 operating system. As mentioned earlier, the method can be used for fast offline as well as online QRS detection. In the offline implementation, the preprocessing is done blockwise, but the peak detection stage uses the entire signal. On the other hand, in the online implementation, both preprocessing and peak detection are done blockwise. In the following subsections, we give the implementation details and results of both implementations.

5.3.1 Offline implementation details and results

The proposed algorithm has low computational load and can be used for fast and automatic offline QRS detection in long duration ECG records, such as those obtained from a Holter monitor. In the offline application of the proposed method, the preprocessing is carried out blockwise, but in the peak detection stage, the entire signal is used to obtain a smooth envelope, in which the QRS complexes are detected. This can be contrasted with the real-time implementation, in which the peak detection is also carried out blockwise. The choice of various parameters is discussed in the following subsections.

5.3.1.1 Choice of filter order M

As for the bandpass filter described in Section 2.3.1, it is found that the detection errors are high for order values less $M < 40$ and low for $M > 40$, up to about order $M = 700$, beyond which the errors actually begin to increase, as the filter begins to cut off the out-of-band frequencies more sharply. Empirically, order $M = 300$ is found to give the best performance among several order values chosen over this range. Hence, M is set as 300.

5.3.1.2 Choice of N

The block size must be large enough to ensure there is at least one QRS complex in each block. A block size greater than 1000 samples (2.8 s) meets this requirement for all records in the MIT-BIH arrhythmia database.

The various considerations in selection of the block size are as follows. The selection of a small block size makes the noise estimate more local, but it comes at the price of an increased processing time. For example, the processing time for a 30-minute record using a block of 5000 samples is 1.25 s, whereas that using a 2000 sample block is 3.57 s on the same computer. This is because of the overheads due to signal padding, I/O etc. Additionally, a smaller block size would give more errors in real-time implementation, because of the possible incorrect detections at block edges in some records. On the other hand, if the block size is too large, the noise estimate would not be as local. In this work, we have used a block size of $N = 5000$ (13.9 s), as it was empirically found to give the best results among the trial block sizes of $N = 2000$, (5.6 s) 5000 and 7000 (19.4 s). Therefore, all the parameters used in the method have been optimized for this block size. To facilitate comparison, the same block size has been used for both the offline and real-time implementation.

5.3.1.3 Choice of $\mathcal{N}_T$

For determination of the threshold for smoothing, $\mathcal{N}_T$, we chose some records from the MIT-BIH database that contain instances of high muscular noise. On computation of TKE directly (before smoothing) in the excessively noisy signal blocks from these records, it was found that the muscular noise intensified, and led to false positives. The amount of noise in these segments and the cleaner segments in these and other records was compared and a threshold for smoothing was then determined. It was observed that the noisy segments contain noise greater than the threshold of $\mathcal{N}_T = 130mV$; hence, this was used as the threshold for smoothing.

5.3.1.4 Choice of C

As discussed in Section 2.3.3, the logarithmic compression should give a high gain to the mid-amplitude range and low gain to the low amplitude range. The constant C can be used to control the shape of the compression curve, to get this desired response. As shown in Fig. 4, for a low value of C, such as $C = 1$, the curve is close to linear, so it does not boost the middle range sufficiently. On the other hand, for a high value of $C = 50$, the gain for not just the mid range, but also the low amplitude range is quite high. So there is a desirable range of values of C lying between the two extremes.

It is empirically found that the desirable range is $1 < C < 45$. For values of C outside this range, no Th and MPP values are found to give satisfactory results. For example, for values of C greater than the upper limit, high Th and MPP values need to be chosen, in order to avoid false detections in records with pointed T-waves. However, this leads to missed detection in records with PVC beats. Similarly, a choice of C less than the lower limit requires selection of a low threshold, because of low enhancement of the mid-range. However, this leads to greater false detections in noisy signals. In this work, we have chosen $C = 5$, and then suitable Th and MPP values have been determined accordingly.

5.3.1.5 Choice of ϵ

The role of the parameter ϵ is to ensure that the denominator term in (5.16) is always non-zero, so that division by zero can be avoided. However, the value of ϵ also affects the weights, which in turn affect WTV denoising. Observing in (5.21) that the overall regularization depends on the value of K, we have chosen a value of $\epsilon = 0.0001$, and then a suitable K value has been found as described in the following subsection.

5.3.1.6 Estimation of optimal ranges of values of K, Th and MPP

A range of suitable values of K can be found experimentally. For this purpose, we use a small subset of the MIT-BIH database as the test set, consisting of ECG signals that have episodes corresponding to two cases: (1) high muscular noise and (2) low amplitude QRS complexes (records 104, 228, 208 and 203). These two cases have conflicting threshold requirements. We set the Th and MPP as zero and the MPS as 200 ms. The average values of sensitivity and positive predictivity as K varies, are shown in the Fig. 5.6. It is seen that as expected, the sensitivity drops sharply after a certain value of K and the positive predictivity rises sharply initially as K increases, because of increased smoothing. For $K > 7 \times 10^{-8}$, there is a sharp drop in sensitivity, therefore, a suitable range of values of K would be $K < 7 \times 10^{-8}$. In this range, an appropriate threshold can be used for reducing the number of false positives.

To determine a suitable value of Th and MPP, the receiver operating characteristics curve (ROC) can be used, as also used for threshold determination in [120]. The ROC curve is a plot of the true positive rate (TPR) against the false positive rate (FPR) at various levels of cut-off. The TPR is the same as *sensitivity* defined in (3.7) and the FPR or (1-*positive predictivity*) is defined as

$$FPR = \frac{FP}{TP + FP}. \tag{5.26}$$

We choose the records 114, 203, 113 and 104 from the MIT-BIH database as the test dataset, which present challenges like presence of different ECG amplitude levels, PVC beats, pointed T- waves and muscular noise. The ROC curve for this test dataset is shown in Fig. 5.7 for MPS of 200 ms, which as mentioned earlier, is the refractory period between QRS complexes and $Th = MPP \in [0 \quad 0.7]$. For $Th = MPP = 0$ the TPR is the highest (.998) but the FPR is also quite high (0.268). At $Th = MPP = 0.2$, though the FPR is very low (0.268), the TPR is also quite low (.001). For $Th = MPP = 0.7$, no R-peaks are detected. As indicated in Fig. 5.7, the point closest to the upper left corner occurs at $Th = MPP = 0.06$ and achieves the best balance between TPR and FPR.

5.3.1.7 Results of offline implementation

The proposed method is evaluated on the MIT-BIH arrhythmia database. We choose $K = 3.4 \times 10^{-8}$ and $Th = MPP = 0.06$. MPS is set as 72 samples (200 ms). The overall algorithm along with the values of the various parameters involved is summarized in the flowchart in Fig. 5.8. The average time taken to process an ECG record of 30

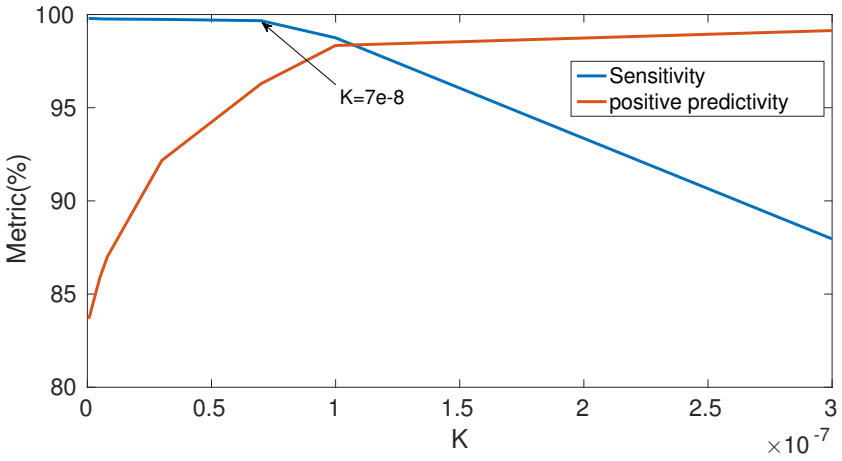

FIGURE 5.6: Variation of sensitivity and positive predictivity with K

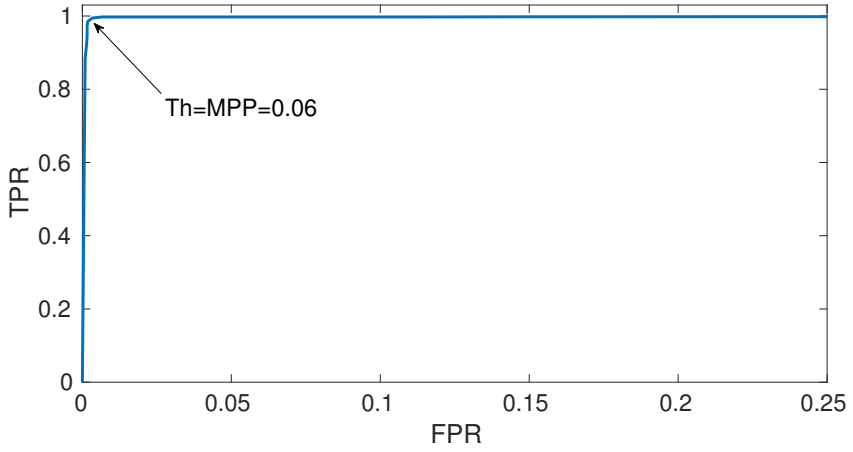

FIGURE 5.7: ROC curve for $Th = MPP \in [0 \quad 0.7]$

minutes duration is 1.25 s. The results obtained on the MIT-BIH database using the proposed method are given in Table-1. The overall $Se = 99.90\%$, $P^{+} = 99.88\%$ and $DER = 0.23\%$.

Fig. 5.9 - 5.12 illustrate how the various steps in the proposed method help in detecting QRS complexes in various challenging scenarios. Fig. 5.9 shows an ECG signal from record 117 with tall and pointed T-waves. These waves have a relatively larger frequency overlap with QRS complexes. It is seen in Fig. 5.9(b) that the T-waves have been effectively suppressed after WTV minimisation based filtering, because of the use of Teager-Kaiser energy as weights. Hence, there are no false positives because of the T-waves.

Fig. 5.10 shows an even more challenging scenario from the record 108, where the signal has pointed P-waves, which are difficult to differentiate from the similar looking reversed-polarity QRS complexes. Therefore, it is seen in Fig. 5.10(b) that even after

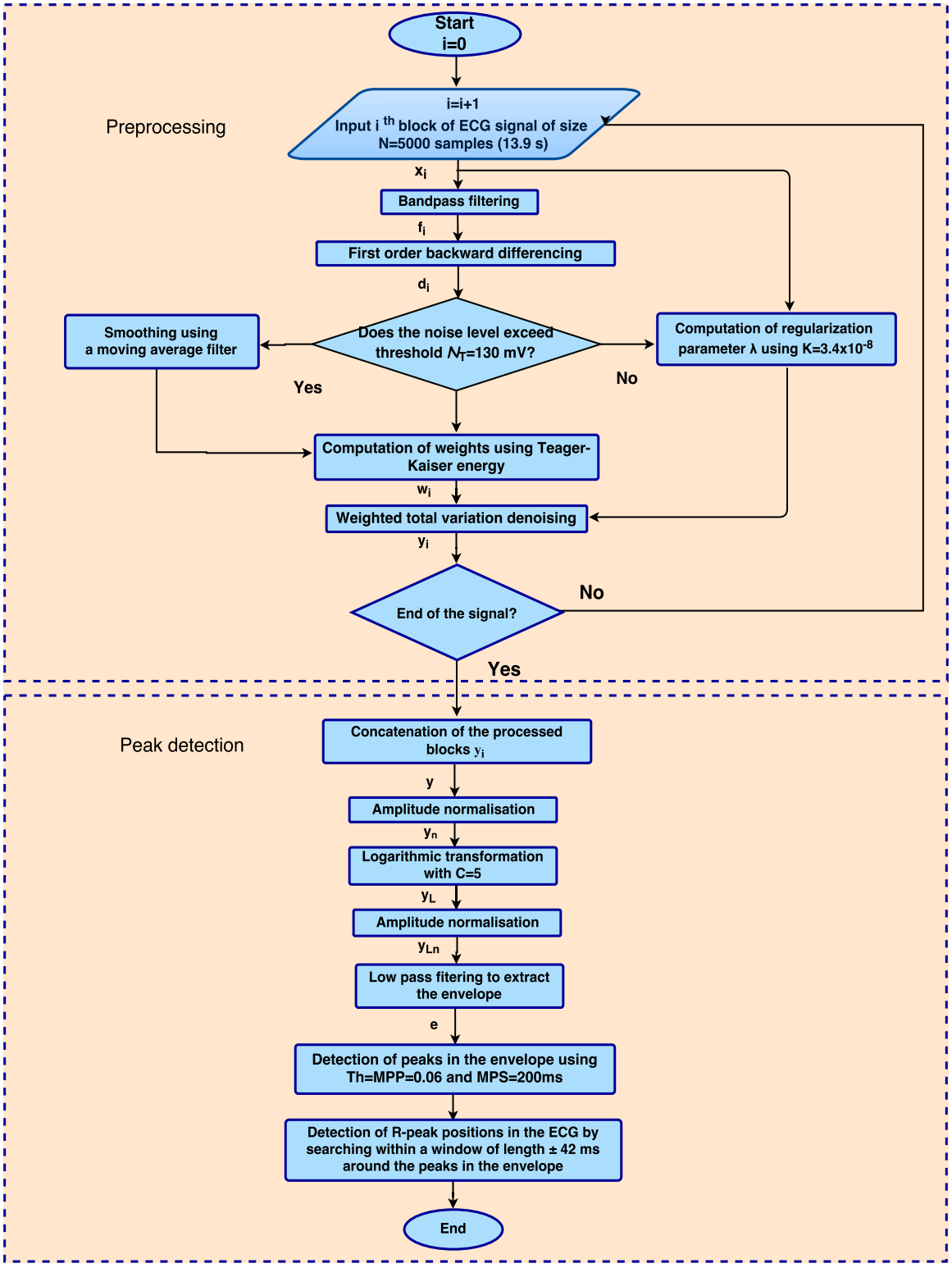

FIGURE 5.8: Flow chart of the proposed method (Offline implementation). In this example, it is assumed that the signal length is a multiple of the block length N.

TABLE 5.1: Results for QRS detection on the MIT-BIH arrhythmia database

Record	TotalBeats	TP	FN	FP	Se(%)	P+(%)	DER (%)
100	2273	2273	0	0	100.00	100.00	0.00
101	1865	1864	1	4	99.95	99.79	0.27
102	2187	2187	0	0	100.00	100.00	0.00
103	2084	2084	0	0	100.00	100.00	0.00
104	2229	2222	7	8	99.69	99.64	0.68
105	2572	2557	15	32	99.42	98.76	1.84
106	2027	2027	0	2	100.00	99.90	0.10
107	2137	2136	1	0	99.95	100.00	0.05
108	1763	1756	7	10	99.60	99.43	0.97
109	2532	2532	0	0	100.00	100.00	0.00
111	2124	2123	1	2	99.95	99.91	0.14
112	2539	2539	0	1	100.00	99.96	0.04
113	1795	1795	0	0	100.00	100.00	0.00
114	1879	1879	0	5	100.00	99.73	0.27
115	1953	1953	0	0	100.00	100.00	0.00
116	2412	2392	20	2	99.17	99.92	0.92
117	1535	1535	0	2	100.00	99.87	0.13
118	2278	2278	0	2	100.00	99.91	0.09
119	1987	1987	0	0	100.00	100.00	0.00
121	1863	1862	1	0	99.95	100.00	0.05
122	2476	2476	0	0	100.00	100.00	0.00
123	1518	1518	0	0	100.00	100.00	0.00
124	1619	1619	0	1	100.00	99.94	0.06
200	2601	2601	0	3	100.00	99.88	0.12
201	1963	1962	1	0	99.95	100.00	0.05
202	2136	2134	2	0	99.91	100.00	0.09
203	2980	2950	30	12	98.99	99.59	1.42
205	2656	2653	3	0	99.89	100.00	0.11
207	1860	1860	0	4	100.00	99.79	0.22
208	2955	2938	17	6	99.42	99.80	0.78
209	3005	3005	0	0	100.00	100.00	0.00
210	2650	2649	1	3	99.96	99.89	0.15
212	2748	2748	0	0	100.00	100.00	0.00
213	3251	3251	0	0	100.00	100.00	0.00
214	2262	2259	3	3	99.87	99.87	0.27
215	3363	3363	0	0	100.00	100.00	0.00
217	2208	2207	1	2	99.95	99.91	0.14
219	2154	2154	0	0	100.00	100.00	0.00
220	2048	2048	0	0	100.00	100.00	0.00
221	2427	2427	0	0	100.00	100.00	0.00
222	2483	2483	0	1	100.00	99.96	0.04
223	2605	2605	0	0	100.00	100.00	0.00
228	2053	2052	1	22	99.95	98.94	1.12
230	2256	2256	0	1	100.00	99.96	0.04
231	1571	1571	0	0	100.00	100.00	0.00
232	1780	1780	0	8	100.00	99.55	0.45
233	3079	3078	1	0	99.97	100.00	0.03
234	2753	2753	0	0	100.00	100.00	0.00
Overall	**109494**	**109381**	**113**	**136**	**99.90**	**99.88**	**0.23**

the preceding operations, including WTV minimisation, the P-wave amplitudes have not been significantly reduced. However, it can be seen in 5.10(c) that in the envelope obtained from lowpass filtering, the QRS complexes have much greater peak prominence in comparison to the P-waves; hence, the use of MPP criterion enables successful detection of the QRS complexes, without any false positives caused by the P-waves, even though the peak amplitudes in the envelope at P-wave locations exceed the threshold.

Fig. 5.11(a) shows a signal from record 104 which has severe muscular noise. It is seen in Fig. 5.11(b) that bandpass filtering is not able to suppress this noise completely because it spectrally overlaps with the QRS complexes. However, as seen in Fig. 5.11(c), WTV minimization very effectively suppresses this noise while preserving the QRS complexes. The regularization parameter λ is automatically adapted to a suitable value to remove

the higher amount of noise, because of the adaptation in (5.20).

Fig. 5.12(a) shows an ECG signal from record 203. This signal contains variations in QRS amplitudes and has an episode of ventricular tachycardia resulting in several PVCs in a row, and also a little muscular noise. Because of their lower frequency content, PVCs are reduced in amplitude by bandpass filtering. It is seen in 5.12(b) that again the regularisation parameter λ is automatically adapted to an appropriate value and the low amplitude QRS complexes as well as the PVCs are preserved and successfully detected.

In determining the various parameters of this algorithm, small subsets of the MIT-BIH database have been used, as described earlier in this section. In order to ensure that there is no bias, we evaluate the algorithm on records from two other databases. We choose 20 records from the European ST-T database and 20 records from the Fantasia database. In all these records, we have used the first one million samples (nearly 67 minutes) in the evaluation. No modification was required in the algorithm for application to these records. The results of the evaluation are given in Table-5.2 and Table-5.3, respectively. It can be seen that the algorithm gives over 99% average values of Se and P^+ values for these records also.

TABLE 5.2: Results for QRS detection on the European ST-T database

Record	Total Beats	TP	FN	FP	Se(%)	P+(%)	DER (%)
e0103	4068	4063	5	55	99.88	98.66	1.48
e0105	3698	3697	1	2	99.97	99.95	0.08
e0107	3952	3951	1	7	99.97	99.82	0.20
e0112	2989	2988	1	82	99.97	97.33	2.78
e0121	5290	5284	6	16	99.89	99.70	0.42
e0127	5089	5072	17	34	99.67	99.33	1.01
e0133	3702	3700	2	16	99.95	99.57	0.49
e0136	3841	3841	0	0	100.00	100.00	0.00
e0147	3535	3535	0	1	100.00	99.97	0.03
e0154	3927	3927	0	12	100.00	99.70	0.31
e0202	5615	5601	14	2	99.75	99.96	0.29
e0205	6058	5978	78	1	98.71	99.98	1.32
e0208	4852	4840	12	11	99.75	99.77	0.48
e0213	5982	5938	44	7	99.26	99.88	0.86
e0303	4834	4829	5	5	99.90	99.90	0.21
e0403	5173	5170	3	3	99.94	99.94	0.12
eo411	5355	5352	3	1	99.94	99.98	0.07
e0418	6299	6299	0	0	100.00	100.00	0.00
e0509	4552	4552	0	1	100.00	99.98	0.02
e0612	3592	3588	4	32	99.89	99.12	1.00
Overall	**92403**	**92205**	**196**	**288**	**99.82**	**99.63**	**0.56**

5.3.2 Real-time implementation

The algorithm takes a processing time of 0.020 s to process an ECG signal block of length 5000 samples (13.9 s) using the computer configuration mentioned earlier. Thus, the proposed algorithm is implementable in real time in block-by-block processing mode [113]. For non-real-time implementation of the proposed method, e.g. in a case where

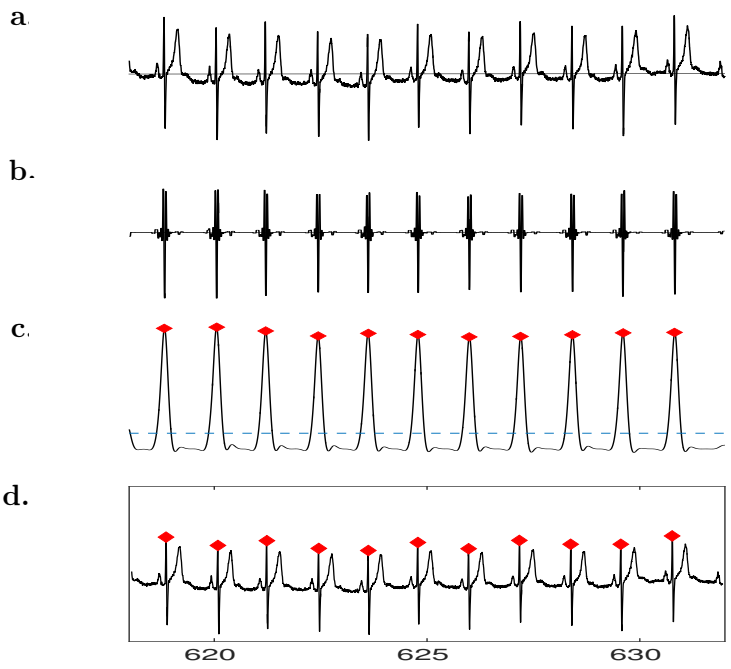

FIGURE 5.9: Outputs obtained at different stages of the algorithm for record 117 (618-632s).(a) The ECG signal (b) Output obtained by WTV minimisation (c) The envelope obtained using lowpass filtering and detected peaks (Threshold indicated by dashed line) and (d) The detected QRS complexes in the ECG.

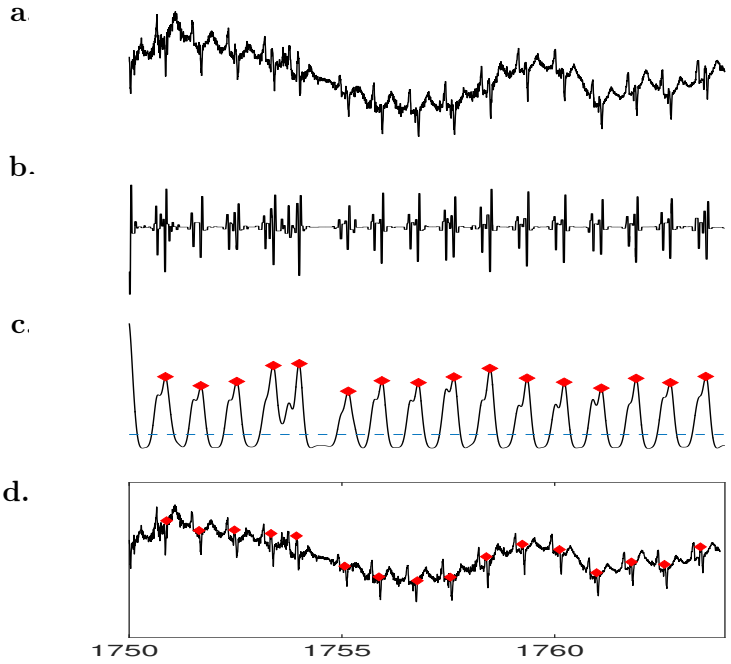

FIGURE 5.10: Outputs obtained at different stages of the algorithm for record 108 (1750-1764s).(a) The ECG signal (b) Output obtained by WTV minimisation (c) The envelope obtained using lowpass filtering and detected peaks (Threshold indicated by dashed line) and (d) The detected QRS complexes in the ECG.

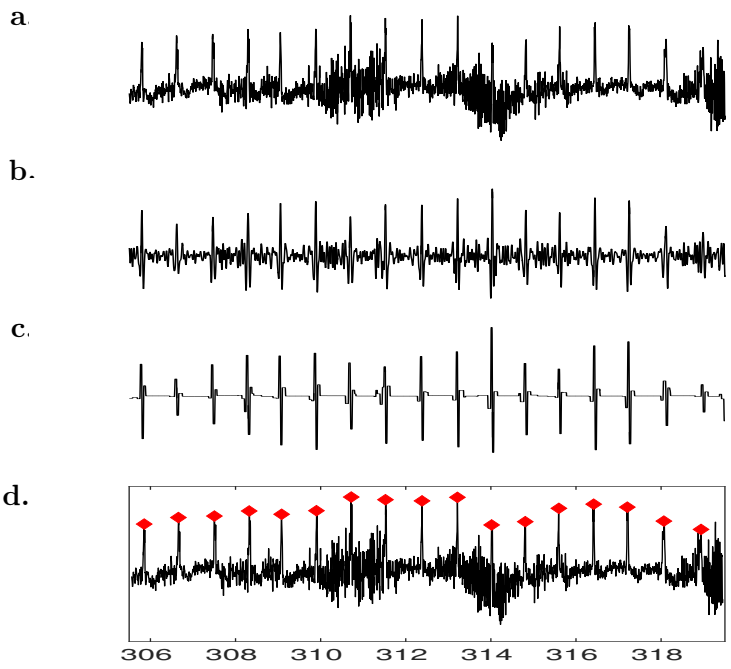

FIGURE 5.11: Outputs obtained at different stages of the algorithm for record 104 (305.5-319.5s). (a) The ECG signal (b) Output obtained by bandpass filtering (c) Output obtained by WTV minimisation and (d) The detected QRS complexes in the ECG.

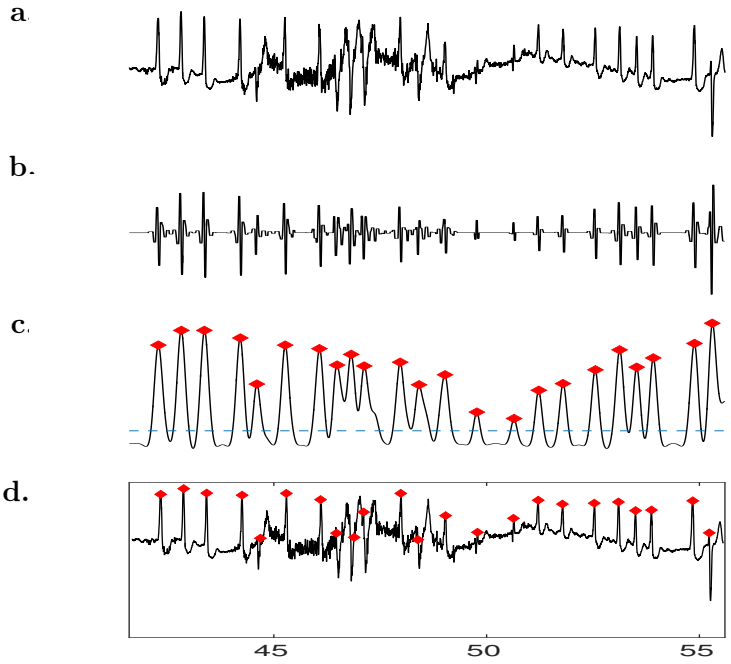

FIGURE 5.12: Outputs obtained at different stages of the algorithm for record 203 (41.6-55.6s). (a) The ECG signal (b) Output obtained by WTV minimisation (c) The envelope obtained using lowpass filtering and detected peaks (Threshold indicated by dashed line) and (d) The detected QRS complexes in the ECG.

TABLE 5.3: Results for QRS detection on the Fantasia database

Record	Total Beats	TP	FN	FP	Se(%)	P+(%)	DER (%)
f1o01	3986	3946	40	18	99.00	99.55	1.47
f1o02	3812	3812	0	74	100.00	98.10	1.94
f1o03	4045	4045	0	50	100.00	98.78	1.24
f1o05	3407	3404	3	16	99.91	99.53	0.56
f1o07	4025	4025	0	13	100.00	99.68	0.32
f1y01	4917	4917	0	12	100.00	99.76	0.24
f1y07	3378	3378	0	7	100.00	99.79	0.21
f1y08	4097	4096	1	23	99.98	99.44	0.59
f1y09	4507	4507	0	12	100.00	99.73	0.27
f1y10	4911	4911	0	12	100.00	99.76	0.24
f2o01	4216	4216	0	0	100.00	100.00	0.00
f2o02	3595	3592	3	2	99.92	99.94	0.14
f2o03	3766	3766	0	27	100.00	99.29	0.72
f2o04	3857	3857	0	0	100.00	100.00	0.00
f2o05	4929	4922	7	4	99.86	99.92	0.22
f2y01	4586	4586	0	14	100.00	99.70	0.31
f2y02	2807	2807	0	2	100.00	99.93	0.07
f2y03	3883	3882	1	26	99.97	99.33	0.70
f2y04	4939	4937	2	18	99.96	99.64	0.41
f2y05	5172	5150	22	4	99.57	99.92	0.50
Overall	**82835**	**82756**	**79**	**334**	**99.95**	**99.73**	**0.32**

a long record obtained from a Holter monitor is to be processed, the signal may be processed blockwise in the preprocessing stage, but in the peak detection stage it is preferable to use the entire signal to obtain the smooth envelope for peak detection, as done in obtaining the results in Table-5.1. If the peak detection is also done blockwise, as would be required in a real-time scenario, the number of false positives can be higher, because at block edges, two peaks may falsely be attributed to the same beat, in spite of the use of a blanking period of 200 ms. This is mostly prominent in cases of signals with tall and pointed P- and T-waves. This can be contrasted with the situation in a non-real-time scenario, where the entire signal is lowpass filtered and hence, all peaks corresponding to a QRS complex are merged into a single smooth pulse and in case of tall and pointed P- and T-waves, the MPP criterion helps in avoiding the false positives, as previously illustrated in Fig. 5.5 and also be observed in Fig. 5.10(c). On lowpass filtering, the P- and the T-waves would have a lower peak prominence and can be rejected by use of the MPP criterion. In the real-time case, the pointed P- and T- waves have higher peak prominence at the edges; therefore, the number of FPs is greater. In order to avoid missed detection of QRS complexes shared between two consecutive blocks, the signal is padded on both ends of the block with repeating boundary values before preprocessing. An illustration of how it helps in avoiding missed detection at the edges is shown in Fig.-5.13.

The overall Se, P^+ and DER values obtained for the real-time implementation of the proposed method are 99.86%, 99.85% and 0.29%, respectively. The results have been computed for $Th = MPP = 0.08$, the rest of the parameters being the same as in the offline implementation.

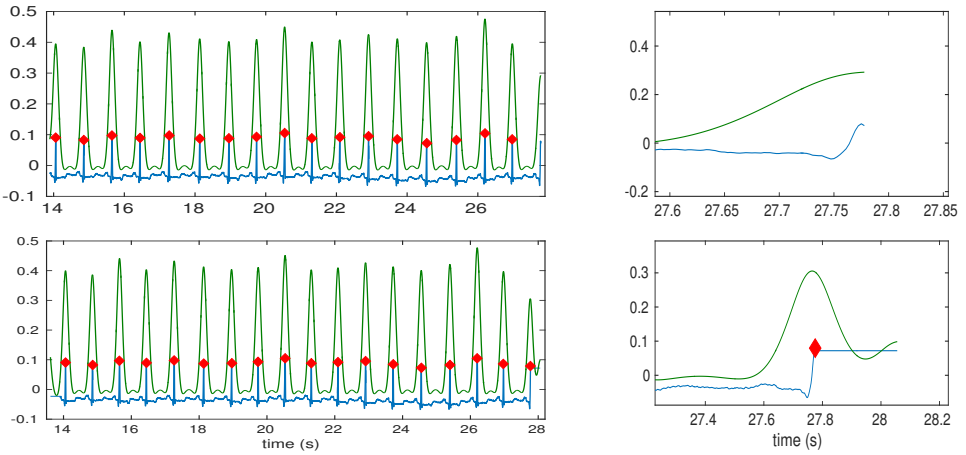

FIGURE 5.13: Top panel: (Left) ECG signal without padding, with the corresponding envelope signal overlaid and detected peaks indicated by diamond shaped markers. The last QRS complex is not detected. (Right) Enlarged view of the last partial QRS complex which goes undetected. Bottom panel: (Left) Padded ECG signal signal with the corresponding envelope signal overlaid and detected peaks indicated by diamond shaped markers. The last QRS complex is detected. (Right) Enlarged view of the last partial QRS complex which is detected.

5.4 Discussion

We compare the results of offline implementation of the proposed method with those of established and state-of-the-art techniques on MIT-BIH arrhythmia database in Table-5.4. It is seen that the proposed method gives improved results over all the referenced methods, except for [121]. The dataset used in [121], however, is significantly smaller [35].

The results of real-time implementation of the proposed method are compared with those of existing real-time methods in Table-5.5. It is observed that though the overall DER is higher than in the offline case, the results obtained using the proposed method are still better than those of the referenced methods, except for the sparse derivative denoising (SDD)-based technique in [35], with which the results are comparable. The algorithm in [35], however, takes a processing time of about 0.8 msec/sample, whereas the proposed method takes a processing time of just 4 μs/sample, on a processor slower than that used in [35]. Also, the offline implementation of the proposed method gives lower DER than [35], as shown in Table-5.4.

Thus, it can be concluded that the proposed work provides an improved method for fast and accurate offline and real-time automatic QRS detection.

TABLE 5.4: Comparison of results of the proposed method with those of existing methods on MIT-BIH arrhythmia database

Reference	Method	FN	FP	Se (%)	P+ (%)	DER (%)
Pan and Tompkins (1985) [21]	First derivative followed by squaring	277	507	99.54	99.75	0.71
Li et al (1995) [121]	Wavelet transform	112	65	99.89	99.94	0.15
Martinez et al (2004) [25]	Discrete wavelet transform	220	153	99.8	99.86	0.34
Chen et al (2006) [26]	Wavelet denoising and moving average filtering	459	529	99.55	99.49	0.96
Jung and Lee (2012) [39]	Singular value decomposition filter	581	579	99.47	99.47	1.05
Ning and Selesnick (2013) [35]	Sparse derivative denoising	138	127	99.87	99.88	0.24
Zidelmal et al (2014) [34]	S- transform and Shannon energy	171	97	99.84	99.91	0.25
Dohare et al (2014) [122]	Median filtering and sixth power of the signal	870	728	99.21	99.34	1.46
Bouaziz et al (2014) [123]	Discrete wavelet transform	140	232	99.87	99.79	0.34
Phukpattaranont (2015) [37]	Quadratic filtering	202	210	99.82	99.81	0.38
Castellas-Rufas and Carrabina (2015) [38]	Non-linear MaMeMi filter	614	353	99.43	99.67	0.88
Yochum et al (2016) [124]	Continuous wavelet transform	160	574	99.85	99.48	0.67
Farashi (2016) [120]	Multiresolution time-dependent entropy	163	273	99.75	99.85	0.39
Proposed method	Weighted total variation denoising	113	136	99.90	99.88	0.22

5.5 Conclusions

In this chapter, a novel technique for QRS detection which uses WTV denoising for preprocessing is proposed. The regularization parameter in WTV, which determines the amount of noise removed is varied adaptively in proportion to a local measure of noise. The weights are chosen so as to preserve the QRS complexes, while allowing greater smoothing of the P- and T-waves. In the peak detection stage, the signal is logarithmically transformed to equalize the QRS amplitudes, and then a smooth envelope is obtained in which the peaks are detected. Finally, the R-peak locations are determined in the ECG signal using the detected peak positions in the envelope as guides. The proposed method has the advantage of being computationally fast and both the offline and online implementations of the proposed method show improvement in detection accuracy over established and state-of-the-art methods.

TABLE 5.5: Comparison of real-time implementation of the proposed method with existing real-time methods on MIT-BIH arrhythmia database

Reference	**Method**	**FN**	**FP**	**Se (%)**	**P+ (%)**	**DER (%)**
Pan and Tompkins (1985) [21]	First derivative followed by squaring	277	507	99.54	99.75	0.71
Chen et al (2006) [26]	Wavelet denoising and moving average filtering	459	529	99.55	99.49	0.96
Ning and Selesnick (2013)[35]	Sparse derivative denoising	138	127	99.87	99.88	0.24
Dohare et al (2014) [122]	Median filtering and sixth power of the signal	870	728	99.21	99.34	1.46
Castellas-Rufas and Carrabina (2015) [38]	Non-linear MaMeMi filter	614	353	99.43	99.67	0.88
Farashi (2016) [120]	Multiresolution time-dependent entropy	163	273	99.75	99.85	0.39
Proposed method	Weighted total variation denoising	156	165	99.86	99.85	0.29

In this work, the Teager-Kaiser energy of the difference signal has been used as weights; however, WTV minimization is a general framework of denoising and with some other choice of weights, even better results could be obtained. In the real-time implementation of the proposed method, greater false positives occur at the block edges in records with pointed P- and T-waves, as compared to the offline implementation. If these waves could be diminished to a greater degree relative to the QRS complexes, by use of some morphological feature based weights, for example, better detection accuracies can be achieved.

Chapter 6

ECG Classification Using Discrete Signal Processing on Graphs

6.1 Introduction

After segmentation of the ECG into beats, with each beat extracted using a fiducial mark, which is typically the R-peak, the final step in automatic ECG-based heartbeat classification is to categorize each beat into one of the known categories, so as to make a diagnostic decision. As mentioned earlier, many cardiovascular conditions can be diagnosed through their signature ECG patterns. For example, the ECG can be used to detect the presence of arrhythmias. While some arrhythmias are benign, some are life threatening. Also, some arrhythmias occur infrequently; therefore, long term monitoring is required to diagnose them. As discussed earlier, manual analysis of long-term ECG is a tedious task and is prone to errors. Therefore, there is a strong need for automatic ECG classification.

The various types of arrhythmias have already been discussed in detail in Chapter-2. Also, it was highlighted that although many ECG feature extraction schemes have been proposed in the literature, lesser attention has been paid on exploring new methods of classification. Most of the recent methods for ECG classification use SVM as classifier [47, 57–64, 83] . In this chapter, we propose a new method for arrhythmia classification, in which we use a graph-based classifier. We use PCA to reduce the dimensionality of the raw beats, on which no preprocessing is applied. The transformed input beats of reduced dimensionality are combined with the RR-interval information to form the input vectors to be classified. These input vectors are used to build a K-nearest neighbor graph on the basis of their similarities. This graph-based classifier is used to determine the labels of the unlabeled beats. The performance of the proposed method is compared to that

of other techniques that use more sophisticated features. Also, the performance of the graph-based classifier is compared to SVMs, using the same inputs.

The rest of this chapter is organized as follows. In Secction 6.2, we present a brief review of discrete signal processing (DSP) on graphs, considering only the concepts that are relevant to this work. In Section 6.3, we describe the data used for evaluation of the proposed method and give details of the methodology adopted. In Section 6.4, we describe the obtained results and finally, the chapter is concluded in Section 6.5.

6.2 Review of discrete signal processing on graphs

6.2.1 Preliminaries

DSP on graphs is an emerging novel framework of signal processing, in which a dataset is represented as a signal indexed by a graph $G = (\mathcal{V}, \mathbf{A})$, where $\mathcal{V} = \{v_0, ..., v_{N-1}\}$ is the set of nodes and $\mathbf{A}$ is the weighted adjacency matrix of the graph [125]. Each data element is indexed by the node v_n and each weight $\mathbf{A}_{n,m}$ of a directed edge from v_m to v_n reflects the similarity or dependency between the two data elements. The dataset is represented as a *graph signal* indexed by the graph G. The graph signal is defined as a map from the set of nodes $\mathcal{V}$ to the set of complex numbers $\mathbb{C}$ [125]:

$$\mathbf{s} : \mathcal{V} \rightarrow \mathbb{C} \tag{6.1}$$

$$v_n \rightarrow s_n.$$

We can also write graph signals as vectors:

$$\mathbf{s} = [s_0 \; s_1 \; ... \; s_{N-1}]^T \in \mathbb{C}^N \tag{6.2}$$

Graph filters and graph shift

A graph filter can be defined as a system $\mathbf{H}(\cdot)$ that takes a graph signal $\mathbf{s}$ as input and produces the output graph signal $\tilde{\mathbf{s}} = \mathbf{H}(\mathbf{s})$. An example of a basic nontrivial filter is the *graph shift*, which can be interpreted as a local operation that replaces a signal value s_n at node v_n with the linear combination of neighboring values of node v_n [126]:

$$\tilde{s_n} = \sum_{m \in \mathcal{N}_n} \mathbf{A}_{n,m} s_m \tag{6.3}$$

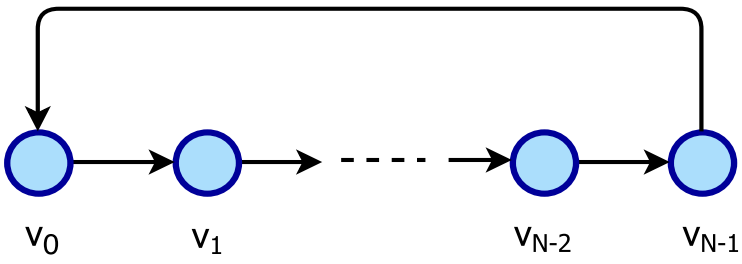

FIGURE 6.1: Graph representation of a finite discrete periodic time series of length N

Thus, the output of the graph shift can be expressed as the product of the input signal and the adjacency matrix of the graph:

$$\tilde{\mathbf{s}} = [s_0 \; s_1 \; ... \; s_{N-1}]^T = \mathbf{A}\mathbf{s}. \tag{6.4}$$

The operation of graph shift is the basic building block of DSP on graphs.

In the DSP on graph framework, a finite (or periodic) time series can be represented as a directed acyclic graph, as shown in Fig. 6.1. The adjacency matrix of this graph is a $N \times N$ circulant matrix, given by

$$\mathbf{A} = \mathbf{C}_N = \begin{bmatrix} & & & 1 \\ 1 & & & \\ & \ddots & & \\ & & & 1 \end{bmatrix}, \tag{6.5}$$

On substituting (6.5) into (6.4), we obtain the standard time-delay, given by

$$\tilde{s}_n = s_{(n-1) \bmod N}, \tag{6.6}$$

which can be represented in vector-matrix notation as

$$\tilde{\mathbf{s}} = \mathbf{C}_N \, \mathbf{s}. \tag{6.7}$$

6.2.2 Total variation on graphs

In case of graph signals, the total variation can be defined based on graph shift [126]. According to classical DSP, the total variation of a signal $\mathbf{s}$ would be expressed as

$$TV(\mathbf{s}) = \sum_{n} |s_n - s_{n-1}|. \tag{6.8}$$

In case of a finite time series, the periodicity condition $s_n = s_{n \bmod N}$ gives the following definition [126]:

$$TV(\mathbf{s}) = \sum_{n=0}^{N-1} |s_n - s_{n-1 \bmod N}|. \tag{6.9}$$

In (6.9), TV compares a signal $\mathbf{s}$ to its shifted version. The higher this difference, the greater the TV. Using (6.6), (6.9) can be written as

$$TV(\mathbf{s}) = \|\mathbf{s} - \mathbf{C}\mathbf{s}\|_1 \tag{6.10}$$

Just as TV in time measures the cumulative difference between consecutive signal samples, the TV on graph measures the cumulative difference between a signal value at each node in the graph and the values at its neighbors.

6.2.3 Classification via regularization on graphs

In [125], Sandryhaila and Moura have proposed a classification algorithm based on TV regularization of graph signals. In this section, we describe the key concept on which this algorithm is based.

Let $G = (\mathcal{V}, \mathbf{A})$ denote a graph with N nodes, representing a dataset with N elements. Two nodes are connected with each other if the corresponding elements are similar. The labels or categories for this dataset form a graph signal, which is indexed by the graph vertices. We first consider the binary classification case, in which the labels can take only two possible values, viz. +1 and -1. The known labels form a signal $\mathbf{s}^{(known)}$, with values

$$s_n^{known} = \begin{cases} +1, & n^{th}\text{element belongs to class 1} \\ -1, & n^{th}\text{element belongs to class 2} \\ 0, & \text{class is unknown.} \end{cases} \tag{6.11}$$

Now, in the graph G, since elements are connected if they are similar to each other and also, since similar elements tend to belong to the same category, therefore, it can be expected that the class labels form a graph signal that does not vary fast from node

to node, i.e., has low total variation. Thus, the predicted labels can be defined as the solution to the optimization problem [125]

$$\mathbf{s}^{\text{predicted}} = \arg\min_{\mathbf{s}\in\mathbb{R}^N} TV_G(\mathbf{s}), \tag{6.12}$$

subject to the constraint that very few of the known labels should be assigned to the wrong class, where $TV_G(\mathbf{s})$ denotes the total variation of the graph G. Thus, the predicted labels can be found assuming that the labels form a graph signal with minimum total variation.

After determining the predicted signal $\mathbf{s}^{(predicted)}$, the unlabeled data elements are assigned to one of the classes by comparing each $s_n^{(predicted)}$ against threshold zero, i.e. if $s_n^{(predicted)} > 0$, then it is assigned class label +1, otherwise class label -1.

6.3 Materials and methods

6.3.1 Data

For evaluation of the proposed method, we have used the MIT-BIH arrhythmia database [106], which is the standard database for evaluation of arrhythmia detection algorithms. This database has been described earlier in the previous chapters. We have used the MLII recordings from this database for evaluation of the proposed method. The database has 110109 beat labels in total, each belonging to one of the 16 arrhythmia classes, as listed in Table-6.1. A certain percentage of beats was chosen from each of the 16 classes to constitute the training set, whereas the rest of the beats were used to test the proposed method. As shown in Table-6.1, the training set comprises 12% of normal beats, which constitute the largest class in the database. From the left bundle branch block, right bundle branch block, atrial premature contractions, premature ventricular contractions and paced categories, 30% of the beats have been used. From the remaining smaller classes, 50% of the beats have been used. The class labels provided with the database are used as the ground truth.

6.3.2 ECG segmentation

For segmentation of the ECG into beats, we use the QRS annotations provided with the database. We do not use an existing QRS detection algorithm here, because no algorithm has 100% accuracy and we want to use all the beats in the evaluation of the proposed method. For segmentation of the ECG into beats, we take 100 samples preceding and

TABLE 6.1: Training and test data selection from the MIT-BIH arrhythmia database

Beat type	**Annotation**	**Total beats**	**Training %**	**Training beats**	**Test beats**
Normal	N	75017	12.00%	9013	66004
Left bundle branch block	L	8072	30.00%	2422	5650
Right bundle branch block	R	7255	30.00%	2177	5078
Atrial premature contraction	A	2546	30.00%	764	1782
Premature ventricular contraction	V	7129	30.00%	2139	4990
Paced beat	/	7024	30.00%	2108	4916
Aberrated atrial premature beat	a	150	50.00%	75	75
Ventricular flutter	!	472	50.00%	236	236
Fusion of Ventricular and normal beat	F	802	50.00%	401	401
Blocked atrial premature beat	x	193	50.00%	97	96
Nodal	j	229	50.00%	115	114
Fusion of p[aced and normal beat	f	982	50.00%	491	491
Ventricular escape beat	E	106	50.00%	53	53
Nodal premature beat	J	83	50.00%	42	41
Atrial escape beat	e	16	50.00%	8	8
Unclassifiable beat	Q	33	50.00%	17	16

including the R-peak as the pre-R segment and 200 samples after the R-peak as the post-R segment, following [83].

6.3.3 Dimensionality reduction and combining dynamic information

We do not apply any preprocessing to the extracted beat segments. We only apply PCA to reduce the dimensionality of the raw beats. We choose the first 30 principal components (PCs) that account for 99.44% variance. The remaining PCs mainly correspond to noise and are discarded. This dimensionality reduction is necessary to reduce the computational cost in creating the graph.

Since arrhythmia affects not only beat morphology, but also the heart rhythm, we also use the dynamic information along with the morphological information. To obtain the dynamic information, we compute the previous and the post RR interval for each beat, along with the local and the average RR interval. The local RR interval is computed as the average of the RR intervals in the last 5 seconds. On the other hand, the average RR interval is computed as the average of the RR intervals in the last 5 minutes. These four RR interval-based features are first computed for each beat, and then standardized to have mean zero and standard deviation 1. These are then combined with the PCA transformed raw beats to form 34 dimensional input vectors.

6.3.4 Classification using graph

We use the input vectors to create a K-nearest neighbor graph, in which each 34-dimensional input vector is connected to its K nearest neighbors. In constructing the graph, we used the city block distance as the measure of similarity. When two input vectors represented by nodes v_m and v_n are connected, the connecting edge is assigned the weight

$$\mathbf{A}_{n.m} = e^{(-d_{n,m}/\sigma)}, \tag{6.13}$$

where $d_{n,m}$ is the city block distance between the input vectors and σ is the variance of the distance kernel, which has been set equal to the mean of the distances between all connected nearest neighbours.

In Section 2.2.3, binary classification using TV regularization on graph was described. This approach can be extended to multiclass classification by carrying out one-against-all classification for each class [125]; i.e. when one class is being considered, the rest of the classes are all assigned to one other class.

The predicted labels are determined as the solution to the optimization problem

$$\mathbf{s}^{\text{predicted}} = \arg\min_{\mathbf{s}\in\mathbb{R}^N} \frac{1}{2}\|\mathbf{s}^{known} - \mathbf{s}\|_2^2 + TV_G(\mathbf{s}), \tag{6.14}$$

where the first term, which is the data fidelity term imposes the constraint that the predicted signal should be close to the initial signal. In (6.14), equal weights have been given to the data fidelity and the regularization terms.

6.4 Results

The proposed method is applied to the data as described in Table-6.1. In implementation of the proposed method, the graph signal processing toolbox available at `https://lts2.epfl.ch/gsp/` was very helpful. Fig. 6.2 shows the graph representation of the ECG data using K nearest neighbour graph with K=10. Only the nodes are indicated in the figure; the edges have been omitted for better clarity. The top graph shows all the dataset labels (test and train samples). Blue verices indicate label -1 and red vertices indicate label +1. In the middle graph, the test verices are set to zero and are indicated by green. These missing values are to be predicted by the proposed method. The bottom figure shows the solution obtained by the proposed method. The missing values have

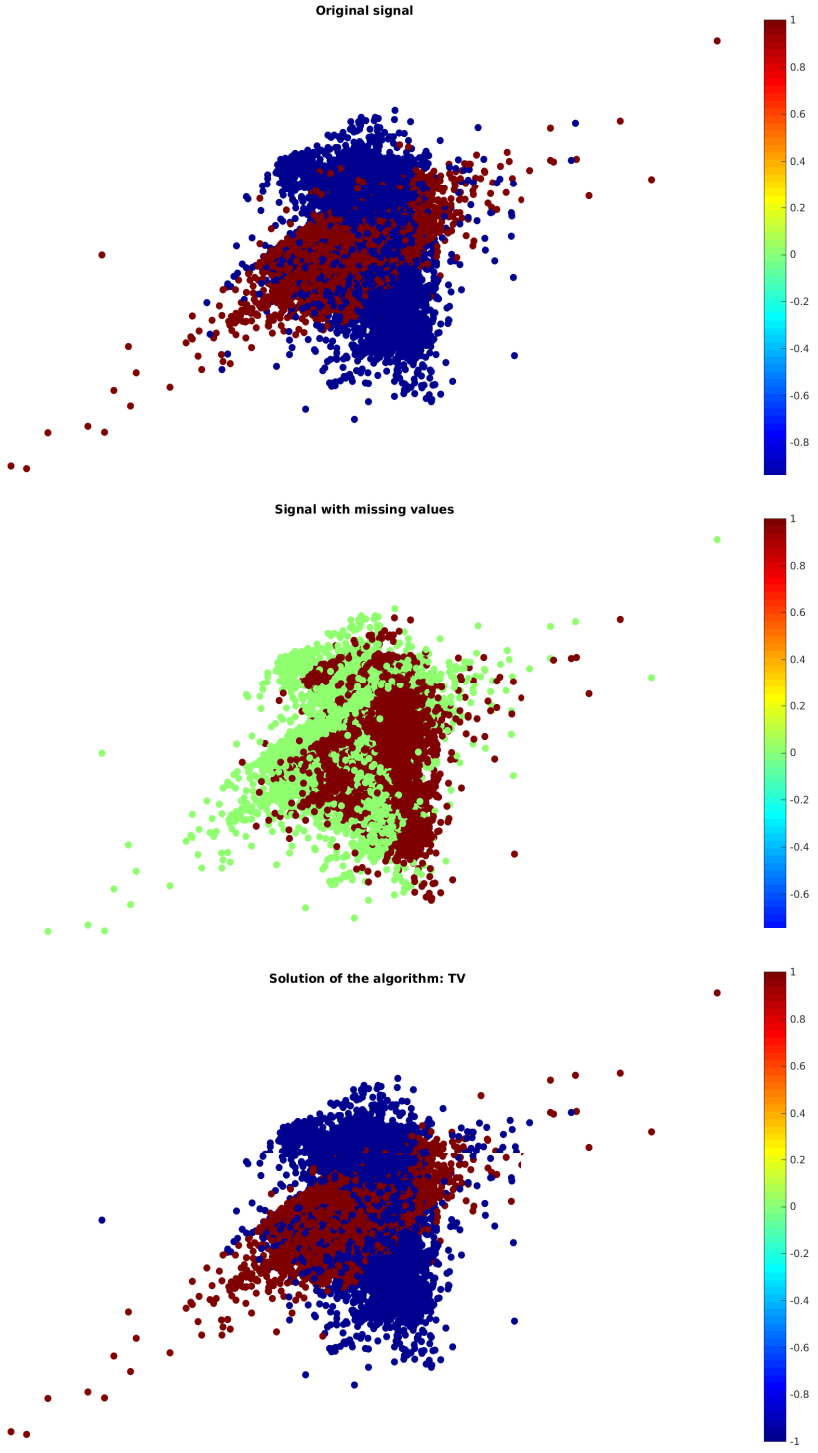

FIGURE 6.2: Graph representation of the ECG data using K nearest neighbour graph with K=10. Only the vertices are indicated; the edges have been omitted for better clarity. Top: Graph representation of the complete dataset (test and train samples). Blue vertices indicate label -1 and red vertices indicate label +1. Middle: The test verices are set to zero and are indicated by green. Bottom: The solution obtained by the proposed method. The missing values have been replaced by the predicted values. It is seen that it resembles the graph in the top figure quite closely.

TABLE 6.2: Accuracies obtained for different neighborhood sizes in the K-nearest neighbor graph

Beat type	**Accuracy** (%)		
	K=3	**K=10**	**K=30**
Normal	88.15	95.59	96.55
Aberrated atrial premature beat	98.27	99.92	99.92
Atrial escape beat	98.66	99.99	99.99
Blocked atrial premature beat	98.64	99.97	99.97
Fusion of Ventricular and normal beat	94.53	99.50	99.68
Fusion of paced and normal beat	96.11	97.16	96.94
Left bundle branch block	95.98	97.52	95.75
Nodal	98.54	99.87	99.87
Atrial premature contraction	96.69	98.49	98.21
Nodal premature beat	98.82	99.45	99.72
Paced beat	95.74	96.86	97.10
Premature ventricular contraction	95.03	99.22	97.97
Unclassifiable beat	95.44	98.35	99.84
Right bundle branch block	94.42	96.85	98.12
Ventricular escape beat	96.11	99.88	99.89
Ventricular flutter	96.10	99.88	99.81
Average	**96.08**	**98.66**	**98.71**

been replaced by the predicted values. It is seen that it resembles the graph in the top figure quite closely. The classification accuracies obtained using different neighborhood sizes K in the graph are tabulated in Table-6.2. It is observed that as K is increased from 3 to 10, there is a relatively large increase in average accuracy. However, on further increasing K to 30, the average accuracy increases only slightly. It may be noted that as K is increased, the processing time also increases.

We compare the average classification accuracy obtained using the proposed method to those of other techniques in Table-6.3. It is seen that the proposed method gives comparable results to techniques that use more sophisticated and a combination of features.

It would also be interesting to compare the accuracy obtained using the proposed methods to that obtained using SVM with the same input vectors. We obtained an average classification accuracy of 96.53 % using an SVM, with the same data, which is 2.18 % lesser than that obtained using the proposed method.

TABLE 6.3: Comparison of the proposed method with other methods

Reference	**Method**	**Accuracy** (%)
Osowski et al [47]	HOS+Hermite+SVM	98.18
Jiang et al [127]	Wavelet+ICA+SVM	98.86
Ye Can et al [83]	Wavelet +ICA+RR	99.30
Raj and Ray [128]	DCT-Based DOST+PSO optimized SVM	98.82
Proposed method	PCA+Graph-based classification	**98.71**

6.5 Conclusions

In this chapter, a classification using a graph-based classifier was proposed. The raw beats were reduced in dimensionality using PCA. The transformed input vectors were combined with the RR interval information to form the input vectors, which were used to construct a K-nearest neighbor graph. The inputs with known categories were assigned the labels +1 and -1, whereas the inputs belonging to unknown categories were assigned label 0. The unknown labels were predicted by finding a smooth graph signal, by regularizing the total variation. The resultant classifier was evaluated on the standard MIT-BIH arrhythmia database. The average classification accuracy obtained using the proposed method is quite close to that obtained using sophisticated features. Additionally, the proposed method gives higher classification accuracy then SVM, for the same inputs.

Chapter 7

Power Line Interference Removal from ECG Signals Using Wavelet Transform based Component-Retrieval

7.1 Overview

During the process of recording and transmission, the ECG signal gets contaminated with various kinds of noise and artefacts, such as power line interference (PLI). PLI is a high frequency additive noise, which occurs because of coupling of power line frequency (50 or 60 Hz) with the signal carrying cables. Usually, the power line frequency is not constant but exhibits variations about the nominal frequency. This kind of noise can mask the finer details of the ECG signal and a strong PLI can completely overwhelm the underlying ECG signal, making signal interpretation impossible. It can also lead to incorrect delineation of wave boundaries and erroneous RR interval measurement [129, 130]. Thus, for reliable interpretation of the ECG by a cardiologist or for further processing by an automatic system, say, a QRS detector, delineator or classifier, it is important to obtain a clean ECG signal.

According to the American Heart Association (AHA) recommendations, most of the diagnostic information in the ECG is contained in frequencies up to 100 Hz in adults, the lower bound being at 0.05 Hz [131]. Thus, 50/60 Hz PLI removal without causing distortion to the underlying ECG signal is challenging because of the overlapping spectra.

It is observed that the PLI component appears in the form of a ridge in the time-frequency representation (TFR) of the contaminated ECG signal. The ridge is actually a sequence of closely spaced amplitude peaks of the WT coefficients. In [100], Daubechies et al used the frequency reassignment technique of synchrosqueezing to enhance the resolution of the TFR. In the reassigned TFR, the signal components appear as concentrated curves due to the reduced smearing. The transform is still invertible after synchrosqueezing, therefore, for retrieval of any signal component, integration of the coefficients can be performed around the ridge. The synchrosqueezed wavelet transform (SSWT) was further analyzed in [90] and the method used for ridge retrieval was based on a standard least-squares ridge estimation technique [132]. In [67], Meignen et al proposed a new fully automatic method for retrieval of components from a multicomponent signal, hereafter called the RCM algorithm, using ideas from the synchrosqueezing framework. Though the technique was based on ideas from the synchrosqueezing framework, it however used the WT instead of SSWT. It was shown that the method of ridge retrieval used in the RCM algorithm is both more accurate and computationally less demanding than the classical method of ridge-searching in the time-frequency plane [132], which was used in [90]. Also, the technique is fully automatic. We use this technique to remove the PLI component from ECG signals.

The advantage of this proposed approach over fixed notch filters is that it can filter out the PLI even in case of variations in the power line frequency. In comparison to adaptive filters, it does not suffer from issues such as slow convergence rate and requirement of an external reference signal. Two quantitative performance evaluation parameters are used to assess the performance of the proposed technique in two worst-case scenarios and significant improvement as compared to these techniques is seen.

The remainder of this chapter is organized as follows. Section 7.2 gives a brief review of the RCM algorithm and Section 7.3 describes the proposed method. In Section 7.4, the results are discussed. Finally, the paper is concluded in Section 7.5.

7.2 Review of the RCM algorithm

In this section, we give an overview of the RCM algorithm [67]. The purpose of the RCM algorithm is to retrieve components from the wavelet representation. The algorithm first computes the wavelet transform. For $s \in L^2(\mathbb{R})$, the continuous wavelet transform (WT) is defined as

$$W_s\,(a,\ t) = \int_{\mathbb{R}} s(x) \frac{1}{a} \overline{\Psi\left(\frac{x-t}{a}\right)}\, dx, \tag{7.1}$$

where a denotes the scale parameter and $\psi \in L2(\mathbb{R})$ is the appropriately chosen mother wavelet function which satisfies the condition

$$\int_0^\infty \frac{\left|\hat{\Psi}(\xi)\right|^2}{\xi} d\xi < \infty, \tag{7.2}$$

where $\hat{\Psi}(\xi)$ denotes the Fourier transform of $\Psi(t)$. It may be noted that the normalization in 7.1 is different from that commonly used for WT. For discretization, the WT of the sampled signal can be computed at the discrete scales $a_j = 2^{j/n_v}\,\Delta t$, with $j = 0,\ ...,\ Ln_v - 1$, where Δt is the time span equal to the sampling period and n_v is the voice number or number of scales per octave. The total number of scales considered is therefore $n_a = Ln_v$. The RCM algorithm aims at retrieving the components s_k of a multicomponent signal $s$of the form

$$s(t) = \sum_{k=1}^{K} A_k(t)\cos(2\pi\phi_k(t)) = \sum_{k=1}^{K} s_k(t), \tag{7.3}$$

where $A_k(t) > 0$ and $\phi'_k(t) > 0$. The RCM algorithm retrieves the components s_k by identifying the corresponding ridges from the magnitude of the WT and then reconstructing them by using the information in the vicinity of these ridges. It consists of the following three steps:

Step-1: *Automatic determination of the number of modes*

First, the number of modes N_s is to be calculated. For this, the following set is defined [67]:

$$C_s(\gamma,\ t) = \{j,\ |W_s(a_j,\ t)| < \gamma \text{ and } |W_s(a_{j+1},\ t)| > \gamma\}, \tag{7.4}$$

where j denotes the scale number, γ is a threshold chosen from a range of choices belonging to the set $\Gamma(t)$, which is described later. Alternatively, the set

$$\{j, |W_s(a_j,\ t)| > \gamma \text{ and } |W_s(a_{j+1},\ t)| < \gamma\} \tag{7.5}$$

could also have been chosen. Since a mode appears in the WT in the form of a ridge, therefore givenγ, a mode for a given time t is associated with a set of successive scales a_j such that $|W_s(a_j,\ t)| > \gamma$ and is associated with an index j_0 in the set $C_s(\gamma,\ t)$. First, an estimated number of modes $M_s(t)$ at time t can be calculated as the most frequent number of modes detected as γ varies in t. Mathematically, this can be expressed as [67]

$$M_s(t) = \arg\max_N \left\{ \sum_{\gamma\in\Gamma(t)} \delta_{N,\ \#(C_s(\gamma,\ t))} \right\}, \tag{7.6}$$

where $\#(\cdot)$ denotes the operation of determining cardinality and $\delta_{a,\,b} = 1$ if $a = b$, 0 otherwise. The number of modes can then be determined as the most frequently occurring number of modes over all times t as

$$N_s = \arg\max_{N} \left\{ \sum_{t \in T} \delta_{N,\, M_s(t)} \right\}, \tag{7.7}$$

Step-2: *Determination of wavelet threshold*

For the sets

$$B_0(t) = \{\gamma \in \ \Gamma(t),\ \text{s.t.} \#(\mathrm{C}_s(\gamma,\, t)) = N_s\}, \tag{7.8}$$

let T_0 denote the associated times t. A threshold $\hat{\gamma}(t)$ for the WT and t in T_0 is then computed as [67]

$$\hat{\gamma}(t) = \text{median}(B_0(t)). \tag{7.9}$$

It can be shown [6] that if the range for $\Gamma(t)$ is appropriately chosen as $\Gamma(t)_{\min} < \min_i |W_s(a^i,\ t)|$ and $\Gamma(t)_{\max}(t) = \max_i |W_s(a^i,\ t)|$, where (a^i) are the N_s maxima in $a \rightarrow\ |W_s(a,\, t)|$, then A_0 will be a non-empty set.

Step-3: *Modes Retrieval*

For a time $t \in T_0$, let $N_{\hat{\gamma}}(t) = \#Cs(\hat{\gamma}(t),\ t)$. The sets of integers $I_k(t),\ 1 \leq\ k \leq\ N_{\hat{\gamma}}(t)$ are defined as follows [67]

$$\begin{gathered} I_k(t) = \{j_k,\ \ldots\ ,\ J_k(t)\} \text{ s.t. } \forall j_k(t) \leq j \leq J_k(t) \\ |W_s(a_j,\ t)| > \hat{\gamma}(t)\ |W_s(a_{j_k(t)\,-\,1}, t)|\ \hat{\gamma}(t) \\ \text{and } |W_s(a_{J_k(t)\,+\,1}, t)|\ \hat{\gamma}(t)\ ,\ j_k(t)\ j_{k+1}(t). \end{gathered} \tag{7.10}$$

Thus, each set $I_k(t)$ comprises indices corresponding to scales which can be associated with one of the modes when $t \in T_0$, because $N_{\hat{\gamma}}(t) = N_s$ in that case. For each t in T_0, the set $I_{N_s\,-\,k\,+\,1}(t)$ can be used to reconstruct the k^{th} mode as

$$s_k(t) \approx \frac{2}{C_\Psi} \left[\sum_{j\ \in\ I_{N_s\,-\,k\,+\,1}(t)} W_s(a_j,\ t) \frac{log(2)}{n_v} \right]. \tag{7.11}$$

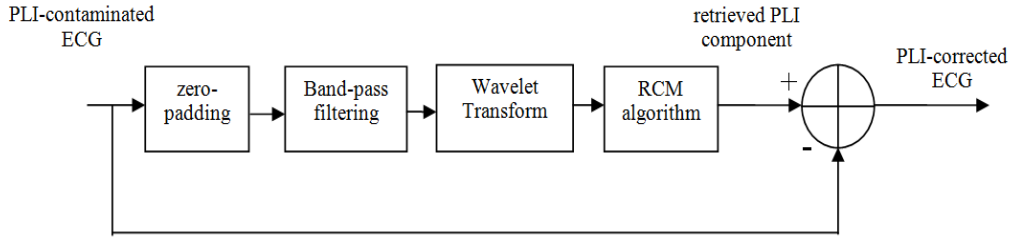

FIGURE 7.1: A schematic representation of the proposed method for PLI removal

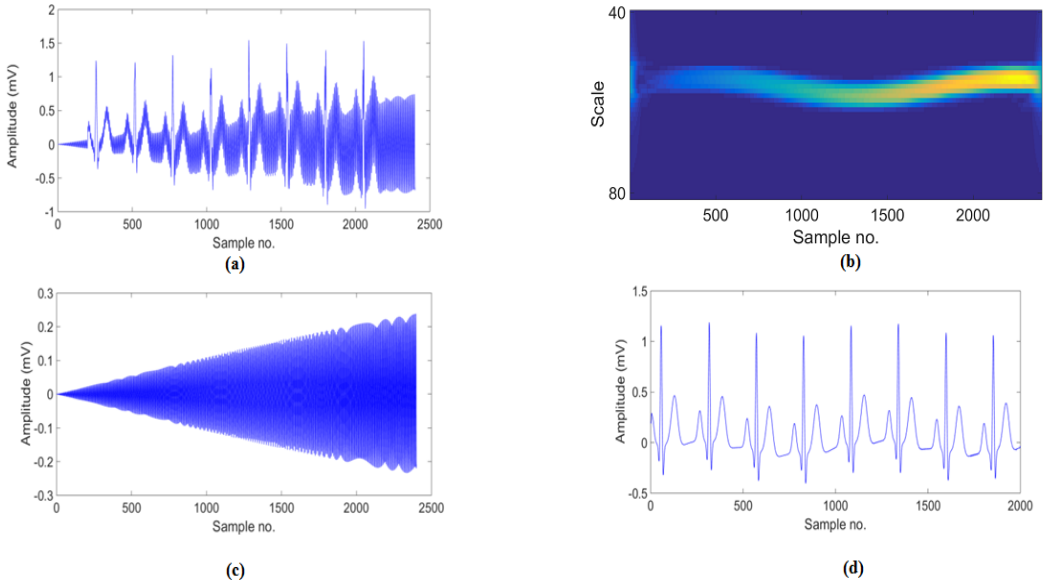

FIGURE 7.2: (a) ECG signal contaminated with PLI of time-varying amplitude and frequency (b) WT magnitude of the band pass filtered ECG obtained using bump wavelet with parameters and . (c) retrieved PLI component using the RCM algorithm and (d) PLI corrected signal obtained by subtracting the retrieved component from the contaminated signal.

7.3 The proposed method

The frequency of PLI is not constant, but actually varies in time about the nominal frequency (50 or 60 Hz). The objective of the proposed method is to remove PLI of nominal frequency 50 Hz from ECG signals. We have focused on 50 Hz PLI, because it is more in-band, i.e. closer to the dominant ECG frequencies, and hence more challenging to remove without causing distortion to the underlying signal. The PLI signal can be modeled as a component of the form $s_k(t) = A_k(t)\cos(2\pi\phi_k(t))$, i.e., a signal with time-varying frequency and amplitude. Consequently, the RCM algorithm described in the previous subsection can be used to retrieve this component. This can be done using two possible approaches. In the first approach, the WT of the contaminated signal can be computed over the scales corresponding to the PLI frequencies and the RCM algorithm can be used to retrieve the PLI component. In the second approach, the contaminated ECG signal can be band-pass filtered with the pass- band equal to the range of PLI

frequencies and then its WT can be computed at the corresponding scales followed by component retrieval using RCM algorithm. These two approaches may appear similar, but in practice, the second approach is more preferable, because some ECG morphologies contribute WT coefficients of comparable magnitude in the vicinity of the ridge, which can cause difficulty in PLI component retrieval. The proposed scheme for PLI removal is depicted in Figure 7.1. The PLI-contaminated ECG signal is first zero padded on both ends to exclude boundary effects. The signal is then band pass filtered around the PLI frequency, with bandwidth chosen so as to accommodate possible PLI frequency variations. In this work, we choose the bandwidth as 47-53 Hz. Subsequently, the WT of the zero-padded signal $s(t)$ is computed using an appropriate mother wavelet over scales corresponding to the same frequency range. We choose the bump wavelet as the mother wavelet which has the Fourier transform

$$\widehat{\Psi}(\xi) = e^{1-\frac{1}{1-\left(\frac{\xi-\mu}{\sigma}\right)^2}} \chi_{[\mu-\sigma,\mu+\sigma]}, \tag{7.12}$$

where, χ_I denotes the indicator function of set I. This wavelet admits the peak frequency $\xi_\Psi = \mu$ and is supported in the frequency range $[\mu-\sigma,\ \mu+\sigma]$. It has been chosen because it has a relatively smaller frequency support, therefore, better frequency localization of the ridge can be achieved. The optimal parameters of this wavelet are determined experimentally, as described in the subsequent section. Next, the PLI component is retrieved from the WT using the RCM algorithm. As the algorithm is fully automatic, no optimisation of parameters is required. The retrieved PLI component is now subtracted from the contaminated signal, to obtain the PLI-corrected ECG signal. For illustration, Fig. 7.2(a) shows an ECG signal contaminated with simulated PLI. The ECG signal is generated using the ECG-simulator [133] available on `www.physionet.org`. The PLI is simulated as a sinusoidal signal with time-varying frequency and amplitude, the nominal frequency being 50 Hz. The WT magnitude of the band pass filtered ECG obtained using the bump wavelet with parameters $\sigma = 0.4$ and $\mu = 5$ is shown in Fig. 7.2(b). The ridge due to PLI can be seen. Fig. 7.2(c) shows the PLI component retrieved using the RCM algorithm and Fig. 7.2(d) shows the PLI-corrected signal obtained by subtracting the retrieved component from the contaminated ECG signal.

7.4 Simulation results and discussion

7.4.1 ECG Data

The ECG signals used in this work are taken from the MIT-BIH Arrhythmia database. The ECG recordings in this database have a sampling rate of 360 samples per second

and duration of 30 minutes each. A total of 30 records from this database are used in this work, from which segments of normal and pathological beat types of length 5000 samples each are obtained. The pathological signals correspond to left bundle branch block (LBBB), right bundle branch block, premature ventricular contraction and atrial premature beats.

7.4.2 PLI Simulation

For performance evaluation of the proposed method, we follow an approach similar to that in [134] and carry out simulations considering two worst-case scenarios of PLI frequency variation with time. Consider a simulated PLI signal of the form

$$p(t) = A(t)\cos(2\pi f(t)t + \phi). \tag{7.13}$$

In the first worst-case scenario, $f(t)$ varies about the central frequency of 50 Hz in a sinusoidal manner, with peak frequency deviation of 2 Hz, i.e. the frequency varies continuously over the range of 48 Hz to 52 Hz, with a period equal to 5 seconds. The amplitude is simulated as a sinusoidal signal with a period of 50 seconds, scaled by appropriate factors so as to achieve input SNRs ranging from -20 to 10 dB in steps of 5 dB . In the second worst case scenario, we consider 2 Hz step-changes in the central frequency, every 6 seconds, rest of the signal parameters being the same as in the first case.

7.4.3 Performance evaluation criteria

In order to evaluate the performance of the proposed method under different noise intensities, the performance measures are calculated at different values of input signal-to-noise ratio (SNR_{in}), defined as

$$SNR_{in} = \frac{\sum_{i=0}^{N-1} x^2(i)}{\sum_{i=0}^{N-1} n^2(i)}, \tag{7.14}$$

where x denotes the clean signal, n denotes the added noise signal, which is the PLI and N denotes the length of the signals. The performance criteria used are output SNR (SNR_o) and mean square error (MSE) defined as

$$SNR_o = 10\log_{10}\frac{\sum_{i=0}^{N-1} x_d^2(i)}{\sum_{i=0}^{N-1}[x(i) - x_d(i)]^2}, \tag{7.15}$$

TABLE 7.1: Values of SNR_o and MSE obtained using different combinations of bump wavelet parameters σ and μ.

μ	σ							
	0.2		0.4		0.6		0.8	
	SNR_o	MSE	SNR_o	MSE	SNR_o	MSE	SNR_o	MSE
3	32.75	1.33E-4	28.33	0.0024	30.75	8.72E-4	30.9	4.24E-4
5	20.97	0.0017	33.96	2.03E-4	25.25	0.0028	25.22	0.0021
7	16.31	0.005	29.81	2.26E-4	34.84	2.57E-4	31.65	0.0025.

TABLE 7.2: Average SNR_o and MSE for different values of input SNR in the first worst case scenario

Method	Input SNR	-20	-15	-10	-5	0	5	10
Notch	SNR_o	0.1159	0.3570	1.042	2.6900	5.6977	9.8137	14.4874
filter	MSE	13.8813	4.3896	1.3881	0.4389	0.1388	0.0439	0.0139
ANC	SNR_o	1.4739	3.4967	6.6060	10.0522	13.0196	15.1580	16.4838
	MSE	0.9671	0.3185	0.1131	0.0480	0.0273	0.0206	0.0184
Proposed	SNR_o	18.7144	23.4801	27.9203	31.6720	34.4686	36.2394	37.1925
method	MSE	0.00505	0.0016	5.55E-4	2.18E-4	1.11E-4	7.66E-5	6.37E-5

$$MSE = \frac{1}{N}\sum_{i=1}^{N}\left[x(i) - x_d(i)\right]^2, \tag{7.16}$$

where x_d denotes the denoised signal. These performance criteria are used to measure the amount of noise removed and also how closely the denoised signal resembles the original clean signal. It is desirable to achieve high values of SNR_o and low values of MSE to ensure that the noise is removed without causing distortion to the underlying signal.

7.4.4 Parameter selection for WT

For determination of optimal bump wavelet parameters, a subset of the ECG signals was used, to which random PLI realizations were added and the average values of the performance evaluation criteria given in 7.15 and 7.16 were calculated. The results are tabulated in Table-7.1 and it can be seen that the values $\sigma = 0.4$ and $\mu = 5$ cause the least distortion to the underlying signal, although comparable results are obtained using $\sigma = 0.6$ and $\mu = 7$. Outside the ranges of μ and σ in the Table, the mode retrieval algorithm was found to fail for one or more signals.

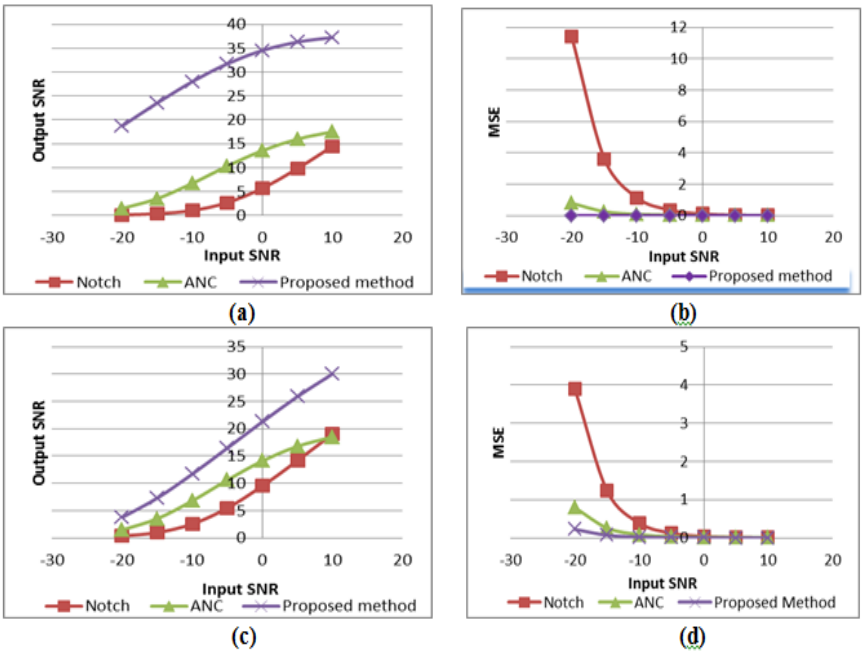

FIGURE 7.3: Variation of output SNR and MSE for pathological cases: (a) Output SNR variation with input SNR for the first worst case scenario (b) MSE variation with input SNR for the first worst case scenario (c) Output SNR variation with input SNR for the second worst case scenario (d) MSE variation with input SNR

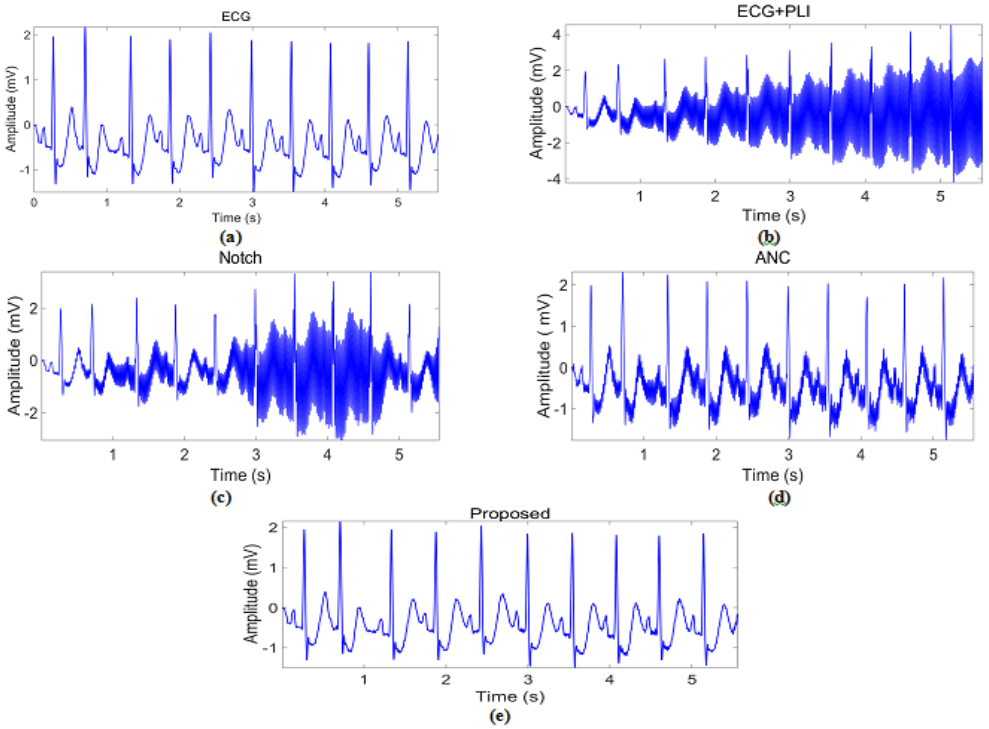

FIGURE 7.4: (a) ECG signal from record 213 of MIT-BIH database (b) the ECG signal contaminated with PLI at -5 dB SNR corresponding to the first worst-case scenario (c) Notch filter output (d) ANC output (e) output using the proposed method

TABLE 7.3: Average Output SNR and MSE for different values of input SNR in the second worst case scenario

Method	Input SNR	-20	-15	-10	-5	0	5	10
Notch filter	SNR_o	0.3354	0.9789	2.5472	5.4647	9.5232	14.1726	19.0374
	MSE	4.7375	1.4982	0.4738	0.1498	0.0474	0.015	0.00475
ANC	SNR_o	1.4561	3.5004	6.7086	10.3777	13.6481	16.0462	17.5224
	MSE	0.965	0.3139	0.1078	0.0425	0.0217	0.0150	0.0129
Proposed method	SNR_o	3.7568	7.2920	11.6896	16.4436	21.2427	25.8429	29.9287
	MSE	0.2706	0.0856	0.02715	0.0086	0.0028	9.17E-4	3.33E-4

7.4.5 Results of PLI removal

The results of PLI removal using the proposed method are compared with notch filtering [135] and adaptive noise cancellation (ANC) [136]. The notch filter is designed as an IIR filter with the notch at 50 Hz and a -3 dB bandwidth of 1Hz. For the ANC, the convergence step-size is set to 0.05 and the regularization factor is chosen as 10-6 as in [10]. All simulations were carried out in MATLAB software. The results for the two worst-case scenarios (for the healthy records) are averaged over all records and tabulated in Table-7.2 and 7.3 respectively. The results for the pathological cases are separately shown in Fig. 7.3(a)-(d). It is observed that the proposed method performs significantly better than the two reference methods in both the scenarios at all input SNR levels. Also, the proposed method performs equally well for healthy and pathological cases. For visual comparison, the contaminated and denoised ECG signals obtained using the proposed and reference methods for the first worst case scenario are shown in Figure 7.4. As expected, the fixed notch filter is unable to track the PLI frequency variations and performs poorly. Though the ANC performs much better than the notch filter, it however is significantly less effective in PLI removal than the proposed method.

7.5 Conclusions

PLI is a major source of noise in ECG signals which can adversely affect its interpretation. In this chapter, we proposed a novel method for PLI removal from ECG signals based RCM algorithm, which is inspired by synchrosqueezing. The main motivation of the proposed technique is that the PLI component appears in the form of a ridge in the contaminated ECG signal, which can be retrieved and reconstructed using the RCM algorithm. By subtracting this component from the contaminated ECG, the PLI can be removed. The proposed method is evaluated in two worst case scenarios of PLI frequency and amplitude variations is found to significantly outperform the existing fixed and adaptive filtering techniques.

Chapter 8

Conclusions and Future Scope

CVDs are the leading cause of death globally. In order to mitigate mortality risks due to CVDs, their timely detection and better management is necessary. The ECG is a low cost and noninvasive tool for diagnosis of many cardiac disorders. Particularly, arrhythmias can be identified through their signature ECG patterns. Manual identification of arrhythmias in long-term ECG obtained from Holter monitor after several hours or days of recording, is a tedious task and is prone to human errors. Therefore, there is a strong motivation for automatic arrhythmia classification, which is the focus of this work. This consists of two main steps: (1) heartbeat segmentation and (2) beat classification. For heart beat segmentation, the location of QRS complexes is required. Using the R-peak as the fiducial mark, usually fixed intervals are chosen on either side of the mark for beat segmentation. Thus, in this thesis, we have focused on QRS detection and beat classification.

Five novel algorithms were proposed in this thesis. Three algorithms for QRS detection, and one algorithm for ECG classification was proposed. In addition, one algorithm for power line interference removal was also proposed as additional work. The key results of this thesis are summarized as follows:

- One of the objectives of this thesis was to develop a technique for QRS detection, which may not necessarily be real-time implementable, but gives improved detection accuracy over existing techniques. In this direction, a technique for QRS detection using the SSWT in the preprocessing stage was proposed in Chapter-3. The key advantage of SSWT is that it's largely invariant to the underlying mother wavelet. This property proved to be very useful for QRS detection, as ECG signals have diverse QRS morphologies. This technique also employed a nonlinear transformation that is novel in the context of QRS detection, to equalize the QRS

amplitudes before peak detection. The proposed algorithm gives quite a low detection error rate of 0.15 %, outperforming existing techniques in the literature. However, a limitation of this algorithm is its high computational and memory requirements.

- Another objective of this thesis was to develop a QRS detection algorithm with low computational load, suitable for implementation in wearable devices. The accuracy of the proposed algorithm was aimed to be higher than existing QRS detection techniques for wearable devices. In this direction, a new method based on least squares optimization techniques was proposed in Chapter-4. The algorithm employed WLS and Savitzky-Golay filtering. The proposed algorithm was implemented in NXP LPC1768 microcontroller, based on ARM Cortex M3 core and was shown to be real-time implementable on it. Additionally, the algorithm was shown to outperform existing real time techniques. The overall DER obtained was 22% in the offine implementation and 0.67% in the real-time implementation.

- In the direction of developing real-time implementable algorithms, another algorithm based on WTV denoising was proposed in Chapter-5. While the algorithm in Chapter-4 was based on ℓ_2 norm minimization, this algorithm uses ℓ_1 norm minimization. Also, this technique used Teager-Kaiser energy to compute weights instead of signal derivative, as used in the WLS-based technique. The main motivation behind this algorithm was to see if this TV norm based technique gives better results than the least squares based technique proposed in Chapter-4. To solve the WTV minimization problem, a recently proposed fast solver was utilized, and it was found that the technique is much faster than the WLS based technique. The offline implementation of this method gives nearly the same accuracy as the WLS-based method, whereas the real-time implementation of this method gives much higher accuracy than the WLS based method. The DER obtained using this method for real-time implementation is 0.29%, whereas that for the WLS-based method is 0.67%.

- Another objective of the thesis was to develop an improved ECG classification method. It was observed that in the literature, more attention had been paid on the feature extraction stage as compared to the classifier stage. We attempted to explore new classification techniques which did not require sophisticated features for classification. In this direction, we developed a graph based classifier in Chapter-6. To the best of our knowledge, graphs have not been used earlier for ECG classification. The proposed method yielded classification accuracy nearly equal to those obtained using more sophisticated features. Additionally, the graph based classifier was shown to outperform SVM classifiers with the same inputs.

- As an additional work, a method for PLI removal from ECG signals was also proposed in Chapter-7. The motivation for this method emerged from the observation that PLI is observed in the form of a ridge in the wavelet representation, around the PLI frequency. Thus, RCM algorithm was used for retrieval of the ridge corresponding to PLI component, which was reconstructed and then subtracted from the ECG, to remove PLI. The proposed method was evaluated in two worst-case scenarios of PLI variation for both healthy and pathological cases, and was shown to outperform fixed and adaptive notch filters.

Future scope

In the real-time implementation of the techniques proposed in Chapter-4 and Chapter-5, it was observed that false positive detection occur at the block edges, specially in signals with pointed P- and T-waves. In a future work, some strategy to overcome this issue may be developed.

Also, the WLS optimization based algorithm in Chapter-4 and the WTV minimization based algorithm in Chapter-5 can be seen as general frameworks of denoising. In WLS based technique, the inverse of signal derivative values were used a weights. On the other hand, in the WTV-based algorithm in Chapter-5, the Teager-Kaiser energy values were used as weights. In a future work, some other measure of weights could be explored to achieve even greater accuracies.

With the emergence of low cost multichannel sensor technology, there is greater need for multivariate denoising techniques. The recently proposed multivariate denoising algorithm [141] that uses synchrosqueezing of both CWT and STFT can be used for this purpose. This synchrosqueezing-based multivariate denoising algorithm can be used for preprocessing the multilead ECG signal, leading to higher QRS detection accuracies.

In the proposed method of graph-based classification in Chapter-6, single lead ECG data was used for classification. In a future work, another study can be conducted to see if fusion of data from multiple leads gives improved accuracies.

Recently, a synchrosqueezing-based selective time-frequency algorithm [142] is also available which is inspired by the RCM algorithm that was used in Chapter-7. This algorithm attempts to identify and localize only the signal components of interest, unlike the RCM algorithm, which also localizes the noise components. The use of this algorithm can be explored to achieve improved PLI removal as compared to the RCM-based algorithm used in Chapter-7.

Appendix A

List of publications

The following publications have arised out of the research work presented in this thesis:

Journal Publications:

1. T. Sharma and K. K. Sharma, "QRS Complex Detection in ECG Signals Using the Synchrosqueezed Wavelet Transform," *IETE Journal of Research* (Taylor and Francis), vol. 62, no. 6, pp. 885-892 2016.

2. T. Sharma and K. K. Sharma, ": A New Method for QRS Detection in ECG Signals using QRS-Preserving Filtering Techniques," *Biomedical Engineering/Biomedizinische Technik* (De Gruyter), Published online (5-5-2017).

3. T. Sharma and K. K. Sharma, "QRS complex detection in ECG signals using locally adaptive weighted total variation denoising," *Computers in Biology and Medicine* (Elsevier), vol. 87, pp. 187-199, 2017.

4. T. Sharma and K. K. Sharma, "ECG classification using total variation regularization on graph," *to be communicated.*

Conference Publication:

1. T. Sharma & K. K. Sharma, "Power Line Interference Removal from ECG Signals Using Wavelet Transform based Component-Retrieval", Intl. Conference on Advances in Computing, Communications and Informatics (ICACCI), Sept. 21-24, 2016, Jaipur, India, pp.96-101.

Bibliography

[1] M. K. Homoud, "Monophasic action potential." http://ocw.tufts.edu/data/50/634463/634544_xlarge, 2007. Retrieved: 14-06-18. Under Creative Commons license Attribution-ShareAlike 3.0 Unported.

[2] "Monophasic action potential." http://ocw.tufts.edu/data/50/634463/634544_xlarge. Retrieved: 14-06-18. Under Creative Commons license.

[3] "ECG tracing correlated to the cardiac cycle." http://cnx.org/contents/nx-78gVf@1/OU-Human-Physiology-Cardiac-Mu. Retrieved: 14-06-18. Under Creative Commons license Attribution-ShareAlike 3.0 Unported.

[4] "Einthoven's triangle." https://lifeinthefastlane.com/ecg-library/limb-lead-reversals/. Retrieved: 15-06-18. Under Creative Commons Attribution-NonCommercial ShareAlike 4.0.

[5] M. Haggstrom, "Einthoven's triangle." https://en.wikipedia.org/wiki/File:Precordial_leads_in_ECG.png. Retrieved: 15-06-18. Under CC0 1.0 Universal Public Domain Dedication.

[6] Chikumaya, "Premature atrial contraction on ii-lead ecg.." https://commons.wikimedia.org/wiki/File:PAC.png. Retrieved: 15-06-18. Public Domain.

[7] J. Heilman, "Premature ventricular contraction." https://en.wikipedia.org/wiki/Premature_ventricular_contraction#/media/File:PVC10.JPG. Retrieved: 15-06-18. Attribution-ShareAlike 3.0 Unported.

[8] J. Heilman, "Ventricular bigeminy." https://commons.wikimedia.org/w/index.php?curid=9445046. Retrieved: 15-06-18. Attribution-CC BY-SA 3.0.

[9] Glenlarson, "Ventricular tachycardia." ByGlenlarson-Ownwork,PublicDomain, https://commons.wikimedia.org/w/index.php?curid=51194100. Retrieved: 15-06-18. Attribution-ShareAlike 3.0 Unported.

[10] Jer5150, "Ventricular fibrillation." https://commons.wikimedia.org/w/index.php?curid=19669589. Retrieved: 15-06-18. Attribution-CC BY-SA 3.0.

[11] "First degree AV block." https://lifeinthefastlane.com/ecg-library/basics/first-degree-heart-block/. Retrieved: 15-06-18. Attribution-Creative commons ShareAlike 4.0.

[12] "Left bundle banch block." https://lifeinthefastlane.com/ecg-library/basics/left-bundle-branch-block/. Retrieved: 15-06-18. Attribution-Creative commons ShareAlike 4.0.

[13] "World Health Organization, Global status report on noncommunicable diseases." http://www.who.int/mediacentre/factsheets/fs317/en/. Accessed: 2017-05-28.

[14] D. C. Reddy, *Biomedical Signal Processing: Principles and Techniques*. New Delhi: Tata McGraw-Hill Education, 2005. Second reprint.

[15] L. Crevasse and M. Ariet, *Computers in cardiology, J.W (Ed.): Hurst, The Heart.* New York: McGraw-Hill, 7 ed., 1990.

[16] B.-U. Kohler, C. Hennig, and R. Orglmeister, "The principles of software QRS detection," *IEEE Engineering in Medicine and Biology Magazine*, vol. 21, no. 1, pp. 42–57, 2002.

[17] W. P. Holsinger, K. M. Kempner, and M. H. Miller, "A QRS Preprocessor Based on Digital Differentiation," *IEEE Transactions on Biomedical Engineering*, vol. BME-18, no. 3, pp. 212–217, 1971.

[18] M. Okada, "A digital filter for the QRS complex detection.," *IEEE transactions on Biomedical Engineering*, vol. 26, no. 12, pp. 700–3, 1979.

[19] J. Fraden and M. R. Neuman, "QRS wave detection," *Medical and Biological Engineering and Computing*, vol. 18, no. 2, pp. 125–132, 1980.

[20] A. Ligtenberg and M. Kunt, "A robust-digital QRS-detection algorithm for arrhythmia monitoring," *Computers and Biomedical Research*, vol. 16, no. 3, pp. 273–286, 1983.

[21] J. Pan and W. J. Tompkins, "A real-time QRS detection algorithm," *IEEE transactions on Biomedical engineering*, no. 3, pp. 230–236, 1985.

[22] L. Keselbrener, M. Keselbrener, and S. Akselrod, "Nonlinear high pass filter for R-wave detection in ECG signal," *Medical Engineering & Physics*, vol. 19, no. 5, pp. 481–484, 1997.

[23] V. Di Virgilio, C. Francaiancia, S. Lino, and S. Cerutti, "ECG fiducial points detection through wavelet transform," in *Engineering in Medicine and Biology Society, 1995., IEEE 17th Annual Conference*, vol. 2, pp. 1051–1052, IEEE, 1995.

[24] S. Kadambe, R. Murray, and G. F. Boudreaux-Bartels, "Wavelet transform-based QRS complex detector," *IEEE Transactions on Biomedical Engineering*, vol. 46, no. 7, pp. 838–848, 1999.

[25] J. P. Martínez, R. Almeida, S. Olmos, A. P. Rocha, and P. Laguna, "A wavelet-based ECG delineator: evaluation on standard databases," *IEEE Transactions on Biomedical Engineering*, vol. 51, no. 4, pp. 570–581, 2004.

[26] S.-W. Chen, H.-C. Chen, and H.-L. Chan, "A real-time QRS detection method based on moving-averaging incorporating with wavelet denoising," *Computer Methods and Programs in Biomedicine*, vol. 82, no. 3, pp. 187–195, 2006.

[27] Z. Zidelmal, A. Amirou, M. Adnane, and A. Belouchrani, "QRS detection based on wavelet coefficients," *Computer Methods and Programs in Biomedicine*, vol. 107, no. 3, pp. 490–496, 2012.

[28] Y. H. Hu, W. J. Tompkins, J. L. Urrusti, and V. X. Afonso, "Applications of artificial neural networks for ECG signal detection and classification.," *Journal of Electrocardiology*, vol. 26, pp. 66–73, 1992.

[29] Q. Xue, Y. H. Hu, and W. J. Tompkins, "Neural-network-based adaptive matched filtering for QRS detection," *IEEE Transactions on Biomedical Engineering*, vol. 39, no. 4, pp. 317–329, 1992.

[30] K. P. Lin and W. H. Chang, "QRS feature extraction using linear prediction.," *IEEE Transactions on Biomedical Engineering*, vol. 36, no. 10, pp. 1050–1055, 1989.

[31] P. E. Trahanias, "An Approach to QRS Complex Detection Using Mathematical Morphology," *IEEE Transactions on Biomedical Engineering*, vol. 40, no. 2, pp. 201–205, 1993.

[32] D. A. Coast, R. M. Stern, G. G. Cano, and S. A. Briller, "An approach to cardiac arrhythmia analysis using hidden Markov models," *IEEE Transactions on Biomedical Engineering*, vol. 37, no. 9, pp. 826–836, 1990.

[33] M. E. Nygards and L. Sornmo, "Delineation of the QRS complex using the envelope of the ECG," *Medical and Biological Engineering and Computing*, vol. 21, pp. 538–547, 1983.

[34] Z. Zidelmal, A. Amirou, D. Ould-Abdeslam, A. Moukadem, and A. Dieterlen, "QRS detection using S-Transform and Shannon energy," *Computer Methods and Programs in Biomedicine*, vol. 116, no. 1, pp. 1–9, 2014.

[35] X. Ning and I. W. Selesnick, "ECG enhancement and QRS detection based on sparse derivatives," *Biomedical Signal Processing and Control*, vol. 8, no. 6, pp. 713–723, 2013.

[36] M. Merino, I. M. Gómez, and A. J. Molina, "Envelopment filter and K-means for the detection of QRS waveforms in electrocardiogram.," *Medical engineering & Physics*, vol. 37, no. 6, pp. 605–9, 2015.

[37] P. Phukpattaranont, "QRS detection algorithm based on the quadratic filter," *Expert Systems with Applications*, vol. 42, no. 11, pp. 4867–4877, 2015.

[38] D. Castells-Rufas and J. Carrabina, "Simple real-time QRS detector with the MaMeMi filter," *Biomedical Signal Processing and Control*, vol. 21, pp. 137–145, 2015.

[39] W.-H. Jung and S.-G. Lee, "An R-peak detection method that uses an SVD filter and a search back system.," *Computer methods and programs in biomedicine*, vol. 108, no. 3, pp. 1121–32, 2012.

[40] J. L. Semmlow, *Biosignal and Medical Image Processing MATLAB-Based Applications (Signal Processing and Communications), CRC Press.* 2004, pp. 180.

[41] P. D. Chazal, M. O. Dwyer, R. B. Reilly, and S. Member, "Automatic Classification of Heartbeats Using ECG Morphology and Heartbeat Interval Features," *IEEE transactions on Biomedical engineering*, vol. 51, no. 7, pp. 1196–1206, 2004.

[42] P. De Chazal and R. B. Reilly, "A patient-adapting heartbeat classifier using ECG morphology and heartbeat interval features," *IEEE Transactions on Biomedical Engineering*, vol. 53, no. 12, pp. 2535–2543, 2006.

[43] M. Llamedo and J. P. Mart, "An Automatic Patient-Adapted ECG Heartbeat Classifier Allowing Expert Assistance," *IEEE Transactions on Biomedical engineering*, vol. 59, no. 8, pp. 2312–2320, 2012.

[44] D. Lannoy, D. Franc, J. Delbeke, and M. Verleysen, "Weighted Conditional Random Fields for Supervised Interpatient Heartbeat Classification," *IEEE Transactions on Biomedical engineering*, vol. 59, no. 1, pp. 241–247, 2012.

[45] T. H. Linh, S. Osowski, M. Ieee, and M. Stodolski, "On-Line Heart Beat Recognition Using Hermite Polynomials and Neuro-Fuzzy Network," *IEEE Transactions on Instrumentation and Measurement*, vol. 52, no. 4, pp. 1224–1231, 2003.

[46] W. Jiang, S. Member, S. G. Kong, and S. Member, "Block-Based Neural Networks for Personalized ECG Signal Classification," *IEEE Transactions on Neural Networks*, vol. 18, no. 6, pp. 1750–1761, 2007.

[47] S. Osowski, L. T. Hoai, and T. Markiewicz, "Support Vector Machine-Based Expert System for Reliable Heartbeat Recognition," *IEEE Transactions on Biomedical Engineering*, vol. 51, no. 4, pp. 582–589, 2004.

[48] T. Ince, S. Kiranyaz, M. Gabbouj, and S. Member, "A Generic and Robust System for Automated Patient-Specific Classification of ECG Signals," *IEEE Transactions on Biomedical Engineering*, vol. 56, no. 5, pp. 1415–1426, 2009.

[49] S. Kiranyaz, T. Ince, and M. Gabbouj, "Real-Time Patient-Specific ECG Classification by 1-D Convolutional Neural Networks," *IEEE Transactions on Biomedical Engineering*, vol. 63, no. 3, pp. 664–675, 2016.

[50] M. Javadi, S. Ali, A. Abbaszadeh, A. Sajedin, and R. Ebrahimpour, "Biomedical Signal Processing and Control Classification of ECG arrhythmia by a modular neural network based on Mixture of Experts and Negatively Correlated Learning," *Biomedical Signal Processing and Control*, vol. 8, no. 3, pp. 289–296, 2013.

[51] R. Ceylan, Y. Özbay, and B. Karlik, "A novel approach for classification of ECG arrhythmias: Type-2 fuzzy clustering neural network," *Expert Systems with Applications*, vol. 36, no. 3 PART 2, pp. 6721–6726, 2009.

[52] M. Barni, S. Member, P. Failla, R. Lazzeretti, and A.-r. Sadeghi, "Privacy-Preserving ECG Classification With Branching Programs and Neural Networks," *IEEE Transactions on Information Forensics and Security*, vol. 6, no. 2, pp. 452–468, 2011.

[53] S. Shadmand and B. Mashoufi, "Biomedical Signal Processing and Control A new personalized ECG signal classification algorithm using Block-based Neural Network and Particle Swarm Optimization," *Biomedical Signal Processing and Control*, vol. 25, pp. 12–23, 2016.

[54] J. A. Gutierrez-Gnecchi, R. Morfin-Magana, D. Lorias-Espinoza, A. d. C. Tellez-Anguiano, E. Reyes-Archundia, A. Mendez-Patino, and R. Castaneda-Miranda, "DSP-based arrhythmia classification using wavelet transform and probabilistic neural network," *Biomedical Signal Processing and Control*, vol. 32, pp. 44–56, 2017.

[55] O. Castillo, P. Melin, E. Ramírez, and J. Soria, "Hybrid intelligent system for cardiac arrhythmia classification with Fuzzy K-Nearest Neighbors and neural networks combined with a fuzzy system," *Expert Systems with Applications*, vol. 39, no. 3, pp. 2947–2955, 2012.

[56] J.-S. Wang, W.-C. Chiang, Y.-L. Hsu, and Y.-T. C. Yang, "ECG arrhythmia classification using a probabilistic neural network with a feature reduction method," *Neurocomputing*, vol. 116, pp. 38–45, 2012.

[57] F. Melgani and Y. Bazi, "Classification of electrocardiogram signals with support vector machines and particle swarm optimization," *IEEE Transactions on Information Technology in Biomedicine*, vol. 12, no. 5, pp. 667–677, 2008.

[58] F. Alonso-atienza, E. Morgado, L. Fern, L. R. Alvarez, and S. Member, "Detection of Life-Threatening Arrhythmias Using Feature Selection and Support Vector Machines," *IEEE Transactions on Biomedical Engineering*, vol. 61, no. 3, pp. 832–840, 2014.

[59] A. F. Khalaf, M. I. Owis, and I. A. Yassine, "A novel technique for cardiac arrhythmia classification using spectral correlation and support vector machines," *Expert Systms with Applications*, July 2015.

[60] S. Jain, V. Bajaj, and A. Kumar, "Efficient algorithm for classification of electrocardiogram beats based on artificial bee colony-based least-squares support vector machines classifier," *Electronic Letters*, vol. 52, no. 14, pp. 14–15, 2016.

[61] L. Sun, Y. Lu, K. Yang, and S. Li, "ECG analysis using multiple instance learning for myocardial infarction detection.," *IEEE Transactions on Biomedical Engineering*, vol. 59, pp. 3348–56, Dec 2012.

[62] Y. J. Kim, J. Heo, K. S. Park, and S. Kim, "Proposition of novel classification approach and features for improved real-time arrhythmia monitoring," *Computers in Biology and Medicine*, vol. 75, pp. 190–202, 2016.

[63] F. A. Elhaj, N. Salim, A. R. Harris, T. T. Swee, and T. Ahmed, "Arrhythmia recognition and classification using combined linear and nonlinear features of ECG signals.," *Computer Methods and Programs in Biomedicine*, vol. 127, pp. 52–63, 2016.

[64] S. Raj, K. C. Ray, and O. Shankar, "Cardiac arrhythmia beat classification using DOST and PSO tuned SVM," *Computer Methods and Programs in Biomedicine*, vol. 136, pp. 163–177, 2016.

[65] I. Daubechies, J. Lu, and H.-T. Wu, "Synchrosqueezed wavelet transforms: An empirical mode decomposition-like tool," *Applied and Computational Harmonic Analysis*, vol. 30, no. 2, pp. 243–261, 2011.

[66] Z. Farbman, R. Fattal, D. Lischinski, and R. Szeliski, "Edge-preserving decompositions for multi-scale tone and detail manipulation," *ACM Transactions on Graphics (Proceedings of ACM SIGGRAPH 2008)*, vol. 27, Aug. 2008.

[67] S. Meignen, T. Oberlin, and S. McLaughlin, "A new algorithm for multicomponent signals analysis based on synchrosqueezing: With an application to signal sampling and denoising," *IEEE Transactions on Signal Processing*, pp. 5787–5798, 2012.

[68] Rangayyan, R. M. , *Biomedical signal analysis: A case-study approach.* Piscataway, NJ: IEEE Press, 2002.

[69] G. D. Clifford, F. Azuaje, and P. McSharry, *Advanced Methods And Tools for ECG Data Analysis.* Norwood, MA, USA: Artech House, Inc., 2006.

[70] S. Banerjee, R. Gupta, and M. Mitra, "Delineation of ECG characteristic features using multiresolution wavelet analysis method," *Measurement*, vol. 45, no. 3, pp. 474–487, 2012.

[71] P. Langley, E. J. Bowers, and A. Murray, "Principal component analysis as a tool for analyzing beat-to-beat changes in ECG features: application to ECG-derived respiration," *IEEE Transactions on Biomedical Engineering*, vol. 57, no. 4, pp. 821–829, 2010.

[72] S. Banerjee and M. Mitra, "Application of cross wavelet transform for ECG pattern analysis and classification," *IEEE Transactions on Instrumentation and Measurement*, vol. 63, no. 2, pp. 326–333, 2014.

[73] A. S. Alvarado, C. Lakshminarayan, and J. C. Principe, "Time-based compression and classification of heartbeats," *IEEE Transactions on Biomedical Engineering*, vol. 59, pp. 1641–1648, June 2012.

[74] G. Wübbeler, M. Stavridis, D. Kreiseler, R.-D. Bousseljot, and C. Elster, "Verification of humans using the electrocardiogram," *Pattern Recognition Letters*, vol. 28, no. 10, pp. 1172–1175, 2007.

[75] P. S. Hamilton and W. J. Tompkins, "quantitative investigation of qrs detection rules using the mit/bih arrhythmia database," *IEEE Transactions on Biomedical Engineering.*

[76] C. Li and C. Zheng, "Detection of ECG Characteristic," *IEEE transactions on Biomedical Engineering*, vol. 42, no. 1, 1995.

[77] S. Pal and M. Mitra, "Empirical mode decomposition based ECG enhancement and QRS detection," *Computers in Biology and Medicine*, pp. 83–92, 2012.

[78] E. J. d. S. Luz, W. R. Schwartz, G. Camara-Chavez, and D. Menotti, "ECG-based heartbeat classification for arrhythmia detection: A survey," *Computer Methods and Programs in Biomedicine*, vol. 127, pp. 144–164, 2016.

[79] T. P. Exarchos *et al.*, "A platform for wide scale integration and visual representation of medical intelligence in cardiology: the decision support framework," *Computers in cardiology*, vol. 68, pp. 167–170, 2005.

[80] T. P. Exarchos *et al.*, "A methodology for the automated creation of fuzzy expert systems for ischaemic and arrhythmic beat classification based on a set of rules obtained by a decision tree.," *Artificial Intelligence in Medicine*, vol. 40, pp. 187–200, 2007.

[81] S. Mitra, M. Mitra, and B. B. Chaudhuri, "A rough-set-based inference engine for ECG classification," *IEEE Transactions on Instrumentation and Measurement*, vol. 55, no. 6, pp. 2198–2206, 2006.

[82] I. Güler and Elif Derya Übeyli, "Ecg beat classifier designed by combined neural network model," *Pattern Recognition*, vol. 38, pp. 199–208, 2005.

[83] C. Ye, S. Member, B. V. K. V. Kumar, and M. T. Coimbra, "Heartbeat Classification Using Morphological and Dynamic Features of ECG Signals," *IEEE Transactions on Biomedical Engineering*, vol. 59, no. 10, pp. 2930–2941, 2012.

[84] Y. Kutlu and D. Kuntalp, "Feature extraction for ECG heartbeats using higher order statistics of WPD coefficients.," *Computer Methods and Programs in Biomedicine*, vol. 105, pp. 257–67, mar 2012.

[85] C. Lin, Y. Du, and T. Chen, "Adaptive wavelet network for multiple cardiac arrhythmias recognition," *Expert Systems with Applications*, vol. 34, pp. 2601–2611, may 2008.

[86] F. M. Ham and S. Han, "Classification of cardiac arrhythmias using fuzzy artmap," *IEEE Transactions on Biomedical Engineering*, vol. 43, pp. 425–429, April 1996.

[87] A. K. Mishra and S. Raghav, "Local fractal dimension based ecg arrhythmia classification," *Biomedical Signal Processing and Control*, vol. 5, pp. 114–123, 2010.

[88] J. Rodriguez, A. Goni, and A. Illarramendi, "Real-time classification of ecgs on a pda," *IEEE Transactions on Information Technology in Biomedicine*, vol. 9, pp. 23–34, March 2005.

[89] E. J. D. S. Luz, T. M. Nunes, V. H. C. de Albuquerque, J. P. Papa, and D. Menotti, "ECG arrhythmia classification based on optimum-path forest," *Expert Systems with Applications*, vol. 40, pp. 3561–3573, jul 2013.

[90] G. Thakur, E. Brevdo, N. S. Fučkar, and H. T. Wu, "The Synchrosqueezing algorithm for time-varying spectral analysis: Robustness properties and new paleoclimate applications," *Signal Processing*, vol. 93, pp. 1079–1094, 2013.

[91] R. H. Herrera, J. B. Tary, M. V. D. Baan, and D. W. Eaton, "Body Wave Separation in the Time-Frequency Domain," *IEEE Geoscience and Remote Sensing Letters*, vol. 12, no. 2, pp. 364–368, 2015.

[92] P. Wang, J. Gao, and Z. Wang, "Time-Frequency Analysis of Seismic Data Using Synchrosqueezing Transform," *IEEE Geoscience and Remote Sensing Letters*, vol. 11, no. 12, 2044, pp. 2042–2014.

[93] M. Mihalec, J. Slavi, and M. Boltezr, "Synchrosqueezed wavelet transform for damping identification," *Mechanical Systems and Signal Processing*, vol. 80, pp. 324–334, 2016.

[94] H. T. Wu, Y. H. Chan, Y. T. Lin, and Y. H. Yeh, "Using synchrosqueezing transform to discover breathing dynamics from ECG signals," *Applied and Computational Harmonic Analysis*, vol. 36, no. 2, pp. 354–359, 2014.

[95] M. M. Kabir and L. G. Tereshchenko, "Development of analytical approach for an automated analysis of continuous long-term single lead ecg for diagnosis of paroxysmal atrioventricular block," in *Proceedings of the Computing and Cardiology Conference*, pp. 913–916, 2014. Cambridge, MA.

[96] I. Daubechies and S. Maes, "*A nonlinear squeezing of the continuous wavelet transform based on auditory nerve models,*" *Wavelets in Medicine and Biology*, Boca Raton, FL:CRC Press, 1996.

[97] F. Auger and P. Flandrin, "Improving the readability of time-frequency and time-scale representations by the reassignment method," *IEEE Transactions on Signal Processing*, vol. 43, pp. 1068–1089, May 1995.

[98] E. Chassande-Mottin, I. Daubechies, F. Auger, and P. Flandrin, "Differential reassignment," *IEEE Signal Processing Letters*, vol. 4, pp. 293–294, Oct 1997.

[99] E. Chassande-Mottin, F. Auger, and P. Flandrin, *Time-Frequency/Time-Scale Reassignment*, pp. 233–267. Boston, MA: Birkhauser Boston, 2003.

[100] I. Daubechies, J. Lu, and H. T. Wu, "Synchrosqueezed wavelet transforms: An empirical mode decomposition-like tool," *Applied and Computational Harmonic Analysis*, vol. 30, no. 2, pp. 243–261, 2011.

[101] N. E. Huang, Z. Shen, S. R. Long, M. C. Wu, H. H. Shih, Q. Zheng, N.-C. Yen, C. C. Tung, and H. H. Liu, "The empirical mode decomposition and the Hilbert spectrum for nonlinear and non-stationary time series analysis," *Proceedings of the Royal Society of London A: Mathematical, Physical and Engineering Sciences*, vol. 454, no. 1971, pp. 903–995, 1998.

[102] J. Xiao and P. Flandrin, "Multitaper Time-Frequency Reassignment for Nonstationary Spectrum Estimation and Chirp Enhancement," *IEEE Transactions on Signal Processing*, vol. 55, no. 6, pp. 2851–2860, 2007.

[103] H. Yang, "Robustness Analysis of Synchrosqueezed Transforms," *arXiv:1410.5939*, no. October 2014, pp. 1–27, 2015.

[104] D. Iatsenko, P. V. E. Mcclintock, and A. Stefanovska, "Linear and synchrosqueezed timeâĂŞfrequency representations revisited: Overview, standards of use, resolution, reconstruction, concentration, and algorithms," *Digital Signal Processing*, vol. 42, pp. 1–26, 2015.

[105] H. Yang, "Synchrosqueezed wave packet transforms and diffeomorphism based spectral analysis for 1D general mode decompositions," *Applied and Computational Harmonic Analysis*, vol. 39, no. 1, pp. 33–66, 2015.

[106] "MIT-BIH arrhythmia database." `http://www.physionet.org/physiobank/database/mitdb/`. Accessed: 2017-01-18.

[107] "MATLAB synchrosqueezing toolbox." `http://web.math.princeton.edu/~ebrevdo/synsq`. Accessed: 2016-06-10.

[108] S. A. and G. M.J.E., "Smoothing and differentiation of data by simplified least squares procedures," *Analytical chemistry*, vol. 36, pp. 1627–1639, 1964.

[109] S. J. Orfanidis, *Introduction to Signal Processing.* Englewood Cliffs, NJ: Prentice-Hall, 1996.

[110] S. McGinn and P. D. White, "The duration of the QRS complex in the normal and abnormal electrocardiograms.," *American Heart Journal*, vol. 9, pp. 642–654, 1934.

[111] "Ambulatory electrocardiographs," tech. rep., American National Standard Institute, 1994.

[112] "Recommended practice for testing and reporting performance results of ventricular arrhythmia detection algorithms," tech. rep., Association for the Advancement of Medical Instrumentation, 1987.

[113] S. Kuo, B. Lee, and W. Tian, *Real-time signal processing implementations and applications.* West Sussex, England: John Wiley and Sons, 2 ed., 2006.

[114] L. I. Rudin, S. Osher, and E. Fatemi, "Nonlinear total variation based noise removal algorithms," *Physica D: Nonlinear Phenomena*, vol. 60, no. 1, pp. 259–268, 1992.

[115] I. W. Selesnick, M. Lang, and C. S. Burrus, "Constrained least square design of FIR filters without specified transition bands," *IEEE Transactions on Signal Processing*, vol. 44, no. 8, pp. 1879–1892, 1996.

[116] A. Barbero and S. Sra, "Modular proximal optimization for multidimensional total-variation regularization," *arXiv:1411.0589*, 2014.

[117] J. F. Kaiser, "Some useful properties of teager's energy operators," in *Acoustics, Speech, and Signal Processing, 1993. ICASSP-93., 1993 IEEE International Conference on*, vol. 3, pp. 149–152, IEEE, 1993.

[118] F. Thomas Quatieri, *Discrete-time speech signal processing, principles and practice*. Singapore: Pearson Education Pvt. Ltd., 2004.

[119] A. V. Oppenheim, R. W. Schafer, and B. J. R., *Discrete-Time Signal Processing*. Upper Saddle River, NJ: Prentice Hall.

[120] S. Farashi, "A multiresolution time-dependent entropy method for QRS complex detection," *Biomedical Signal Processing and Control*, vol. 24, pp. 63–71, 2016.

[121] C. Li, C. Zheng, and C. Tai, "Detection of ECG characteristic points using wavelet transforms," *IEEE Transactions on Biomedical Engineering*, vol. 42, no. 1, pp. 21–28, 1995.

[122] A. K. Dohare, V. Kumar, and R. Kumar, "An efficient new method for the detection of QRS," *Computers and Electrical Engineering*, vol. 40, no. 5, pp. 1717–1730, 2014.

[123] D. Boutana, M. Benidir, and F. Bouaziz, "Multiresolution wavelet-based QRS complex detection algorithm suited to several abnormal morphologies," *IET Signal Processing*, vol. 8, pp. 774–782, sep 2014.

[124] M. Yochum, C. Renaud, and S. Jacquir, "Biomedical Signal Processing and Control Automatic detection of P , QRS and T patterns in 12 leads ECG signal based on CWT," *Biomedical Signal Processing and Control*, vol. 25, pp. 46–52, 2016.

[125] A. Sandryhaila, "Classification via Regularization on Graphs," *IEEE Global Conference on Signal and Information Processing (GlobalSIP)*, no. 3, pp. 495–498, 2013.

[126] A. Sandryhaila, "Discrete Signal Processing on Graphs : Frequency Analysis," *IEEE Transactions on Signal Processing*, vol. 62, no. 12, pp. 3042–3054, 2014.

[127] X. Jiang, L. Zhang, Q. Zhao, and S. Albayrak, "ECG Arrhythmias Recognition System Based on Independent Component Analysis Feature Extraction," *TENCON 2006 - 2006 IEEE Region 10 Conference*, pp. 1–4, 2006.

[128] S. Raj, S. Member, and K. C. Ray, "ECG Signal Analysis Using DCT-Based DOST and PSO Optimized SVM," *IEEE Transactions on Instrumentation amd Measurtement*, vol. 66, no. 3, pp. 470–478, 2017.

[129] J. S. Sahambi, S. N. Tandon, and R. K. P. Bhatt, "Quantitative analysis of errors due to power-line interference and base-line drift in detection of onsets and offsets in ECG using wavelets," *Medical and Biological Engineering and Computing*, vol. 35, no. 6, pp. 747–751, 1997.

[130] C. Levkov, G. Mihov, R. Ivanov, I. Daskalov, I. Christov, and I. Dotsinsky, "Removal of power-line interference from the ECG : a review of the subtraction procedure," *Biomedical Engineering Online*, vol. 18, pp. 1–18, 2005.

[131] P. Kligfield *et al.*, "Recommendations for the standardization and interpretation of the electrocardiogram Part I: the electrocardiogram and its technology," *Circulation*, vol. 18, pp. 1306–1324, 2007.

[132] R. A. Carmona, W. L. Hwang, and B. Torresani, "Characterization of signals by the ridges of their wavelet transforms," *IEEE Transactions on Signal Processing*, vol. 45, pp. 2586–2590, Oct 1997.

[133] P. E. McSharry, G. D. Clifford, L. Tarassenko, and L. A. Smith, "A dynamical model for generating synthetic electrocardiogram signals," *IEEE Transactions on Biomedical Engineering*, vol. 50, pp. 289–294, March 2003.

[134] M. Zivanovic and M. González-Izal, "Simultaneous powerline interference and baseline wander removal from ECG and EMG signals by sinusoidal modeling," *Medical Engineering and Physics*, vol. 35, no. 10, pp. 1431–1441, 2013.

[135] S.-C. Pei and C.-C. Tseng, "Elimination of ac interference in electrocardiogram using iir notch filter with transient suppression," *IEEE Transactions on Biomedical Engineering*, vol. 42, pp. 1128–1132, Nov 1995.

[136] M. H. Costa and M. C. Tavares, "Removing harmonic power line interference from biopotential signals in low cost acquisition systems," *Computers in Biology and Medicine*, vol. 39, no. 6, pp. 519–526, 2009.

[137] N. Rehman and D. P. Mandic, " Multivariate empirical mode decomposition," *Proceedings of the Royal Society of London A: Mathematical, Physical and Engineering Sciences*, vol. 466, no. 2117, pp. 1291-1302, 2010.

[138] M. A. Colominas, G. Schlotthauer, M. E. Torres, and P. Flandrin, "Noise-assisted EMD methods in action," *Advances in adaptive data analysis*, vol. 4. no. 4, pp. 1250025-1-11, 2012.

[139] N. U. Rehman, C. Park, N. E. Huang and D. P. Mandic, "EMD via MEMD: Multivariate noise-aided computation of standard EMD," *Advances in adaptive data analysis*, vol. 5, no. 2, pp. 135007-1-25, 2013.

[140] T. Chanwimalueang, W. V. Rosenberg and D. P. Mandic, "Enabling R-peak detection in wearable ECG: Combining matched filtering and Hilbert transform," IEEE Conference on Digital Signal Processing, pp. 134-138, 2015.

[141] A. Ahrabian and D. P. Mandic, "A class of multivariate denoising algorithms based on synchrosqueezing," *IEEE Transactions on Signal Processing*, vol. 63, no. 9, pp. 2196-2208, 2015.

[142] A. Ahrabian and D. P. Mandic, "Selective time-frequency reassignment based on synchrosqueezing,." *IEEE Signal Processing Letters*, vol. 22, no.11, pp. 2039 -2043, 2015.